# COMPARISON OF COMPUTATIONAL IMAGE INPAINTING METHODS

A THESIS SUBMITTED TO
THE GRADUATE SCHOOL OF NATURAL AND APPLIED SCIENCES
OF
MIDDLE EAST TECHNICAL UNIVERSITY

CANDE KURT

IN PARTIAL FULFILLMENT OF THE REQUIREMENTS
FOR
THE DEGREE OF MASTER OF SCIENCE
IN
STATISTICS

SEPTEMBER 2018

Approval of the thesis:

**COMPARISON OF COMPUTATIONAL IMAGE INPAINTING METHODS**

submitted by **CANDE KURT** in partial fulfillment of the requirements for the degree of **Master of Science in Statistics Department, Middle East Technical University** by,

Prof. Dr. Halil Kalıpçılar
Dean, Graduate School of **Natural and Applied Sciences** ______________

Prof. Dr. Ayşen Akkaya
Head of Department, **Statistics** ______________

Prof. Dr. İnci Batmaz
Supervisor, **Statistics Department, METU** ______________

Prof. Dr. İlkay Ulusoy
Co-supervisor, **Electric Electronic Eng. Dept., METU** ______________

**Examining Committee Members:**

Assoc. Prof. Dr. Ceylan Talu Yozgatlıgil
Statistics Department, METU ______________

Prof. Dr. İnci Batmaz
Statistics Department, METU ______________

Assist. Prof. Dr. Fatma Yerlikaya Özkurt
Industrial Engineering Department, ATILIM UNIVERSITY ______________

Date:

**I hereby declare that all information in this document has been obtained and presented in accordance with academic rules and ethical conduct. I also declare that, as required by these rules and conduct, I have fully cited and referenced all material and results that are not original to this work.**

Name, Last Name: CANDE KURT

Signature :

# ABSTRACT

## COMPARISON OF COMPUTATIONAL IMAGE INPAINTING METHODS

Kurt, Cande
M.S., Department of Statistics
Supervisor : Prof. Dr. İnci Batmaz
Co-Supervisor : Prof. Dr. İlkay Ulusoy

September 2018, 103 pages

Image processing plays an important role in today's world. It has been using in medicine, quality control, defense industry, fine arts to ease for our lives. There are many applications in these fields such as tumor detection, license plate detection, edge detection, recognition of handwritten digits, filtering for noise reduction, restoring old photographs, and the like. The aim of image processing can be divided into five groups: visualization to observe the objects that are not visible, image sharpening or restoration to create a better visual, image retrieval to seek for the image of interest, measurement of pattern and image recognition to analyze the objects in an image. Inpainting, also known as image restoration or completion is one of the hot topics of image processing. The basic idea of image inpainting is filling lost or missing parts of an image using information from the neighboring of background with different techniques. In this research, performances of widely used image in painting algorithms, Partial Differential Equations (PDE), Kriging and Artificial Neural Networks (ANNs) are compared to those of Multivariate Adaptive Regression Splines (MARS) and Conic Multivariate Adaptive Regression Splines (CMARS) which are novel in

this domain. According to the results, the PDE method overperforms the others while the rest have similar performances; particularly, with respect to Structural Similarity Index (SSMI) criterion which represents human visual evaluation.

Keywords: Image Restoration/Completion, Partial Differential Equations, Kriging, Artificial Neural Networks, Conic Multivariate Adaptive Regression Splines.

# ÖZ

## HESAPLAMALI GÖRÜNTÜ İÇBOYAMA YÖNTEMLERİNİN KARŞILAŞTIRILMASI

Kurt, Cande

Yüksek Lisans, İstatistik Bölümü

Tez Yöneticisi : Prof. Dr. İnci Batmaz

Ortak Tez Yöneticisi : Prof. Dr. İlkay Ulusoy

Eylül 2018 , 103 sayfa

Günümüz dünyasında görüntü işleme önemli bir rol oynar. Tıpta, kalite kontrolde, savunma sanayide ve güzel sanatlarda hayatımızı kolaylaştırmak için kullanılmaktadır. Tümor saptama, plaka tespiti, kenar saptama, el yazısı tanıma, gürültü azaltmak için filtreleme, eski fotoğrafların iyileştirilmesi ve benzeri alanlarda pek çok uygulamaları mevcuttur. Görüntü işlemenin amacını görünmez nesneleri gözlemlemek için görselleştirme, daha iyi görsel elde etmek için görüntü keskinleştirme ya da yenileme, görüntünün ilgilenilen alanının araştırılması için yeniden düzenlenmesi, görüntüdeki objeleri analiz etmek adına örüntü ve görüntü tanıma ölçümü olarak beş gruba ayırabiliriz. Görüntü yenileme ya da tamamlama olarak da bilinen içboyama (inpainting) görüntü işlemenin yeni araştırma konularından biridir. İçboyamanın temel amacı kayıp ya da eksik parçaların farklı tekniklerle arka plandaki komşuluklarından yararlanılarak doldurulmasıdır. Bu çalışmada, alanda yaygın olarak kullanılan parçalı diferansiyel denklemler (PDD), kriging ve yapay sinir ağları (YSA) yöntemlerinin göreceli

olarak yeni olan çok değişkenli uyarlamalı regresyon eğrileri (ÇURE) ve konik çok değişkenli uyarlamalı regresyon eğrileri (KÇURE)'leriyle karşılaştırılmaktadır. Elde edilen sonuçlara göre, özellikle yapısal benzerlik indeksi dikkate alındığında PDD yöntemi diğerlerine göre daha iyi performans gösterirken, diğer yöntemler kendi aralarında benzer performanslar göstermişlerdir.

Anahtar Kelimeler: Görüntü Restorasyonu/Tamamlama, Parçalı Diferansiyel Denklemler, Kriging, Yapay Sinir Ağları, Konik Çok Değişkenli Uyarlamalı Regresyon Eğrileri.

To Ayfer, Oğuz and Caner Kurt

# ACKNOWLEDGMENTS

First and foremost, I would like to express my appreciation to my supervisor Prof. Dr. İnci Batmaz for her support, patience and collaboration. Both her academic knowledge and perspective on life support my development. Whole my life, I will always remember her office where surrounding us her father's unique painting works. Also, I would like to thank to my co-advisor Prof. Dr. İlkay Ulusoy. Without their academic knowledge this thesis could not have been finished.

I would like to thank to the members of the examining committee: Assoc. Prof. Dr. Ceylan Talu Yozgatlıgil and Assist. Prof. Dr. Fatma Yerlikaya Özkurt for their contributions.

I am thankful to Dr. Ceyda Yazıcı for her academic support during developing the CMARS stage.

I would like to thank to committee of International Conference on Information Complexity and Statistical Modeling to accept presentation of primal version of this thesis. Also, I am thankful to Assist. Prof. Dr. Elçin Kartal Koç, chair of our session, for her academic support.

I would like to convey my thanks to individuals Ashok Kandimalla, Simone Parisotto and Dr. Wolfgang Schwanghart and Yurdanur Özkan for sharing their knowledge.

I would convey to my thanks to our library staff, especially to Onur Atlı for his support to provide new book to library.

I would also like to express my thanks to Vivaldi, subtle hero of this thesis, for his unique work: The Four Seasons. Whole my study, I only listened to the same concerto, and this method increased my motivation.

I would like to thank you my colleagues Ertan Budak and Yiğit Ünal for sharing their experiences on visual arts.

I am very thankful to Gülşah Serdar, Ebru Korkmaz and Özge Tüzer for their friendship. One of the great things of the master study was meeting with them.

I would like to express my thanks to my dear friends Simge Bican, Nazlı Gürbüz, Tolgahan Araz and Selcen Kökçü. They always believe in and support me throughout my life.

I would like to share my thanks to our family friends, especially to Fatma Şahin, Sabiha Şahin and Necla Tacir for their support.

I would like to thank to my members of family, especially to my grandmother Aysel Sökmen, my aunt Şerife Sökmen Karadağ and my brothers Berk Yiğit Karadağ and Ahmet Alp Sökmen. I am also thankful to my uncles, aunts, cousins and all my close relatives. They always encourage me to finish my thesis.

I would like to express my thanks to Emre Çakır for his patience and continuous encouragement. We always believe in each other to overcome to difficulties.

I would gratitude to my sole family: my parents Ayfer-Oğuz Kurt and my brother Caner Kurt for their endless love, support and providing opportunities. I shall forever remain indebted them.

# TABLE OF CONTENTS

ABSTRACT . . . . . . . . . . v

ÖZ . . . . . . . . . . vii

ACKNOWLEDGMENTS . . . . . . . . . . x

TABLE OF CONTENTS . . . . . . . . . . xii

LIST OF TABLES . . . . . . . . . . xvi

LIST OF FIGURES . . . . . . . . . . xvii

LIST OF ABBREVIATIONS . . . . . . . . . . xxi

CHAPTERS

1 INTRODUCTION . . . . . . . . . . 1

1.1 General . . . . . . . . . . 1

1.2 Motivation . . . . . . . . . . 6

1.3 Structure of the Thesis . . . . . . . . . . 7

2 BACKGROUND . . . . . . . . . . 9

2.1 Image Representation . . . . . . . . . . 9

2.1.1 Pixel and Voxel . . . . . . . . . . 9

2.1.2 Concept of Neighborhood . . . . . . . . . . 11

2.1.3 Fundamental Morphological Operations in Image Processing . . . . . . . . . . . . . . . . . . . . . . 12

2.2 What is Image Inpainting? . . . . . . . . . . . . . . . . . . . . 13

2.3 Application Areas of Inpainting . . . . . . . . . . . . . . . . . 16

3 LITERATURE REVIEW . . . . . . . . . . . . . . . . . . . . . . . . 19

3.1 Review on Inpainting Approaches . . . . . . . . . . . . . . . . 19

3.1.1 Partial Differential Equation (PDE) Based Inpainting 19

3.1.2 Texture Synthesis Based Inpainting . . . . . . . . 20

3.1.3 Exemplar Based Inpainting . . . . . . . . . . . . . 22

3.1.4 Hybrid Based Inpainting . . . . . . . . . . . . . . 22

3.1.5 Fast and Convolution Based Inpainting . . . . . . . 23

3.1.6 Interpolation Based Inpainting . . . . . . . . . . . 24

3.2 Review on Images and Masks . . . . . . . . . . . . . . . . . . 25

3.2.1 Images . . . . . . . . . . . . . . . . . . . . . . . 26

3.2.2 Masks . . . . . . . . . . . . . . . . . . . . . . . . 29

4 METHODS . . . . . . . . . . . . . . . . . . . . . . . . . . . . . . 31

4.1 Computational Inpainting Methods . . . . . . . . . . . . . . . 31

4.1.1 Partial Differential Equations . . . . . . . . . . . . 31

4.1.2 Kriging . . . . . . . . . . . . . . . . . . . . . . . 33

4.1.3 Artificial Neural Networks . . . . . . . . . . . . . 35

4.1.4 Multivariate Adaptive Regression Splines . . . . . 37

4.1.5 Conic Multivariate Adaptive Regression Splines . . 39

4.2 Quality Metrics . . . . . . . . . . . . . . . . . . . . . . . . 43
4.2.1 Mean Squared Error . . . . . . . . . . . . . . . . . 43
4.2.2 Peak Signal-to-Noise Ratio . . . . . . . . . . . . . 45
4.2.3 Structural Similarity Index . . . . . . . . . . . . . 45
4.3 Repeated Measures ANOVA . . . . . . . . . . . . . . . . . 48
5 COMPARATIVE EXPERIMENTS AND RESULTS . . . . . . . . . 51
5.1 Dataset . . . . . . . . . . . . . . . . . . . . . . . . . . . . 51
5.2 Tools . . . . . . . . . . . . . . . . . . . . . . . . . . . . . 56
5.3 Applied Methods . . . . . . . . . . . . . . . . . . . . . . . 57
5.3.1 PDE . . . . . . . . . . . . . . . . . . . . . . . . . 58
5.3.2 Kriging . . . . . . . . . . . . . . . . . . . . . . . 58
5.3.3 Artificial Neural Networks . . . . . . . . . . . . . 59
5.3.4 Multivariate Adaptive Regression Splines . . . . . 61
5.3.5 Conic Multivariate Adaptive Regression Splines . . 61
5.4 Application Results . . . . . . . . . . . . . . . . . . . . . 62
5.4.1 Outputs of Inpainted Images . . . . . . . . . . . . 62
5.4.2 Results with Quality Metrics . . . . . . . . . . . . 68
5.4.3 Three-Way Repeated Measures ANOVA . . . . . . 70
5.4.3.1 Results of PSNR . . . . . . . . . . . . 72
5.4.3.2 Results of MSE . . . . . . . . . . . . 77
5.4.3.3 Results of SSMI . . . . . . . . . . . . 82

6 CONCLUSION . . . . . . . . . . . . . . . . . . . . . . . . . . . . 89

REFERENCES . . . . . . . . . . . . . . . . . . . . . . . . . . . . 91

APPENDICES

A IMAGE TYPES . . . . . . . . . . . . . . . . . . . . . . . . . . . . 101

A.1 Binary . . . . . . . . . . . . . . . . . . . . . . . . . . . . 102

A.2 Indexed . . . . . . . . . . . . . . . . . . . . . . . . . . . . 102

A.3 Grayscale . . . . . . . . . . . . . . . . . . . . . . . . . . . . 102

A.4 RGB . . . . . . . . . . . . . . . . . . . . . . . . . . . . 102

# LIST OF TABLES

TABLES

Table 3.1 Grouped Images . . . . . . . . . . . . . . . . . . . . . . . . . . . 28

Table 5.1 Results of the Lena image . . . . . . . . . . . . . . . . . . . . . . . 68

Table 5.2 Results of the Boat image . . . . . . . . . . . . . . . . . . . . . . . 68

Table 5.3 Results of the Cameraman image . . . . . . . . . . . . . . . . . . . . 69

Table 5.4 Results of the Jet plane image . . . . . . . . . . . . . . . . . . . . . 69

Table 5.5 Results of the Mri image . . . . . . . . . . . . . . . . . . . . . . . . 69

Table A.1 Interpretation of Image Types . . . . . . . . . . . . . . . . . . . . . 101

# LIST OF FIGURES

FIGURES

Figure 1.1 Relief of twelve Hittite Gods of the Underworld . . . . . . . . . . 2

Figure 1.2 View from the Window at Le Gras, 1826 . . . . . . . . . . . . . . . 3

Figure 1.3 The First Color Image . . . . . . . . . . . . . . . . . . . . . . . . 4

Figure 1.4 A Preserving Method: Matting and Framing . . . . . . . . . . . . 5

Figure 2.1 Image Representation . . . . . . . . . . . . . . . . . . . . . . . . 10

Figure 2.2 On a square grid, each pixel represents a square region of the image. 11

Figure 2.3 Neighborhoods on a rectangular grid . . . . . . . . . . . . . . . . 12

Figure 2.4 Combining erosion and dilation to produce an opening or a closing 12

Figure 2.5 Separation of touching features by erosion/dilation . . . . . . . . . 13

Figure 2.6 A house from Tecklenburg, Germany . . . . . . . . . . . . . . . . 13

Figure 2.7 Sample of inpainting . . . . . . . . . . . . . . . . . . . . . . . . 14

Figure 2.8 Image Inpainting Representation . . . . . . . . . . . . . . . . . . 14

Figure 2.9 Mathematical Image Inpainting Representation . . . . . . . . . . . 15

Figure 2.10 A sample of removing large objects from images . . . . . . . . . . 16

Figure 3.1 Block Diagram of PDE Based Inpainting . . . . . . . . . . . . . . 20

Figure 3.2 Block Diagram of Texture Synthesis Based Inpainting . . . . . . . 21

Figure 3.3 Representation of Texture Synthesis Based Inpainting . . . . . . . 21

Figure 3.4 Block Diagram of Exemplar Based Inpainting . . . . . . . . . . . 22

Figure 3.5 Representation of Hybrid Based Inpainting . . . . . . . . . . . . . 23

Figure 3.6 Representation of Fast and Convolution Based Image Inpainting . . 23

Figure 3.7 ANNs Representation . . . . . . . . . . . . . . . . . . . . . . . 25

Figure 3.8 Shade of gray ranging from black to white . . . . . . . . . . . . 28

Figure 4.1 A feed-forward network structure . . . . . . . . . . . . . . . . . 35

Figure 4.2 A sample truncated functions with the knot $t$=0.5 . . . . . . . . . . 38

Figure 4.3 Example of log-log scale curve for various different $\tilde{M}$ values . . . 42

Figure 4.4 The Quality Attributes Tree . . . . . . . . . . . . . . . . . . . . 43

Figure 4.5 Diagram of the SSMI Mechanism . . . . . . . . . . . . . . . . . 45

Figure 5.1 Used Images . . . . . . . . . . . . . . . . . . . . . . . . . . . 54

Figure 5.2 Used Masks . . . . . . . . . . . . . . . . . . . . . . . . . . . 55

Figure 5.3 Finding Neighbors of the known pixels . . . . . . . . . . . . . . 57

Figure 5.4 Masked Lena and Segmentation Results of the AT . . . . . . . . . 58

Figure 5.5 Variogram of Lena-M1. Blue line belongs the model, red squares represents experimental semiveriograms . . . . . . . . . . . . . . . . . 59

Figure 5.6 Results of ANNs . . . . . . . . . . . . . . . . . . . . . . . . . 60

Figure 5.7 Inpainted Images of Lena Image . . . . . . . . . . . . . . . . . . 63

Figure 5.8 Inpainted Images of Boat Image . . . . . . . . . . . . . . . . . . 64

Figure 5.9 Inpainted Images of Cameraman Image . . . . . . . . . . . . . . 65

Figure 5.10 Inpainted Images of Jet plane Image . . . . . . . . . . . . . . . . 66

Figure 5.11 Inpainted Images of Mri Image . . . . . . . . . . . . . . . . . . . . 67

Figure 5.12 Result of Tests of Within-Subjects Effects for Image . . . . . . . . 71

Figure 5.13 Structure of Within-Subjects Factors . . . . . . . . . . . . . . . . . 71

Figure 5.14 Descriptive Statistics of PSNR . . . . . . . . . . . . . . . . . . . . 72

Figure 5.15 Results of Mauchly's Test of Sphericity for PSNR . . . . . . . . . . 72

Figure 5.16 Result of Tests of Within-Subjects Effects for PSNR . . . . . . . . 73

Figure 5.17 Estimated results of method for PSNR . . . . . . . . . . . . . . . . 74

Figure 5.18 Result of Pairwise Comparisons of method for PSNR . . . . . . . . 74

Figure 5.19 Estimated results of mask for PSNR . . . . . . . . . . . . . . . . . 75

Figure 5.20 Result of Pairwise Comparisons of mask for PSNR . . . . . . . . . 75

Figure 5.21 Result of Interaction for PSNR . . . . . . . . . . . . . . . . . . . . 76

Figure 5.22 Descriptive Statistics of MSE . . . . . . . . . . . . . . . . . . . . . 77

Figure 5.23 Results of Mauchly's Test of Sphericity for MSE . . . . . . . . . . 78

Figure 5.24 Result of Tests of Within-Subjects Effects for MSE . . . . . . . . . 78

Figure 5.25 Estimated results of method for MSE . . . . . . . . . . . . . . . . 79

Figure 5.26 Result of Pairwise Comparisons of method for MSE . . . . . . . . 79

Figure 5.27 Estimated results of mask for MSE . . . . . . . . . . . . . . . . . 80

Figure 5.28 Result of Pairwise Comparisons of mask for MSE . . . . . . . . . 80

Figure 5.29 Result of Interaction for MSE . . . . . . . . . . . . . . . . . . . . 81

Figure 5.30 Descriptive Statistics of SSMI . . . . . . . . . . . . . . . . . . . . 82

Figure 5.31 Results of Mauchly's Test of Sphericity for SSMI . . . . . . . . . . 83

Figure 5.32 Result of Tests of Within-Subjects Effects for SSMI . . . . . . . . 83

Figure 5.33 Estimated results of method for SSMI . . . . . . . . . . . . . . . . . 84

Figure 5.34 Result of Pairwise Comparisons of method for SSMI . . . . . . . . . 84

Figure 5.35 Estimated results of mask for SSMI . . . . . . . . . . . . . . . . . . 85

Figure 5.36 Result of Pairwise Comparisons of mask for SSMI . . . . . . . . . . 85

Figure 5.37 Result of Interaction for SSMI . . . . . . . . . . . . . . . . . . . . . 86

Figure A.1 Representation of RGB and HSL values . . . . . . . . . . . . . . . . 103

# LIST OF ABBREVIATIONS

| | |
|---|---|
| 2-D | Two-Dimensional |
| 3-D | Three-Dimensional |
| ANNs | Artificial Neural Networks |
| ANOVA | Analysis of variance |
| ARPANET | Advanced Research Projects Agency Network |
| AT | Ambrosio-Tortorelli |
| BFs | Basis Functions |
| BLUE | Best Linear Unbiased Estimation |
| CFD | Computational Fluid Dynamics |
| CMARS | Conic Multivariate Adaptive Regression Splines |
| CQP | Conic Quadratic Programming |
| DF | Degrees of freedom |
| DWT | Discrete Wavelet Transform |
| FAX | Facsimile Automatic Xerox |
| FMM | Fast Marching Method |
| GCV | Generalized Cross-Validation |
| HSL | Hue, Saturation and Lightness |
| HVS | Human Visual System |
| LM | Levenberg-Marquardt |
| LRM | Linear Regression Model |
| LSE | Least Squares Estimation |
| MARS | Multivariate Adaptive Regression Splines |
| MCA | Morphological Component Analysis |
| MSE | Mean Squared Error |
| NNs | Neural Networks |
| OCR | Optical Character Recognition |
| PCA | Principal Component Analysis |
| PDE | Partial Differential Equations |

| | |
|---|---|
| PRSS | Penalized Residual Sum of Squares |
| PSNR | Peak Signal-to-Noise Ratio |
| RANOVA | Repeated Measures Analysis of Variance |
| ReV | Regionalized Variable |
| RGB | Red, Green and Blue |
| RSS | Residual Sum of Squares |
| SSD | Sum of Squared Differences |
| SSMI | Structural Similarity Index |
| SVD | Singular Value Decomposition |
| TR | Tikhonov Regularization |
| TV | Total Variational |
| UQI | Universal Quality Index |
| USC | University of Southern California |
| VQ | Vector Quantization |
| WWW | World Wide Web |

# CHAPTER 1

# INTRODUCTION

"What I like about photographs is that they capture a moment that's gone forever, impossible to reproduce."
—Karl Lagerfeld
"A good snapshot keeps a moment from running away."
— Eudora Welty

## 1.1 General

Photography is the strongest and easiest way to keep memories. In today's world almost everybody has a smartphone and automatically two cameras, front and back. If we look back in the period before the 2000s, we will notice that we had hard copy photographs. When we go back much further in time, cave arts, instead of photographs, will welcome us. Prehistoric people made cave art, and there are some theories about the reasons they made it; however, some mysteries remain. For instance, it is still controversial what the oldest painting known in the world is. Archaeologists have long been exploring temples, caves and other historical sites, and discovered many interesting artworks. To illustrate, they have found out that in Hattusa, the capital city of the Hittite Empire, the row of twelve gods with sickle-shaped swords on their shoulders at the end of the $13^{th}$ century BC is preserved. Figure 1.1 shows a representation of twelve gods of the Hittite underworld in the relief.
What is common to all the cultures in history is that they are all interested in painting. Thanks to the developing technology, manpower has decreased and digital art has began to play an important role in today's world. The first photograph was taken by Nicéphore Niépce in June/July 1827. He used two methods to obtain images: copying

Source: Photographed by the author

Figure 1.1: Relief of twelve Hittite Gods of the Underworld

from engraving and yielding camera obscura (meaning dark room in Latin). During his experiments on the method of copying from engraving, he worked with his son. The Nicéphore Niépce's son was an talented artist, and he was rendering the pictures which was a lithograph or engraving. Then, they coated the plates with the bitumen which is a sensitive substance to light. Existing varnished rendered picture was put on the coated stone. After that, they exposed both of them together to light. Whereas bitumen beneath inked lines of picture was conserved, bitumen beneath the bare paper became unsolved. Lavender oil was used for bath solution, and the unexposed parts on the plate dissolved. Finally, plate was ready to use for biting plate, inking and printing it. His invention is called "photogravue". Today's off-set printing has been founded upon his invention [2, 49].

After his son joining the army, he had to find another way to obtain images without drawing them. In those years, he continued to the experiments to develop and improve lithography, and he added to the literature one more word: “heliography”, meaning sun drawing. He made use of the camera obscura and some chemical materials such as pewter. A sheet of glass which is covered by bitumen was exposed for eight hours long exposure in a camera obscura. Finally, exposed material was bathed with oil. After this procedure, he obtained gray scale image by employing bitumen on a pewter plate [2, 51]. The first photograph belonged the Niépce's estate view is represented in Figure 1.2.

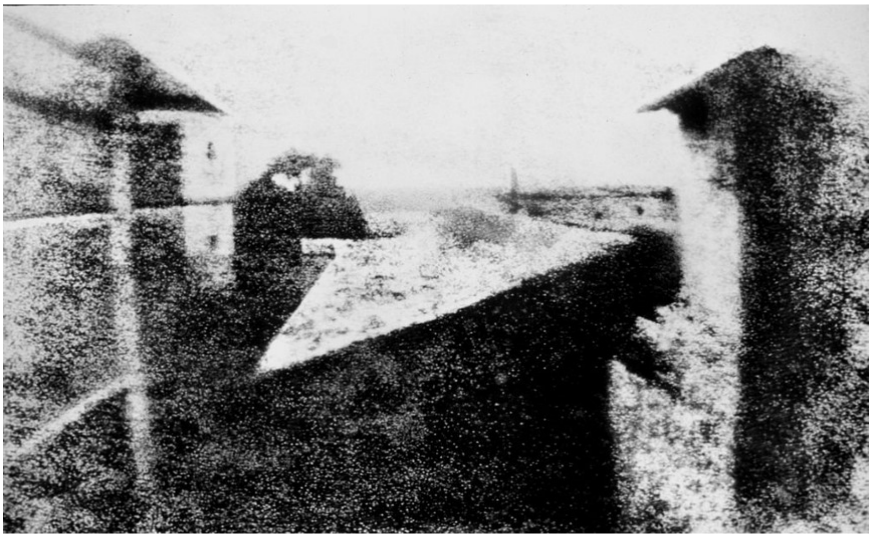

Source: Courtesy of Mahon [51]

Figure 1.2: View from the Window at Le Gras, 1826

If his son had not joined the army, the birth of photography might have been occurred by others. He was the pioneer of the black and white photography, and lots of people have improving his invention. Actually, the term of photography emerged after its invention. In 1839, the world gained a new word: "photography", which is derived from the Greek words for "light" and "writing". The name is given by Sir John Herschel whose invention yields from positive/negative process to obtain photograph [51].

As black and white photography developed, Scottish mathematical physicist James Clerk Maxwell had already started a new era: color photography. At the beginning, Maxwell's purpose was to be an invited lecturer at the Royal Institution. Instead of delivering a theoretical speech, he decided to conduct an experiment at the Royal Institution in the presence of public. In May 1861, Thomas Sutton took the picture of a tartan ribbon three times, under the supervision of Maxwell. Then, he developed the plates, and filtered them by red, green and blue (RGB) filters. Their outcome is demonstrated in Figure 1.3. That was a great fortune for The Royal Institution audience being a witness of the historical movement [51].
Thanks to the developing technology, people are advancing art of the photography, which is still an important part of our lives. The author of this thesis has a personal interest in the analogue photography. She remembers her grandfather's negative films. They were the same size as the hard copies. In those years photographers modified

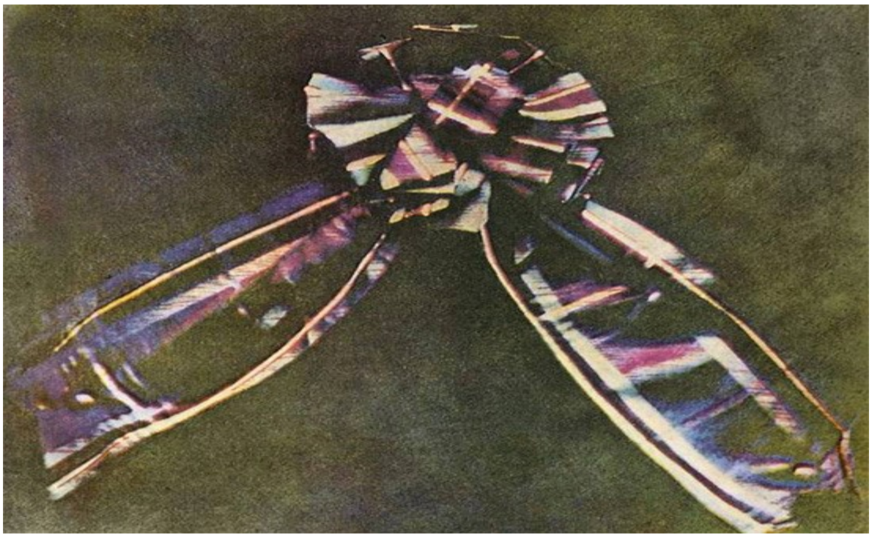

Source: Courtesy of Mahon [51]

Figure 1.3: The First Color Image

the photographs manually. Unlike today, they did not have the chance to modify images by automatic tools such as Photoshop program. After developing the films with chemical materials, they worked on negatives. Their equipment was limited: negatives, a pencil and a light. They changed the unwanted parts of the photograph by drawing those areas. In this way, people looked better in photographs than their real appearances by the agency of the manual effort of the photographers.

As the years go by, printed photographs have started to deteriorate particually when people do not take good care of them. Michele Hamill [36] states that handling, environment, housing, matting and framing, albums and labeling, duplication, disaster preparedness and digital imaging are the most important precautions for keeping the family heritage. According to the Michele Hamill, there are several causes of the deterioration, and some precautions are needed to be taken to protect them from those undesirable facts. First of all, handling should be done with care. Viewing the photographs in unclear environments with rushed hand movements can bring about scratches, cracks and rucked. And, touching them without gloves can cause stain because of the perspiration on hands. The environment in which photographs are kept should be chosen carefully. Keeping them in basements and attics can destroy the photographs due to a temperature higher than 68°F and humidity rate of %30-50. More importantly, sunlight destroys the colors of photographs. Extra light on printed photographs can cause them to look as if they are over-exposed. Another important criterion is knowing how to house photographs. If people do not keep them in folders, envelopes and boxes, their chance of being destroying increases. They can come under the light, dust and other environment conditions. The ideal hosing is keeping them separately in different places but in case of storage problem small bulks can be grouped without paper clips, labels and tapes. Being careful with matting and framing is the fourth important precaution to protect photographs. Matting and framing preserving procedure is depicted in Figure 1.4. All the while, the fundamental step is to avoid attaching photographs directly to the frame or glazing. Also, you should remove the photograph carefully from the frame because it may have been stuck to the glazing and the photograph for a long time.

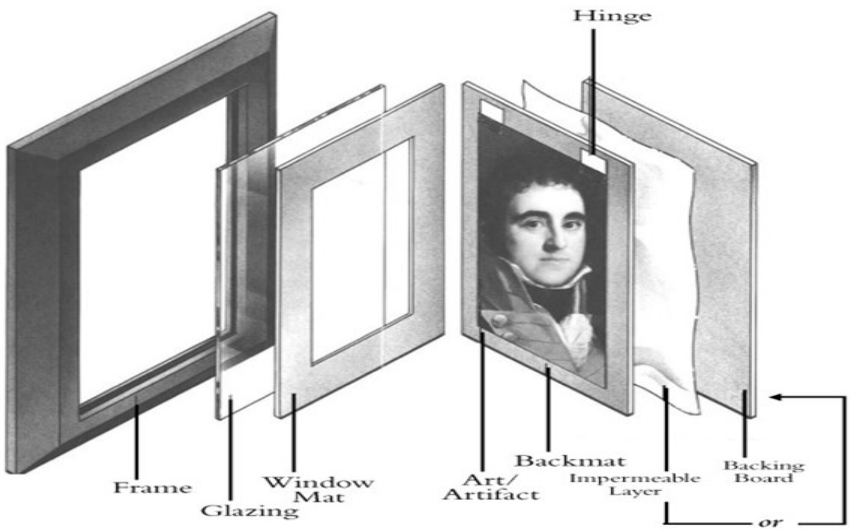


Source: New york State Archives, Managing Records. [61]

Figure 1.4: A Preserving Method: Matting and Framing

Furthermore, using albums and labels can damage photographs. It is true that storing the photographs conserves them from light, dust and other environmental effects and labeling them to remember dates of the special memories is a nice habit; however it is necessary to avoid sticking labels directly to photographs in order to prevent them from destruction. People can write the reminder on the back side of the photograph with a soft graphite pencil. The sixth preservation method is duplicating the photographs. When negatives are available, photographs can be recreated. On the other hand, color photographing can be a good solution to create copies with acid-free quality papers. The last but not the least, disaster preparedness is essential. Keeping the negatives and printed version of heirloom photographs in separate places can create an opportunity to reprint them from the negatives.

The precautions which are mentioned above can make photographs endure longer. However, if these precautions are ignored after a while, it leads to corruption of photographs. Today; however, this problem can be solved with the use of digital imaging, which transfers the hard-copy photographs to soft-copy images. Now, printed photographs are scanned by high resolution printers to keep them in a digital platform. After the scanning procedure, the scratches, cracks, imperfections, oils, and so forth on the photographs will be transferred to the digital form as well. These image-corruption problems actually provide an opportunity to the image processing field. Researchers have developed methods not only to solve these problems but also to remove unwanted contents from the image such as people, text and watermarks. This method is called "Image Inpainting."

## 1.2 Motivation

This thesis research topic is predicting the corrupted parts of the old photographs. Initially, literature review was done on image processing, and the image inpainting has been detected a rising topic. It has also been discovered that there are two main research topics on the image inpainting: removing physical determinations; in other words, completing the destroyed parts, and eliminating unwanted contents. The former refers to erasing scratches, cracks, red eye correction, dust and blur; the latter refers to erasing unwanted contents such as people, text, logo and watermarks.

Image inpainting algorithms are employed in this research focusing on the popular photograph deteriorations, mentioned in the previous paragraph. As will be discussed later, five methods are employed to compare their performance in this thesis. The first three methods are: Partial Differential Equations (PDEs), Kriging and Artificial Neural Networks (ANNs), which are widely used in the field of image inpainting. In addition to these methods, our particular contribution is the Multivariate Adaptive Regression Splines (MARS) and Conic Multivariate Adaptive Regression Splines

(CMARS) methods, where their use in this area is novel.

## 1.3 Structure of the Thesis

The thesis consists of five main chapters. It is structured as follows:

- Chapter 1 provides an introduction to the history of photography and the problems of photograph corruptions. Also, the motivation of the thesis research is stated in this chapter.
- Chapter 2 presents definition of computer vision, briefly history of digital image and image representation; also the method of inpainting.
- Chapter 3 includes related works in the image inpainting literature and state-of-art image datasets.
- Chapter 4 describes the theory and formulations of the chosen techniques: PDEs, Kriging, ANNs, MARS and CMARS. This chapter also includes quality metrics, and the method of repeated measures analysis of variance (RANOVA) used in performance comparisons.
- Chapter 5 is concerned with explaining the method of application via an instance image, chosen dataset with causes under the light of image classifications presented in Section 3.2. It also includes application tools and results.
- Chapter 6, the conclusion part, dwells on comparative results of the five methods mentioned in Chapter 4.
- Appendix A describes image types.

# CHAPTER 2

# BACKGROUND

Digital image was invented a decade before the color photography. Frederick Bakewell (1800-1869), born in England, was the inventor of the image telegraph. The mechanical process of his device was similar to drum scanner. After his first facsimile machine, Arthur Korn, in Germany and Edouard Belin, in France, developed different facsimile machines which have different methods for sensing tonal images. Whereas Korn used a selenium cell for scanning, Berlin's machine made use of relief etching technique which allowed the photography to scan with stylus. Finally, in 1920 the British Inventors Harry G. Bartholomew and Maynard D. McFarlane achieved to produce the first digital image. Their method is called Bartlane method, mix of the inventor's surnames. Bartlane method used a series of negatives on zinc five plates which were exposed to different lengths of time. Their method was tested for 15 levels in 1929. The more plates they used, the more levels of gray they gained [81].

## 2.1 Image Representation

There are several ways to represent image in the field of image processing. Spatial representation of a digital image is the most popular way [34]. It consists of two major components: 1- pixel and voxel 2- neighborhood relations.

### 2.1.1 Pixel and Voxel

An image is a continuous function of two spatial variables: x and y. Continuous images are represented by two-dimensional (2-D) arrays of point. Pixel or pel words come from the abbreviations of the word "picture element". A pixel is a value of x and y coordinates corresponding to grid position. f(x,y) includes M rows and N columns, where x= 0, 1, 2, . . . , M-1 and y= 0, 1, 2, . . . , N-1.

*Lena* is a popular gray scale test image used for image processing with $256 \times 256$ pixels. Figure 2.1a is a close-up view of Lena's eye in order to show some of the gray scale values. The image consists of an array of intensity values which ranges from zero to 255. Those coordinates correspond with gray colors as shown in Figure 2.1b, and Figure 3.8 can be a guide of the gray values.


(a) Image displayed as a visual intensity array

| | | | | | | | | | | | |
|---|---|---|---|---|---|---|---|---|---|---|---|
| 39 | 39 | 39 | 39 | 39 | 39 | 39 | 39 | 39 | 39 | 39 | 39 |
| 39 | 101 | 112 | 109 | 107 | 111 | 113 | 107 | 63 | 99 | 144 | 39 |
| 39 | 90 | 86 | 88 | 71 | 68 | 68 | 62 | 48 | 61 | 80 | 39 |
| 39 | 66 | 54 | 57 | 54 | 52 | 50 | 48 | 50 | 51 | 50 | 39 |
| 39 | 51 | 51 | 52 | 53 | 48 | 46 | 45 | 47 | 61 | 90 | 39 |
| 39 | 48 | 50 | 50 | 49 | 48 | 43 | 53 | 60 | 98 | 163 | 39 |
| 39 | 55 | 77 | 60 | 61 | 59 | 34 | 57 | 77 | 85 | 183 | 39 |
| 39 | 66 | 102 | 80 | 73 | 89 | 57 | 70 | 85 | 67 | 181 | 39 |
| 39 | 71 | 104 | 114 | 71 | 77 | 85 | 79 | 63 | 121 | 205 | 39 |
| 39 | 61 | 102 | 120 | 108 | 74 | 63 | 73 | 117 | 187 | 207 | 39 |
| 39 | 82 | 100 | 114 | 132 | 126 | 117 | 138 | 179 | 198 | 202 | 39 |
| 39 | 39 | 39 | 39 | 39 | 39 | 39 | 39 | 39 | 39 | 39 | 39 |

(b) Image shown as a 2-D numerical array

Source: Created by the author, inspired by [34], page 55

Figure 2.1: Image Representation

Matrix (2.1) illustrates the image representation in 2-D array, in a matrix form. It can be interpreted as follows: Digital image is represented as an $M \times N$ matrix in which M is the number of rows, and N the number of columns. Result of multiplying M and N is the total number of pixels of the image.

The Origin of an image is represented as (x,y) = (0,0), and the next coordinate values of the first column can be defined as f(1,0). Complete image can be written as in the following $M \times N$ matrix:

$$f(\mathbf{X,Y}) = \begin{bmatrix} f(0,0) & f(0,1) & \dots & f(0,N-1) \\ f(1,0) & f(1,1) & \dots & f(1,N-1) \\ \vdots & \vdots & & \vdots \\ f(M-1,0) & f(M-1,1) & \dots & f(M-1,N-1) \end{bmatrix}. \tag{2.1}$$

Hence, per element of matrix (2.1) is named as pixel, picture element, pel or image element whereas in three-dimensional (3-D) space: depth, row and column pixels turn into a volume element called voxels. Five representations of the same image with different number of pixels is given in Figure 2.2.

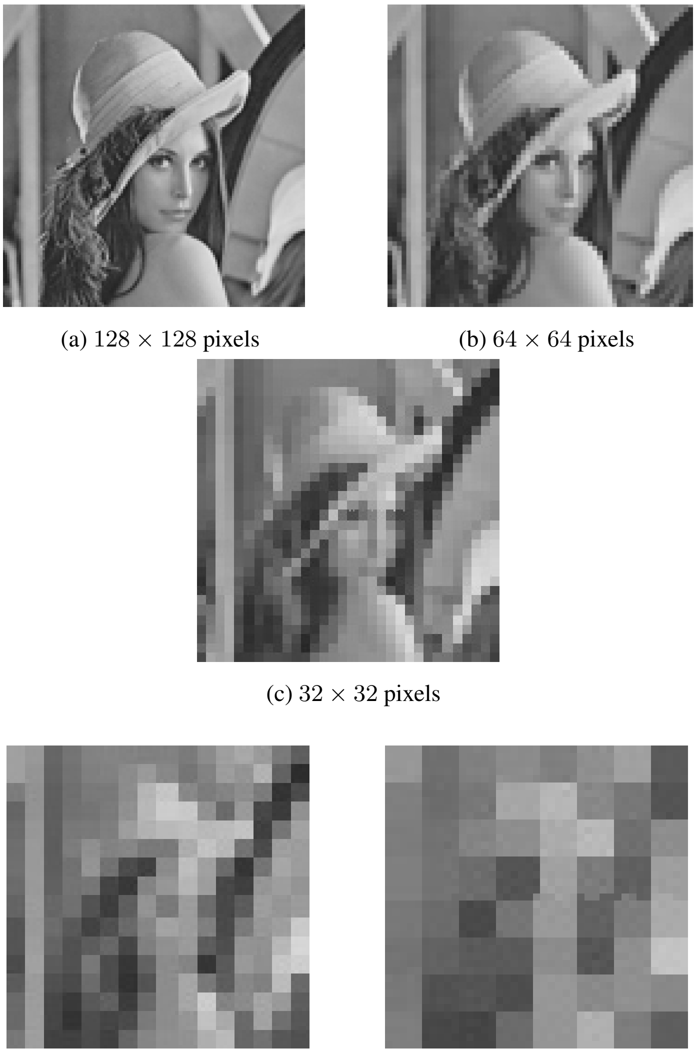

(a) 128 × 128 pixels (b) 64 × 64 pixels

(c) 32 × 32 pixels

(d) 16 × 16 pixels (e) 8 × 8 pixels

Source: Created by the author, inspired by [42]

Figure 2.2: On a square grid, each pixel represents a square region of the image.

It is obvious that decreasing the total pixels causes lost of the details in the image. Hence, in this thesis, $256 \times 256$ pixels images are employed in order to effectively compare the performances of the methods considered.

### 2.1.2 Concept of Neighborhood

A selected center pixel of a rectangular grid could have neighbor in two ways: having a joint edge or at least one joint corner. Hence, a center pixel defines as an (m,n) tuple could have four or eight neighbors. Figure 2.3 highlights the neighborhood relations.

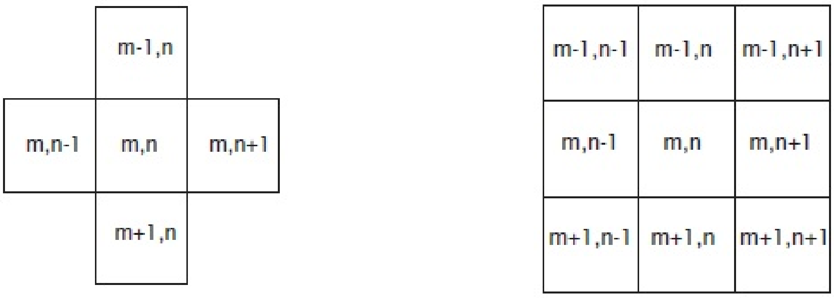


(a) 4-neighborhood (b) 8-neighborhood

Source: Courtesy of Bernd Jähne, [42]

Figure 2.3: Neighborhoods on a rectangular grid

### 2.1.3 Fundamental Morphological Operations in Image Processing

Cambridge Dictionary defines morphology as: "the scientific study of the structure and form of animals and plants" in biology; "the study of the form of words and phrases" in language. In image processing morphology refers to structure or form of the related objects. Morphological operations are popular in image segmentation, a branch of the image processing which is related to clustering the pixels with the same purpose. Some of the popular morphological transactions are: dilation, erosion, opening and closing. *Dilation* is expanding the pixels, which is a useful attempt for filling small holes and connecting disjoint objects. *Erosion* is the opposite transaction of the dilation operator with a capability of shrinking the pixels. That operation is convenient for removing the image components, noise and very thin scratches [42]. In Figure 2.4 these operations are exemplified.

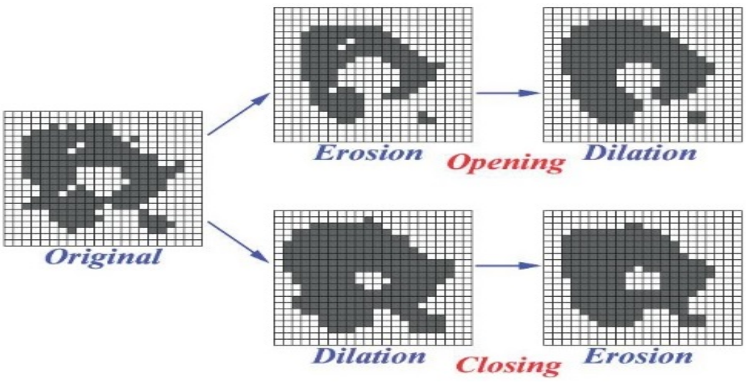


Source: Courtesy of Russ [71], page 472

Figure 2.4: Combining erosion and dilation to produce an opening or a closing

*Opening* and *closing* is a combination of dilation and erosion operations. When the erosion operation follows the dilation operation, it is called *opening* operation; on

the other hand, when the dilation operation comes before the erosion operation it is named as *closing*, a process is closing breaks in objects. These transactions can be applied on the images with multi-iterations.
In Figure 2.5 opening and closing operations are applied several times for segmentation.

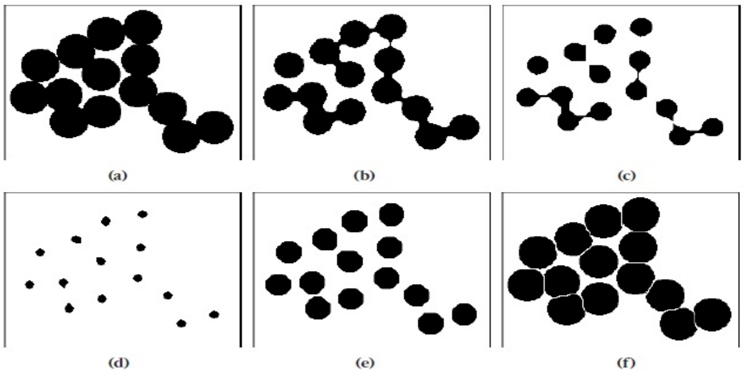


Source: Courtesy of Russ [71], page 472

Figure 2.5: Separation of touching features by erosion/dilation

## 2.2 What is Image Inpainting?

Human perception simply interprets the 3-D structure of the world. When people look around, they can recognize people, buildings and other objects owing to having an innate capability of sense. There is no doubt that people can distinguish objects of Figure 2.6 even if the image includes occluded parts. Human perception can complete the vision of chairs; for instance, in spite of the fences [81].

Source: Photographed by the author

Figure 2.6: A house from Tecklenburg, Germany

Inpainting originates from art restorers who manually revert the cracked parts of oil painting. They paint from outside of the corrupted areas to inside thanks to using the same color/structures of surrounding areas. Definitely this process can be occurred by the talented artists in order to keep the originality of the valuable paintings. A talented restorer Leo Tsai restorated the oil painting named as "the Flowers", painted by Italian famous artist Paolo Porpora. His work is represented in Figure 2.7 as a manual form of inpainting. This process is also called restoration, conservation or retouching.

Source: BBC News, The costliest art mishaps. [87]

Figure 2.7: Sample of inpainting

In Section 2.1, the image representation was mentioned. With the same image, *Lena*, representation of image inpainting is given visually in Figure 2.8.


(a) Inpainted Image displayed as a visual intensity array

| | | | | | | | | | | | |
|---|---|---|---|---|---|---|---|---|---|---|---|
| 39 | 39 | 39 | 39 | 39 | 39 | 39 | 39 | 39 | 39 | 39 | 39 |
| 39 | 101 | 112 | 109 | 107 | 111 | 0 | 0 | 0 | 99 | 144 | 39 |
| 39 | 90 | 86 | 88 | 71 | 68 | 0 | 0 | 48 | 61 | 80 | 39 |
| 39 | 66 | 54 | 57 | 54 | 52 | 0 | 0 | 50 | 51 | 50 | 39 |
| 39 | 51 | 51 | 52 | 53 | 48 | 0 | 0 | 47 | 61 | 90 | 39 |
| 39 | 48 | 50 | 50 | 49 | 48 | 0 | 0 | 60 | 98 | 163 | 39 |
| 39 | 55 | 77 | 60 | 61 | 59 | 0 | 0 | 77 | 85 | 183 | 39 |
| 39 | 66 | 102 | 80 | 73 | 0 | 0 | 0 | 85 | 67 | 181 | 39 |
| 39 | 71 | 104 | 0 | 0 | 0 | 85 | 79 | 63 | 121 | 205 | 39 |
| 39 | 0 | 0 | 0 | 0 | 0 | 63 | 73 | 117 | 187 | 207 | 39 |
| 39 | 0 | 0 | 0 | 0 | 126 | 117 | 138 | 179 | 198 | 202 | 39 |
| 39 | 39 | 39 | 39 | 39 | 39 | 39 | 39 | 39 | 39 | 39 | 39 |

(b) Image shown as a 2-D numerical array

Source: Created by the author

Figure 2.8: Image Inpainting Representation

In this example, image is masked via randomly black lines, and then *Lena* is divided into subregions, and eye part is taken. Corresponding grayscale values of the corrupted image is given in juxtaposition. As mentioned before black is coded with zero in the image processing area. Fundamental aim of image inpainting algorithms is predicting the corrupted parts of the image. Black areas will be predicted from the nonzero informations which surround the zero values. The mathematical aspect of image inpainting algorithm can be expressed as follows:

$$\mathbf{I} = \begin{bmatrix} \Omega \subset R_e^n \to R_e^m \\ \mathbf{X} \to \mathbf{I(X)} \end{bmatrix}, \tag{2.2}$$

in which **X** is the image matrix with x and y coordinates in gray scale space. Here, n=2 and m=3 represent 2-D and 3-D, respectively. $\Omega$ is the missing region.
In Figure 2.9, corrupted part, the target of inpainting algorithm is represented by $U_I(\Omega)$. Region $S_I$ is the subset of the original Image $I_0$, and known part of the image. $\partial\Omega$ is the boundary of the corrupted part [3].

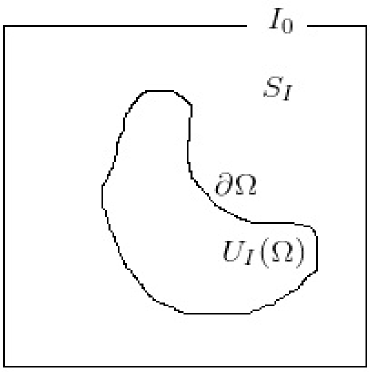


Source: Recreated by the author, inspired by [3]

Figure 2.9: Mathematical Image Inpainting Representation

During the data transmission and coding processes some image structures and/or blocks have damaged or lost in the field of the telecommunication. Necessity is the mother of invention, and image inpainting algorithms appeared at the beginning of 2000s. While a variety of definitions of the term "image inpainting" have been suggested, this term will emerged firstly as error concealment [3]. Later, this process also called disocclusion, error concealment, image completion, image filling-in, image denoising, image deblurring, image decomposition, image synthesis and image inpainting [3, 75].

## 2.3 Application Areas of Inpainting

Today image and video inpainting has taken on important role in the field of the image processing with various applications. These applications could be subdivided as follows: image restoration, text or object removal and disocclusion [3].

### Image Restoration

Image restoration algorithms work on image degradation. Some of the causes of image degradation are looked more closely in Chapter 1. Degradations can be defined as follows: Scratches, cracks, blur and dust spots on printed old photographs and red eye corrections. Furthermore, image restoration techniques are used for automatic finger-print identification systems [3, 13].

### Text or Object Removal

Another inpainting workplace is removing the unwanted contents such as people, text, logo or watermarks. After removing foreground objects, there is a large target to inpaint [3]. Moreover, adding special effects in images or videos belong to this group. Figure 2.10, illustrates the object removing capability of image inpainting algorithm [3].

(a) Original image (b) Inpainted Image

Source: Courtesy of Criminisi et al. [16]

Figure 2.10: A sample of removing large objects from images

**Disocclusion**

Oxford Dictionary defines disocclusion as [3]: "The exposure of something to view or reappearance of something hidden from view (as a result of a change in the observer's perspective, removal of an obstruction in the line of sight, and the like, or as a phenomenon in various types of image production); an instance of this." In Chapter 2, Figure 2.6 is given to illustrate application area of disocclusion.

# CHAPTER 3

# LITERATURE REVIEW

> "The modification of images in a way that is non-detectable for an observer who does not know the original image is a practice as old as artistic creation itself. Medieval artwork started to be restored as early as the Renaissance, the motives being often as much to bring medieval pictures “up to date” as to fill in any gaps [26, 92]. This practice is called retouching or inpainting. The object of inpainting is to reconstitute the missing or damaged portions of the work, in order to make it more legible and to restore its unity [26]"
> — Bertalmio, Sapiro, Caselles and Ballester [5]

## 3.1 Review on Inpainting Approaches

Image inpainting algorithms consist of two groups: Blind inpainting and non-blind inpainting. In blind inpainting algorithm, we must find the corrupted parts, whereas in non-blind inpainting missing parts are given to the algorithm [101]. Results of the literature review is given below.

### 3.1.1 Partial Differential Equation (PDE) Based Inpainting

Digital image inpainting, date backs to 2000. Bertalmio et al. [5] improved a novel algorithm which allows the users to select the corrupted parts. After the selection, these parts are filled with isophote lines; in other words, linear equal gray value belonged the edges of surrounding area. This technique also known as "diffusion based method", and the first application in image processing area is named as "image in-

painting". The remarkable point of this method is that it is fast, especially on small missing parts. Then, Bertalmio et al. [6] continued to their research inspired by computational fluid dynamics (CFD) yielding Navier Strokes Equations to diffuse the isophote lines into the corrupted parts to fill [6]. Subsequently, Chan and Shen [12] proposed Total Variational (TV) and Curvature Driven Diffusion (CDD) inpainting algorithm. TV algorithm makes use of the second order PDE and the Euler-Lagrange model [3]. Then, aim of the CDD algorithm is eliminating the previous algorithm's drawbacks on the capability of large areas by taking into account the geometric information of the isophotes [3, 14].
In 2004, Telea [85] published a paper in which the writer described the Fast Marching Method (FMM). The method fills the missing parts as a weighted average of the surrounding area [3, 85].
According to these researches, the PDE method is good at inpainting the small areas. However, algorithm may produce unsatisfactory results during inpainting to large areas. Also, algorithm takes a long time for large areas. Mechanism of PDE is given in Figure 3.1.

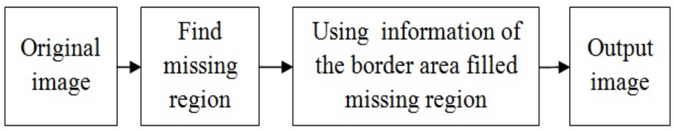


Source: Courtesy of Thanki [86]

Figure 3.1: Block Diagram of PDE Based Inpainting

### 3.1.2 Texture Synthesis Based Inpainting

Texture synthesis based inpainting, which is indicated in Figure 3.2, is reproducing the textures from the known points. Performances of PDE based image inpainting algorithms are high on the small corruptions; but they are low on regular patterns and/or textured locations. Banday and Sharma [3] list two reasons why the PDE based methods are failed on texture synthesis based inpainting. These are: 1- Textures have high intensity gradients, and this structure can be interpreted as edges and corrupted part even if they are belonging the original image. 2- Boundary condition can not recognize among the structures, textured areas or regular patterns of trivial amount of information [3]. Texture synthesis algorithms have the capability of synthesizing

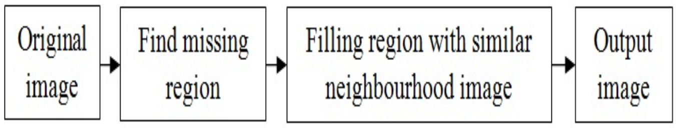


Source: Courtesy of Thanki [86]

Figure 3.2: Block Diagram of Texture Synthesis Based Inpainting

similar neighborhoods of the inpainted area. The first application of texture synthesis algorithms are employed by sampling, and then copying pixels which belong to the surrounding neighborhood. Procedure of copying pixel by pixel was a time consuming method; therefore Efros and Freeman [25] proposed a faster algorithm employed by the fragment based algorithm. These kind of algorithms copy entire blocks. Criminisi et al. [17] improved the previous presented algorithm by Efros and Freeman [25] in terms of assigning inpainting priority to edges according to a proximity measure. Later, researchers demonstrated that inpainting is possible via generating texture in differing brightness conditions. These process is called "multiresolution texture synthesis" approach. Fang et al. [29] continued this approach, and add value in terms of yielding Vector Quantization (VQ) and Principal Component Analysis (PCA) based methods. The term "multiresolution texture synthesis" has come to be used to refer to the fast multiresolution texture synthesis. To sum up, texture synthesis techniques may be divided into two main sub-groups: parametric and non-parametric. Statistical techniques are categorized under parametric whereas both pixel and patch based techniques are belonging to the group of non-parametric. Parametric techniques have capability of inpainting irregular and/or stochastic textures [86]. The main differences between the pixel and patch based is filling the corrupted parts pixel by pixel and patch by patch, respectively. This process is illustrated below.

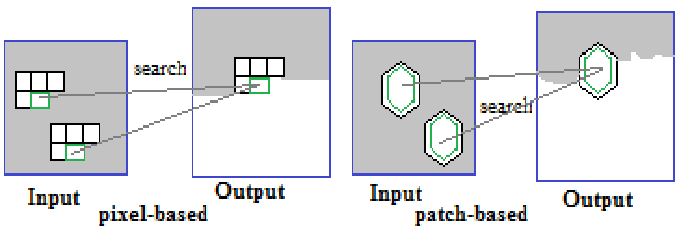


Source: Courtesy of Banday and Sharma [3]

Figure 3.3: Representation of Texture Synthesis Based Inpainting

### 3.1.3 Exemplar Based Inpainting

Images may involve both structures and textures, and existed techniques have obstacles to inpaint those joint images such as natural images. This technique is generated by inspiring PDE and texture synthesis method. The algorithm utilizes applying texture synthesis approach under the light of isophote driven principle. Mechanism of the approach is given in Figure 3.4. There are two steps: The first step is determining the priority assignment, and the second step is synthesizing the patches in accordance with iteratively searching similarity between the patches of the original image. In recent years, researchers have investigated a variety of approaches to exemplar based inpainting. During their approaches segmenting images into regions, inpainting using fragment based method, hybrid algorithm which is using both the diffusion based and texture synthesis, choosing the best matching patch via Sum of Squared Differences (SSD) criterion and using local optimization criteria [16, 17, 86, 105].


Source: Courtesy of Thanki [86]

Figure 3.4: Block Diagram of Exemplar Based Inpainting

### 3.1.4 Hybrid Based Inpainting

Hybrid inpainting is a kind of mixture approach such as exemplar based method. The aim is preserving texture and structure details of the objective image. This method works decomposing the image into texture and structure regions, and represented in Figure 3.5.

A considerable amount of study has been published on hybrid inpainting. These studies make use of the TV method to separate the texture and the structure parts, removing occlusion problem via splinting the image into mode functions, using sparse representation and layers called Morphological Component Analysis (MCA) [100, 105].

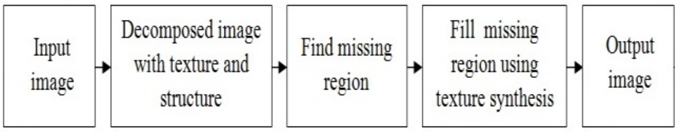


Source: Courtesy of Thanki [86]

(a) Block Diagram of Hybrid Based Inpainting

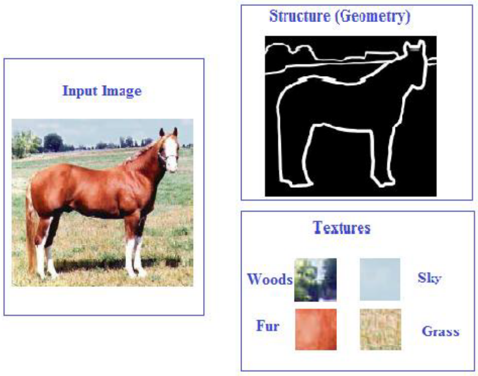


Source: Courtesy of Banday and Sharma [3]

(b) Sample of Hybrid Based Inpainting

Figure 3.5: Representation of Hybrid Based Inpainting

### 3.1.5 Fast and Convolution Based Inpainting

Nevertheless, all the previously mentioned methods are time consuming. In order to reduce the duration of inpainting process researchers provide fast algorithms. These researches include the followings: modifying PDE techniques in terms of computing smoothness and using the weighted average kernel iteratively [62, 85]. This approach is summarized in Figure 3.6.

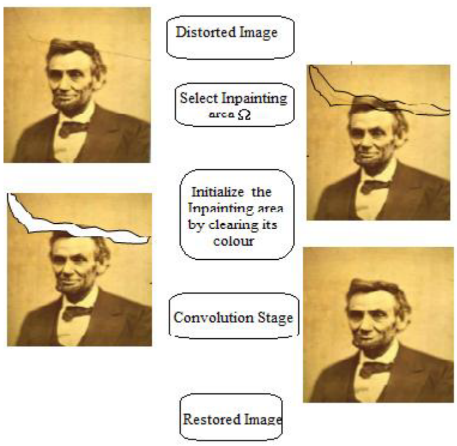


Source: Courtesy of Banday and Sharma [3]

Figure 3.6: Representation of Fast and Convolution Based Image Inpainting

### 3.1.6 Interpolation Based Inpainting

Nearest neighbor, bilinear, bicubic, b-splines, discrete wavelet transform (DWT) and Kriging are members of the image inpainting family as a subset of interpolation techniques. Fundamentally, those algorithms are solved by measuring the distances via defined weighted of kernel scale. Nearest neighbor is the primitive version of the interpolation technique in which each interpolated output pixel is assigned as the value of the nearest sample point in the input image. Furthermore, bilinear interpolation yields a 4-connected pixels of corrupted part whereas effect area of the bicubic interpolation is 16-connected pixels. The kernel value includes polynomials, cubic or cubic convolution expressions. B-splines solve the problems by connecting polynomials with pieces [74, 91]. Wavelet analysis is a widespread method to represent data. Set of basis functions (BFs), wavelets, are obtained via DWT from dilations and shifting the single prototype wavelet. Instead of storing the image by pixel blocks, this transformation gives an opportunity to store the image more efficiently. After decomposition process, reconstruction occurs [35, 91]. Weights for each point according to its distance from the missing value is taking into account in the Kriging algorithm.
Also, ANNs and MARS are performed on the field of image inpainting. There is a large volume of published studies describing the role of ANNs in real world applications, included image processing. Yadav et al. [102] state that emerging of ANNs date backs to 1940s. The written first book is titled as The Organization of Behavior which displayed a specific learning law for the synapses of neurons. This idea gives an opportunity for building a qualitative explanation of some experimental results from psychology. In 1951, Marvin Minsky found neuro-computer called the Snart which works great in terms of technical stand point information processing functions. At the end of 1950s, successful neuro-computer, called the Mark I perceptron, based on pattern recognition and perceptron was invented. During 1970s, publishing on adaptive signal processing, pattern recognition and biological modelling occurred.
Conferences on ANNs and journals were established at the end of 1980s, and they have became a key instrument in research, and are even rising today [102].
Jain and Seung [43] presented their ANNs algorithm in order to remove the noise of images. Xie et al. [101] made use of deep NNs to solve image noise problem. Fawzi et al. [30] proposed an algorithm to complete too large missing places. For this

aim, they employed hallucinations of pre-trained NNs. Figure 3.7 is exemplifying the ANNs structure.

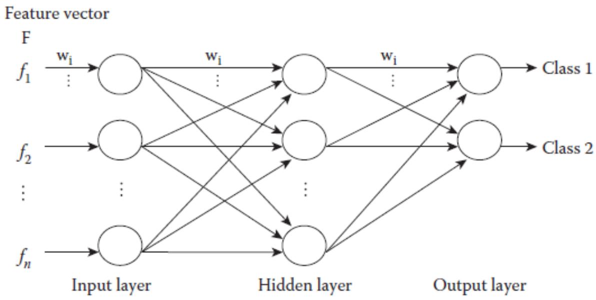


Source: Courtesy of Umbaugh [89], page 373

Figure 3.7: ANNs Representation

MARS, the method of Friedman [31], is used in the field of economy, data mining applications, and so forth. In economic models Estrella and Mishkin [76] present their probit method. Furthermore, the MARS method is used in the field of image processing. Some of the researchers are employed in facial image verification, land cover classification of satellite images, and the like [1, 66]. Nevertheless, there is no application of MARS in image inpainting area.

CMARS is a novel method relatively to MARS approach, and to the best of authors' knowledge, this is the first study to undertake the analysis of image processing. In different research areas CMARS produces better results compared to the MARS approach. We came up with contributions to gain better images.

In Chapter 4, PDE, ANNs, Kriging MARS and CMARS methods which are used in this research, are described in detail.

## 3.2 Review on Images and Masks

Researchers apply their algorithms to some test images in order to evaluate performances of the algorithms. In addition to literature review on image inpainting approaches, literature is elaborated as to images and masks. Results of the literature review on images and masks is given below.

### 3.2.1 Images

Yuan and Ghanem [104] introduced their TV based image inpainting method in the Conference on Computer Vision and Pattern Recognition (annual meeting since 1985). They preferred standard test images: walk bridge, pepper, mandrill, Lena, jet plane, cameraman, boat, pirate and house.

Some popular natural test images of the image processing area, Lena, Barbara, boat and pepper, were used for their novel deep neural algorithm on superimposed text removing problem [101].

He and Sun [45] presented their research in the European Conference on Computer vision in 2012 (semi-annual meeting since 1992). The research is about removing the unwanted objects; in other words, completing the missing parts of an image. For the purpose of proving the capability of the method three common situations of unwanted objects were included: linear structures, regular/random textures and repeated objects which are convenient schemes .

Some test images are chosen according to capability of the algorithms. Bertalmio et al. [7] proposed that their algorithm was qualified enough to fill the missing parts as their belonged features: texture or structure. In order to present their simultaneous structure and texture image inpainting algorithm, mixture of structure and texture images were employed.

The algorithm of Gandhi et al. [33] is capable of patch based image restoration in case of Gaussian, speckle, poisson and salt and pepper noise types. Their investigation's remarkable point is applying the algorithm which outperforms state-of-the art restoration methods to different fields of image processing. Image processing has a wide range of usage fields some of which are: medical, natural, aviation, geographical information systems and astronomy. To present their method's capability medical, natural and aviation fields are preferred. Chosen images for the medical field are bone and brain; for the natural field are baboon and house, and lastly for the aviation field are planet and chemical plant.

Lena is one of the most popular test image in image processing field. In the literature, the researchers indicate Lena image's preferability by different point of views. Lena has been a popular test image in the image processing area since July of 1973. At that time, researchers from University of Southern California (USC) wanted to employ a different face image instead of usual test images for their image processing research which is supported by Advanced Research Projects Agency Network (ARPANET) the pioneer of the world wide web (WWW) [39]. At that time, they wanted to use a human face. Then, they scan the Lena's image by Muirhead wirephoto scanner; thus, they converted analog image to digital image. During converting process, there is a slight and surprising image inpainting attempt. After converting the image, converter's error noticed by one of the researcher. The top line of the image was absent. Instead of rescanning the image, researchers preferred to replicate the top line to absent line because of lack of time [39]. Lena image has also remarkable features such as having shading, details and being mix of texture [84]. Lena includes different areas: light and dark, fuzzy and sharp [39]. Her face is symmetric and the image includes fine details: hair, scarf, fingers and hat. In image processing, zero values represent black pixels of the image. When image matrix includes few zeros that situation indicates that image is more convenient for the four arithmetical operations. Multiplying zero values with a constant, and obtaining again the zero limits the researchers [99]. Lena image includes all the gray values and after multiplying corresponding value of the pixels would be obtained. This feature demonstrates prefability of Lena. In addition to image properties mentioned above, the image processing area under men majority and using an attractive woman image was remarkable [57]. Lena test image had another role in the world. Those researchers used the image without permission. Her situation pointed out the copyright infringement issue. In 1991, they got agreement to using the image for research and education [39].
According to literature review, images are preferred by the researchers for five main reasons:

1 Popularity

2 Methods and image conformity

3 Different fields of image processing

4 Face image

5 Including more details

Those images are divided into five groups in terms of fields and given in Table 3.1:

Table3.1: Grouped Images

| | |
|---|---|
| Portrait | Einstein, Lena, woman dark hair |
| Human,<br>animal/plants | Barbara,<br>Cameraman, living room, Mandril, peppers, pirate |
| Outdoor/<br>Architecture and structure | Boat,<br>lake gray, walk bridge, house |
| Aviation | Chemical plant, jet plane |
| Medical | Mri, bone |

**Image Histogram and its Interpretation**

Image histogram, which is the graphical representation of light, dark and mid-tones is an exposure meter widely used among the photographers. Every tonal value corresponds to a luminosity value [46]. Histograms can be obtained simultaneously taking the photograph process with up to date cameras. Another histogram gaining option is using image processing programs. In this research, the images are transformed to grayscale image, and their histograms are created via MATLAB ®.
In the field of image processing, interpreting the image histogram is a good guide not only to determine whether the images are over-exposed, under-exposed or well-exposed but also to obtain information about luminosity interval of scene [38].
The vertical axis of histogram demonstrates the scale of luminosity from black (zero) to white (255) tones. The horizontal axis of histogram represents the tonal values as shown in Figure 3.8.

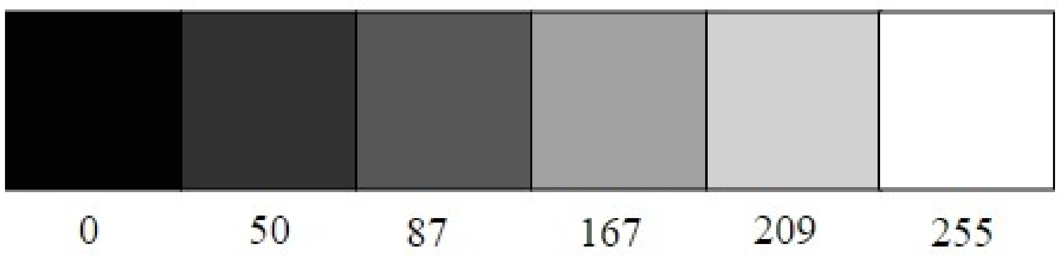


Source: Courtesy of Shiffman, D. [77]

Figure 3.8: Shade of gray ranging from black to white

Right-skewed image histogram indicates that image consists of dark areas while left-skewed image histogram shows overly light areas [46]. Having skewed shape does not determine whether image is over-/under-exposed. The important thing is interpreting the histogram corresponding to the scene type. If the photograph includes base on bright areas, expectation is getting left-skewed image histogram. On the other hand, if dark areas have been shot, expectation is obtaining right-skewed image histogram. Unless expectation is met, photograph could be interpreted as over-/under-exposed.

### 3.2.2 Masks

In the literature, the general aim is removing the text and scratches. To represent these cases, researchers are preferred arbitrary masks.

Firas [44] states that kriging interpolation technique is a favorable candidate for image reconstruction. In that research, four types of masks are employed: thin scratch, thick scratch, low text and heavy text. Those masks are implemented to test images to demonstrate the performance of proposed novel algorithm.

Commonly, researchers determine text content arbitrary. Size of 18 to 36 pixels text content in form of italic, bold and normal types are employed by Xie et al. to assess the performance of the method [101].

Similarly, Chang and Chongxiu [15] assign arbitrary scratches and texts on the images. In the article, width of pixels (7-12 pixels) and number of recovered pixels are declared. For the text image inpainting case, 48pt font size is preferred.

# CHAPTER 4

# METHODS

In this chapter, methods and quality metrics which are used throughout the thesis are described. As mentioned before, these methods and quality metrics are as follows: PDEs, Kriging, ANNs, MARS and CMARS; Mean Squared Error (MSE), Peak Signal-to-Noise Ratio (PSNR) and Structural Similarity Index (SSMI). Besides, RANOVA, which is used to compare the methods' performances statistically is described.

## 4.1 Computational Inpainting Methods

### 4.1.1 Partial Differential Equations

In this thesis, the Mumford-Shah image model is employed for solving the minimization problem via the Ambrosio-Tortorelli (AT) approximation.

#### Mumford-Shah Image Model

The work of Mumford and Shah is one of the biggest improvements in the field of image segmentation and denoising [56]. Their model is acknowledged thanks to including decomposing an image into piecewise smooth parts in the image inpainting area.

The general idea behind the Mumford and Shah's image model is minimizing an energy function. This function consists of the summation of the three parts: smoothing, data fidelity and punishing part. Smoothing part provides piecewise smooth approximation of original image to stay smooth within each region. Measurement of the least squares distance to the given image is possible with data fidelity part. The last part measures the length of the edges. This function is given as follows [107]:

$$E_{MS}(u, \mathbf{C}) = \alpha \int\limits_{\mathbf{\Omega}-\mathbf{C}} |\nabla u|^2 \, \partial x + \beta \int\limits_{\mathbf{\Omega}} (u - \mathbf{I})^2 \partial x + \mu \int\limits_{\mathbf{C}} \partial s, \tag{4.1}$$

in which $\mathbf{I}$ is the original image and belongs to the image domain $\mathbf{\Omega}$. $\mathbf{C}$ and $u$ represent the set of edge curves and a piecewise smooth approximation of the original image, respectively. Other parameters $\alpha$, $\beta$ and $\mu$ are the positive constant parts of the Mumford and Shah image model.

During to numerical implementation stage of minimizing the Equation 4.1, researchers encountered the problem of non-differentiability and the discretisation of the unknown edge set. In order to overcome this problem, Ambrosio and Tortorelli proposed an approach [75].

### Ambrosio-Tortorelli Approximation

AT proposed elliptic approximation of the Mumford-Shah image model by replacing the $\int\limits_{\mathbf{C}} \partial s$ part of the given by Equation 4.1 to the $\frac{1}{2}\left(\rho|\nabla \nu|^2 + \frac{(1-\nu)^2}{\rho}\right)$.

Substituting into the Equation 4.1, Equation 4.2 is obtained [107]:

$$E_{AT}(u, \nu) = \int\limits_{\mathbf{\Omega}} \left( \alpha(\nu^2 \, |\nabla u|^2) + \beta(u - \mathbf{I})^2 + \frac{1}{2}\left(\rho|\nabla \nu|^2 + \frac{(1-\nu)^2}{\rho}\right)\right) \partial x, \tag{4.2}$$

in which $\nu$ is the smooth edge indicator function which defines the parameter $\rho$.

$$\nu(x) \approx \begin{cases} 0 & \text{if} \quad x \in \mathbf{C}, \\ 1 & \text{otherwise.} \end{cases} \tag{4.3}$$

The aim is minimizing the Equation 4.2. Initially, its gradient is determined and equated to zero. Then, $E_{AT}$ is derived at $u$ and $\nu$. After obtaining the equations, smooth function u and the edge indicator function $\nu$ become ready to use.

### 4.1.2 Kriging

In 1960s, the term kriging was emerged to express a technique of best linear unbiased estimation (BLUE) of a regionalized variable (ReV) by Matheron [78]. In those years, kriging is used in mineral resource investigation such as gold-mining in South Africa [44, 91]. The algorithm has the ability of predicting the unknown locations, this approach is used in the field of the image inpainting.

Kriging method predicts the missing pixels according to distance and the amount of variation between neighbors of the missing values. $\boldsymbol{\lambda}$ which provides a BLUE of the predicted point is determined according to point of missing value of the location [44]. The general formula of Kriging technique is defined as follows [44]:

$$\hat{\mathbf{z}}^* = \sum_{i=1}^{N} \lambda_i Z_i, \tag{4.4}$$

in which $N$ represents the total number of the observed pixels. $\hat{\mathbf{z}}^*$ and $Z_i$ are values of the predicted and observed pixels, respectively.
Aim of the Kriging algorithm is minimizing $\left(\hat{\mathbf{z}}^* - \sum_{i=1}^{N} \lambda_i Z_i\right)^2$. Moreover, $\lambda_i$ stands for the weights of observed values with the following restriction:

$$\sum_{i=1}^{N} \lambda_i = 1. \tag{4.5}$$

The important point is defining the weights. Lagrange multipliers are employed in order to obtain unbiased estimation error and minimum estimated variance [9].
Weights are defined according to the following equation [78]:

$$\sum_{i=1}^{N} \lambda_i \gamma_{ij} - \lambda_i \sigma_i^2 + \mu = \gamma_{0i} \quad \text{i=1,2,...,n.} \tag{4.6}$$

in which $\gamma_{ij}$ represents gamma values obtained from the Equation 4.7.

In this thesis, ordinary kriging is employed. Ordinary kriging is widespread type of kriging methods in terms of minimizing the variance of the prediction error [74]. It predicts a single output per input combination [4].

The variogram is a great instrument to determine the variance of the differences between two variables belong to two locations. Variogram for lag distance $h$ can be calculated as follows [74, 90]:

$$2\gamma(h) = \frac{1}{n}\sum_{i=1}^{N}[Z(x_i) - Z(x_i + h_i)]^2, \tag{4.7}$$

in which $Z(x_i)$ and $Z(x_i + h_i)$ are the intensity values correspond to the locations of $x$ and $x_i + h_i$, respectively. Kriging system is solving the following equation obtained from the minimization of $\left(\hat{\mathbf{z}}^* - \sum_{i=1}^{N} \lambda_i Z_i\right)^2$ :

$$\boldsymbol{\Gamma} * \boldsymbol{\lambda} = \mathbf{g}$$

or

$$\begin{bmatrix} \gamma_{11} & \dots & \gamma_{1N} & 1 \\ \vdots & \ddots & \vdots & \vdots \\ \gamma_{N1} & \dots & \gamma_{NN} & 1 \\ 1 & \dots & 1 & 0 \end{bmatrix} * \begin{bmatrix} \lambda_i \\ \vdots \\ \lambda_i \\ m \end{bmatrix} = \begin{bmatrix} \gamma_{10} \\ \vdots \\ \gamma_{N0} \\ 1 \end{bmatrix}, \tag{4.8}$$

in which gamma matrix is calculated from the variogram. Slope of the variogram plot is important to obtain semivariance. **g** vector is the distance matrix which measures distances between the known and unknown points. Distance matrix is measured via Euclidean distance. After obtaining inverse matrix of $\boldsymbol{\Gamma}$ following equation is using [91]:

$$\boldsymbol{\lambda} = \boldsymbol{\Gamma^{-1}} * \mathrm{g}. \tag{4.9}$$

After calculating the $\boldsymbol{\lambda}$, Equation 4.4 is employed and predictions for the unknown points are obtained.

### 4.1.3 Artificial Neural Networks

One of the important aim of the technology is reducing manpower and increasing the role of mechanics. Today, ANNs have rising popularity in the field of artificial intelligence in order to meet this aim. They imitates biological Neural Networks (NNs) of nervous system with the following assumptions [102]:

- Neurons are the places for the information processing.
- Connections between the neurons are instruments for transferring to signals.
- At the end of the information processing of neuron, each neuron reproduces only one output even if more than one information receives.
- Strength of the links between the neurons are defined with individual weights.
- Output signals are calculated by applying the threshold function also called activation function to the weighted sum of the inputs.

ANNs have variety of architectures such as: Feed forward, feed backward, radial basis function network, multilayer perceptron NN, cellular network, and so on. In this thesis, feed-forward NN is employed.

#### Feed-forward Neural Network

A feed-forward ANN includes at least one hidden layer which comprises neurons inside. Mechanism of feed-forward ANN is presented in Figure 4.1.

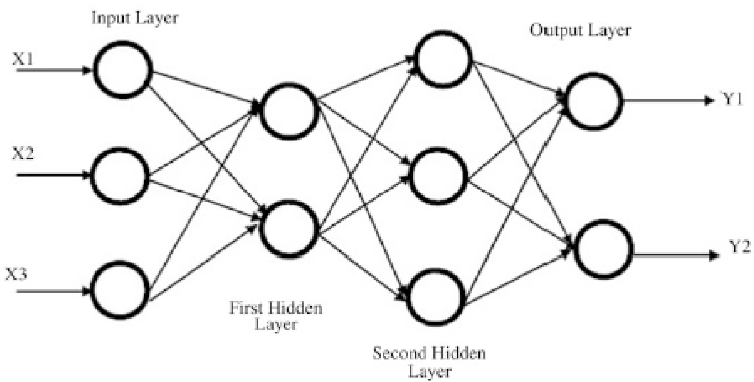


Source: Courtesy of Yadav et al. [102]

Figure 4.1: A feed-forward network structure

in which neurons and arrows are represented by the nodes and the links between the nodes, respectively.

The information has a one direction from the input nodes to hidden nodes with the forward movement. In this architecture model, there are no cycles or loops. The system centers on forwarding the processed elements to distinct layers with each layer receiving input from the previous layer and outputting to the next layer [102].

In this thesis, MATLAB ® Neural Network Toolbox is adopted for obtaining the prediction for the intensity values of the missing parts. Levenberg-Marquardt (LM) algorithm is used to train the ANN [70]. It uses the Newton algorithm and the steepest descent method. The training speed is reduced by using second order derivatives [106]. Equation 4.10, which is generated from the steepest descent and Newton algorithm, represents LM's update rule [106].

$$\Delta \mathbf{w} = (\mathbf{J}^T\mathbf{J} + \mu\mathbf{I})^{-1}\mathbf{J}^T\mathbf{e}, \tag{4.10}$$

in which $\mathbf{w}$, $\mathbf{I}$, $\mu$ are the weight vector, identity matrix, combination coefficient, respectively. $\mathbf{J}$ shows the Jacobian Matrix and $\mathbf{e}$ represents error vector, which is the difference of desired and actual output [8, 106]. $\mathbf{J}$ has $(P \times M) \times N$ dimensions in which the number of training patters are represented by $P$, $M$ is the number of outputs and $N$ is the number of weights. Dimension $(P \times M) \times 1$ belongs the error vector [8].

Algorithm decides to be acting as steepest descent or Newton according to the following criterion:

$$\mu(n) = \left\{ \begin{array}{ll} \mu(n-1)k & E(n) > E(n-1) \\ \mu(n-1)/k & E(n) \leq E(n-1) \end{array} \right\}, \tag{4.11}$$

where $k$ is a constant, whereas $E$ represents convenience value [106]. First of all, Jacobien matrix is calculated and stored. Then, Equation 4.10 is used as an instrument for weight updates in the Jacobien matrix multiplications. In many cases, owing to the storage problem Equation 4.10 is updated according to the following equation:

$$\Delta \mathbf{w} = (\mathbf{Q} + \mu\mathbf{I})^{-1}\mathbf{g}, \tag{4.12}$$

in which $\mathbf{Q}$ is the quasi-Hessian matrix and $\mathbf{g}$ is the gradient vector. Equation 4.12 has outperformed Equation 4.10 because it does not need to store the Jacobien matrix, $\mathbf{J}$ [8]. The analysis maintains until the last pattern computation is completed.

### 4.1.4 Multivariate Adaptive Regression Splines

Friedman was a famous statistician for being the first person to declare MARS in 1991. In this thesis for the MARS part, R program is used with Earth package, which gives an opportunity to get the MARS model. This package is developed by taking into account Friedman's algorithms [31,32].

MARS evolved from recursive partitioning methodology which has the following form [31]:

$$\text{if} \quad \mathbf{x} \in R_m, \quad \text{then} \quad \hat{f}(\mathbf{x}) = g_m(\mathbf{x} \mid \{a_j\}_1^p), \tag{4.13}$$

in which $\{R_m\}_1^M$ are disjoint subregions representing a partition of D. The functions of $g_m$ are common in a constant function

$$g_m(\mathbf{x} \mid a_m) = a_m. \tag{4.14}$$

The general idea behind the recursive partitioning regression is estimating both a valid set of subregions of data and each subregion's separate functions of parameters. This division progress until detecting the optimal set of subregions. The criteria are penalized both for lack-of-fit and the increasing number of regions. Recursive partitioning methodology has discontinuous structure, which affects the model accuracy. MARS solves this drawback [31]. The MARS algorithm is given in Equation 4.15.

$$\begin{aligned} \hat{f}(\mathbf{x}) &= \sum_{m=1}^{M} a_m \psi_m(\mathbf{x}), \\ \psi_m(\mathbf{x}) &= I[\mathbf{x} \in R_m]. \end{aligned} \tag{4.15}$$

in which $\psi_m$s are the BFs which are illustrated below [37]:

$$(x-t)_+ = \begin{cases} x-t, & \text{if } x > t, \\ 0, & \text{otherwise.} \end{cases} \qquad (t-x)_+ = \begin{cases} t-x, & \text{if } x < t, \\ 0, & \text{otherwise.} \end{cases} \tag{4.16}$$

Figure 4.2 provides sample truncated functions (reflected pair) with $t$=0.5 as the knot value.

Foremost MARS is a multivariate non-parametric continues regression model whose general aim is fitting the relation between a set of predictors and a dependent variables via splines called; BFs. Knot is a point of separation in the piecewise regression model. All possible knot locations, all variables and interactions are searched by the

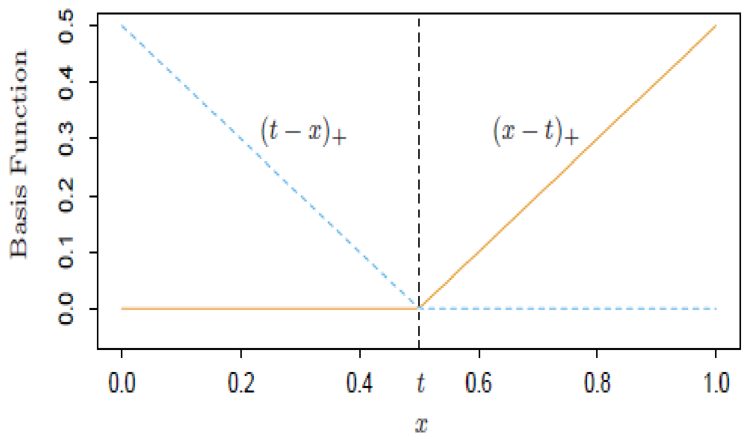


Source: Hastie et al. [37], page 322

Figure 4.2: A sample truncated functions with the knot $t$=0.5

MARS algorithm. Those interactions are obtained by the combinations of BFs. Significant quantities of BFs and knot locations are determined by the MARS algorithm, and then the least squares estimation (LSE) method is used for finding the best final model with trimmed BFs. Friedman [31] argues that there are two broad procedures in the MARS algorithm: the forward stepwise and the backward stepwise regression [31, 76]. At the beginning of the forward phase, due to including a large set of BFs, the model is over-fitting the data, and the model includes all of the possible BFs regardless of their contributions to the performance of the model. The forward stepwise algorithm iterates the splitting procedure till the reached user-determined maximum number of BFs, $M_{max}$. In order to eliminate ineffective BFs, the other phase comes into algorithm called as the backward stepwise regression.

The backward stepwise regression part eliminates some BFs in order to solve the over-fitting problem. Eliminated BFs contribute to the smallest increase in the residual squared error at every stage, and convenient model is obtained [98]. The algorithm stops, after reaching the minimum Generalized Cross-Validation (GCV) value. Friedman [31] makes us of the formula 4.17 in order to detect the optimal number of BFs among the $M_{max}$.

$$LOF(\hat{f_M}) = GCV(M) = \frac{1}{N}\frac{\sum_{i=1}^{N}[y_i - \hat{f_M}(\mathbf{x}_i)]^2}{[1-\frac{\tilde{C}(M)}{N}]^2}, \tag{4.17}$$

in which $N$ represents the number of sample observations. $\tilde{C}(M) = u + dK$, where $K$ is the number of knots obtained at the end of the forward process, $u$ represents the number of linearly independent BFs and $d$ is defined as the cost parameter to optimize BF [98].

### 4.1.5 Conic Multivariate Adaptive Regression Splines

CMARS is a modified version of MARS approach in terms of yielding Tikhonov regularization (TR) and conic quadratic programming (CQP). CMARS is developed from the MARS approach by modifying its backward stage algorithm. As called the method of new approach CMARS, the letter "C" corresponds to conic, convex and continuous [98]. In the literature, researchers are employed the MOSEK™ Optimizastion Toolbox, which is compatible with MATLAB®, C, Java, .NET, R and Python in order to solve CQP problem [55].

In the forward stage of MARS all the BFs are obtained, and Penalized Residual Sum of Squares (PRSS) is minimized in CMARS. After that process, TR also known as ridge regression is solved in the backward stage of CMARS. Then, CQP is used to solve the optimization problem.

#### Tikhonov Regularization

Linear Regression Model (LRM) can be expressed in matrix format:

$$\mathbf{y} = \mathbf{X}\boldsymbol{\beta} + \boldsymbol{\epsilon}. \tag{4.18}$$

Aim of the method of LSE is minimizing the residual sum of squares (RSS). In matrix notation, RSS can be written by the following equation:

$$RSS(\boldsymbol{\beta}) = (\mathbf{y} - \mathbf{X}\boldsymbol{\beta})^T(\mathbf{y} - \mathbf{X}\boldsymbol{\beta}) = \|\mathbf{y} - \mathbf{X}\boldsymbol{\beta}\|_2^2 . \tag{4.19}$$

in which $\boldsymbol{\beta}$ represents $(p + 1) \times 1$ regression coefficients vector. In many cases, the norm of first-order or second-order derivative of $\boldsymbol{\beta}$ is preferred as minimizing target.

Jacques-Salomon Hadamard defined three criteria which are called Hadamard criteria in 1923 [31]. According to these criteria, a problem should meet the following requirements to be defined as well-posed: having a solution, having a unique solution and having a continuous solution. In the field of medicine, physics and economics plenty of problems can not meet the Hadamard's well-posed criteria, and named as ill-posed [40]. TR is an instrument for converting ill-posed problems to well-posed.

If in Equation 4.19, $\mathbf{X}^T\mathbf{X}$ is singular, the singular value decomposition (SVD) method is suitable to solve the minimization problem. Furthermore, a SVD of the coefficient matrix $\mathbf{X}$ and Equation 4.18 can be employed in order to express the Tikhonov solution. Complexity of the possible solution exemplifies the norm of $\boldsymbol{\beta}$ as $\|\boldsymbol{\beta}\|_2$. Difference quotients of $\boldsymbol{\beta}$ are comprised of products $\mathbf{L}\boldsymbol{\beta}$, $\boldsymbol{\beta}$ with a matrix $\mathbf{L}$, which represents the discrete differential operators of the first-order whereas $\boldsymbol{\beta}$ represents the second-order. Weber et al. [98] aimed to optimize Equation 4.19 via TR problem and CQP.
The PRSS equation with $M_{max}$ BFs can be expressed in Equation 4.20 as a CQP:

$$PRSS := \sum_{i=1}^{N}(y_i - f(\tilde{\mathbf{x}}_i))^2 + \sum_{m=1}^{M_{max}} \lambda_m \sum_{\substack{|\boldsymbol{\alpha}|=1 \\ \boldsymbol{\alpha}=(\alpha_1:\alpha_2)^T}}^{2} \sum_{\substack{r<s \\ r,s\epsilon V_m}} \int \theta_m^2 \left[D_{r,s}^{\boldsymbol{\alpha}}\psi_m(\mathbf{t}^m)\right]^2 \partial\mathbf{t}^m. \tag{4.20}$$

A short version of the approximate formula can be rearranged as

$$PRSS \approx \left\|\mathbf{y} - \boldsymbol{\psi}(\tilde{\mathbf{d}})\boldsymbol{\theta}\right\|_2^2 + \sum_{m=1}^{M_{max}} \lambda_m \sum_{i=1}^{(N+1)^{K_m}} L_{im}^2\theta_m^2.$$

$$= \left\|\mathbf{y} - \boldsymbol{\psi}(\tilde{\mathbf{d}})\boldsymbol{\theta}\right\|_2^2 + \sum_{m=1}^{M_{max}} \lambda_m \left\|\mathbf{L}_m\theta_m\right\|_2^2. \tag{4.21}$$

in which $\mathbf{L}_{im} := (L_{1m}, L_{2m}, ..., L_{(N+1)^{K_m},m})^T$ $(m = 1, 2, ..., M_{max})$. After taking the same $\lambda$ for each derivative form, Equation 4.21 is omitted a finite number of tradeoff or penalty parameters $\boldsymbol{\lambda} = (\lambda_1, \lambda_2, ..., \lambda_{M_{max}})^T$. It states a suitable form of TR problem with singleton PRSS:

$$PRSS \approx \left\|\mathbf{y} - \boldsymbol{\psi}(\tilde{\mathbf{d}})\boldsymbol{\theta}\right\|_2^2 + \lambda \left\|\mathbf{L}\boldsymbol{\theta}\right\|_2^2. \tag{4.22}$$

$$\mathbf{L}_{im} := \left[ \left( \sum_{\substack{|\boldsymbol{\alpha}|=1 \\ \boldsymbol{\alpha}=(\alpha_1,\alpha_2)^T}}^{2} \sum_{\substack{r<s \\ r,s\epsilon V_m}} [D^{\boldsymbol{\alpha}}_{r,s}\psi_m(\hat{\mathbf{x}}^m_i)]^2 \right) \Delta\hat{\mathbf{x}}^m_i \right]^{\frac{1}{2}}, \tag{4.23}$$

in which with $(M_{max}+1)\times(M_{max}+1)$ dimensions diagonal matrix **L** is as follows:

$$\mathbf{L} = \begin{bmatrix} 0 & 0 & \cdots & 0 \\ 0 & 0 & \cdots & 0 \\ \vdots & \vdots & \ddots & 0 \\ 0 & 0 & \cdots & L_{M_{max}} \end{bmatrix}. \tag{4.24}$$

Equation 4.22 includes two objective functions: $\left\|\mathbf{y} - \boldsymbol{\psi}(\tilde{\mathbf{d}})\boldsymbol{\theta}\right\|_2^2$ and $\|\mathbf{L}\boldsymbol{\theta}\|_2^2$. TR approach leads to obtaining some challenging combinations of weighted linear sums of objectives. This multi-objective optimization problem is solved by the CQP [98,103];

$$\min \|\mathbf{y} - \mathbf{X}\boldsymbol{\beta}\|_2^2 + \varphi^2 \|\mathbf{L}\boldsymbol{\theta}\|_2^2, \tag{4.25}$$

in which **L= I** (unit matrix).

### Solving Conic Quadratic Programming Problem

The backward stage of the CMARS is solved via the MOSEK™ toolbox of the MATLAB software. An explicit definition of CQP can be written as [83]:

$$\min_{\mathbf{x}} \quad \mathbf{c}^T\mathbf{x}, \quad \text{subject to} \quad \|\mathbf{D}_i\mathbf{x} - \mathbf{d}_i\| \leq \mathbf{p}_i^T\mathbf{x} - \mathbf{q}_i \quad (i = 1, 2, \ldots, k). \tag{4.26}$$

Equation 4.22, TR problem, can be arranged as given in Equation 4.26, which is suitable form of CQP with the following optimization problem:

$$\begin{aligned} &\min_{\boldsymbol{\theta}} \quad \left\|\boldsymbol{\psi}(\tilde{\mathbf{d}})\boldsymbol{\theta} - \mathbf{y}\right\|_2^2 \\ &\text{subject to} \quad \|\mathbf{L}\boldsymbol{\theta}\|_2^2 \leq \tilde{M}. \end{aligned} \tag{4.27}$$

Then, the formula is rearranged as follows:

$$\min_{t,\boldsymbol{\theta}} \quad t,$$

$$\text{subject to} \quad \left\|\boldsymbol{\psi}(\tilde{\mathbf{d}})\boldsymbol{\theta} - \mathbf{y}\right\|_2 \leq t,$$

$$\|\mathbf{L}\boldsymbol{\theta}\|_2 \leq \sqrt{\tilde{M}}$$

$$t \geq 0. \tag{4.28}$$

Indeed, the optimization problem can be gathered in form of a CQP as follows:

$$\mathbf{c} = (1, \mathbf{0}^T_{M_{max}+1})^T, \quad \mathbf{x} = (t, \boldsymbol{\theta}^T)^T,$$

$$\mathbf{D}_1 = (\mathbf{0}_N, \boldsymbol{\psi}(\tilde{\mathbf{d}})), \quad \mathbf{d}_1 = \mathbf{y}, \quad \mathbf{p}_1 = (1, 0, \ldots, 0)^T, \quad \mathbf{q}_1 = 0,$$

$$\mathbf{D}_2 = (\mathbf{0}_{M_{max}+1}, \mathbf{L}), \quad \mathbf{d}_2 = \mathbf{0}_{M_{max}+1}, \quad \mathbf{p}_2 = \mathbf{0}_{M_{max}+2} \quad \text{and} \quad \mathbf{q}_2 = -\sqrt{\tilde{M}}. \tag{4.29}$$

Equation 4.28 is reformulated by Weber et al. [98] divided by the dual problem and the primal dual optimal solution for the problem. There is a relation between the $\lambda$ and the parametrical upper bound $\tilde{M}$ in a constraint of the CQP. The penalty parameter of PRSS:$\lambda$ is calculated by TR. The solution of the optimization problem, Equation 4.22, needs an efficiency curve which is created by plotting of the solutions. In TR, logarithmic scales are instrument to obtain an efficiency boundary point. This logarithmic scales which are obtained for different $\tilde{M}$ values for the problem of CQP create an efficiency curve because of its shape called L-curve. This coordinate scheme includes logarithmic norm of $\mathbf{L}\boldsymbol{\theta}$ (x-axis) and $\sqrt{RSS}$ (y-axis). The closest point to the origin and the corresponding penalty parameter is often the optimum solution regarded as minimizing both complexity and maximizing goodness-of-fit [98]. In order to illustrate this process, the work of Weber et al. is given in Figure 4.3.

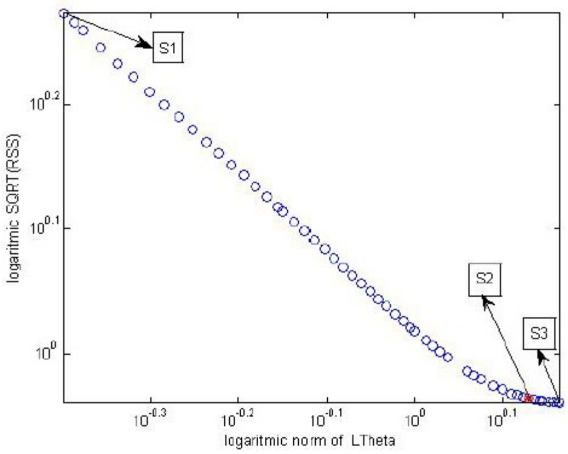


Source: Courtesy of Weber et al. [98]

Figure 4.3: Example of log-log scale curve for various different $\tilde{M}$ values

## 4.2 Quality Metrics

The more image processing application increases, the more image quality metrics have become important in the image processing day by day. Image quality metrics are good guides to compare the performances of the algorithms.
Siv Lindberg [50] states that color gamut, sharpness, contrast, tone quality, detail highlights and shadows, gloss levels and variation, color shift, patchiness, mottle and ordered noise are the most important representative image quality attributes.
Pedersen et al. [65] choose six proposed image quality attributes: sharpness, color, lightness, artifacts, contrast and physical. These quality attributes which keep dimensionality to a minimum are a subset of the literature review results on the image quality attributes. They compare 17 image quality metrics involved SSMI. According to their research, SSMI has a good performance on sharpness and lightness quality attributes. Figure 4.4 demonstrates image quality attributes with subfeatures.

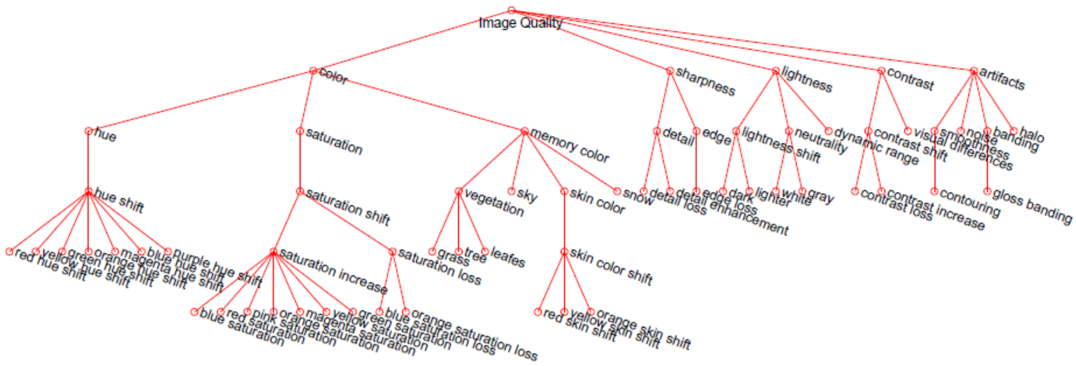


Source: Courtesy of Pedersen et al. [65]

Figure 4.4: The Quality Attributes Tree

### 4.2.1 Mean Squared Error

MSE is a commonly used measure to detect the degradation between the original and inpainted image. MSE can be calculated by the following formula:

$$MSE = \frac{1}{N \times M} \sum_{i=0}^{N-1} \sum_{j=0}^{M-1} [f(i,j) - g(i,j)]^2, \tag{4.30}$$

where $f(i,j)$ and $g(i,j)$ denote the original and inpainted image's $(i,j)$ pixel, respectively. $N$ and $M$ are the dimensions of the images. MSE can approach the zero; this indicates that a smaller MSE value provides higher image quality [53]. Equation 4.30

actually comes from the Minkowski metric which can be written as

$$\|E_p\| = \left( \sum_{i=1}^{N} |x_i - y_i|^p \right)^{\frac{1}{p}}. \tag{4.31}$$

Here, $p$=1 corresponds to the Manhattan metric whereas $p$=2 corresponds to the Euclidean metric, which matches to the MSE given in Equation 4.30 [60]. MSE has been mostly preferable image quality measure for more than half a century because of its following features:

- MSE is a parameter free value so it is simple to calculate. Moreover, it is memoryless in terms of having independency of other samples.
- "All $l_p$ norms are valid distance metrics in $(R^N)$, which satisfy the following convenient conditions, and allow for consistent, direct interpretations of the similarity:

  - non-negativity: $d_p(x, y) \geq 0$
  - identity: $d_p(x, y) = 0$ if and only if $x$=$y$
  - symmetry: $d_p(x, y)$=$d_p(y, x)$
  - triangular inequality: $d_p(x, z) \leq d_p(x, y)$+$d_p(y, z)$

  In particular, the $p$=2 case (proportional to the square root of the MSE) is the ordinary distance metric in N-dimensional Euclidean space [60]."
- Owing to calculating effortless, the gradient and the Hessian matrix of the MSE provide a great opportunity to solve the optimization problems. This advantage comes from non-negativity, identity and symmetry features.
- Lots of researchers compare their algorithms in signal processing applications: filter design, signal compression, restoration, denoising, reconstruction and classification. MSE is one of the most popular image quality metric, and has been using by the researchers. During comparison of the algorithm's performances, using the same quality metric is a convenient method in terms of time consuming and practicality.

### 4.2.2 Peak Signal-to-Noise Ratio

PSNR is the ratio between the dynamic range of pixel values and the MSE; in other words, it represents the power of corrupting noise. Logarithmic decibel scale is employed due to the fluctuation of the signal range. PSNR is given by the Equation 4.32:

$$PSNR = 10\log_{10}\frac{L^2}{MSE}. \tag{4.32}$$

It is apparent that there is an inverse relation between PSNR and MSE measures. Hence, the higher PSNR value shows the higher image quality and less error, and vice versa. PSNR is a convenient quality measure when the image has different dynamic ranges. Furthermore, as mentioned above PSNR has the similar properties with the MSE. Acceptable range of PSNR is defined as 30dB to 50dB by the image processing authorities [74].

### 4.2.3 Structural Similarity Index

In the literature plenty of researchers prefer to support their comparisons with SSMI because it has Human Visual System (HVS) interpretation. SSMI is one of the most popular image quality metric. It consists of the distortion of four image quality attributes: sharpness, lightness and contrast. Sharpness is a quality attribute which takes edges and details into account by focusing on local neighborhoods [65]. Mechanism of SSMI is given in Figure 4.5 where signal **x** belongs to the original image whereas signal **y** represents the inpainted image.

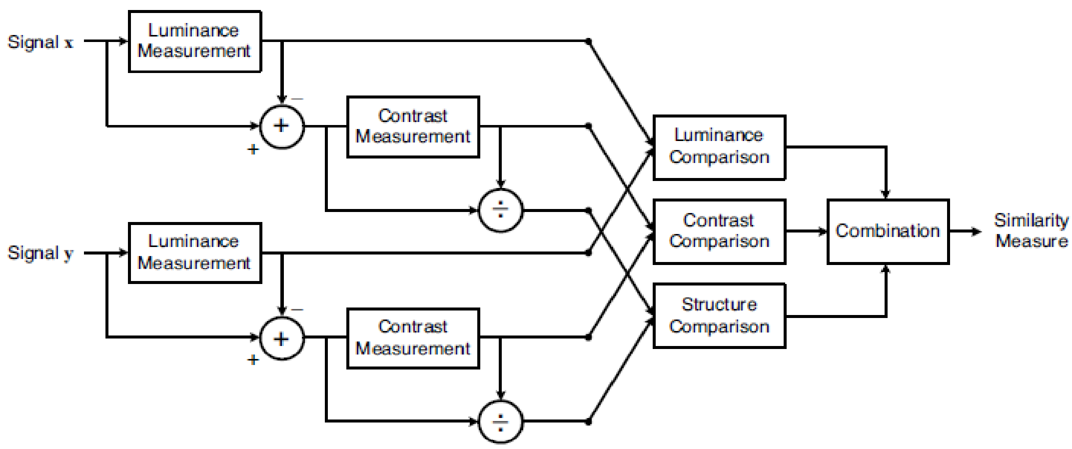


Source: Courtesy of Wang et al. [96]

Figure 4.5: Diagram of the SSMI Mechanism

The first component is luminance, and it is represented by $\ell(\mathbf{x}, \mathbf{y})$, function of $M_x$ and $M_y$, where $M_x$ is the mean intensity of original image and $M_y$ is the mean intensity of inpainted image. First of all, calculating the mean intensity of the original image as the following is necessary to complete the general formula.

$$\mu_x = \frac{1}{N} \sum_{i=1}^{N} x_i. \tag{4.33}$$

Afterwards, the mean intensity from the signal is removed.

$$\sum_{i=1}^{N} x_i = 0. \tag{4.34}$$

An unbiased estimator for the signal contrast is given by

$$\sigma_x = \left( \frac{1}{N-1} \sum_{i=1}^{N} (x_i - \mu_x)^2 \right)^{\frac{1}{2}}. \tag{4.35}$$

Furthermore, normalized signals are preferred to obtain for more exact results. $\frac{(\mathbf{x}-\mu_x)}{\sigma_x}$ and $\frac{(\mathbf{y}-\mu_y)}{\sigma_y}$ are in the normalized signal form. Hence, the crucial note is that there is a relatively independence between the components. For instance, redoubling the contrast and/or luminance will not change the structures of the images. Hence, calculation of SSMI is possible with obtaining the following components' values: luminous $\ell(\mathbf{x}, \mathbf{y})$, contrast $c(\mathbf{x}, \mathbf{y})$ and $s(\mathbf{x}, \mathbf{y})$ as

$$S(\mathbf{x}, \mathbf{y}) = f(\ell(\mathbf{x}, \mathbf{y}), c(\mathbf{x}, \mathbf{y}), s(\mathbf{x}, \mathbf{y})). \tag{4.36}$$

In order to detect the quality of the inpainted image by comparing with the reference image, defining the components of the Equation 4.36 is necessary. $\ell(\mathbf{x}, \mathbf{y})$ is defined by the Wang et al. [96] as follows:

$$\ell(\mathbf{x}, \mathbf{y}) = \frac{2\mu_x\mu_y + C_1}{\mu_x^2 + \mu_y^2 + C_1}, \tag{4.37}$$

where the constant $C_1 = (K_1 L)^2$ includes dynamic range of pixel values and a small nonzero constant. In MATLAB ® program, $K_1$ and $K_2$ are defined 0.01 and 0.03 as default, respectively [80]. $L = 2^b - 1$, where $b$ represents the bits per pixel. In this thesis, 8-bit grayscale images are elaborated thus 255 is a valid value for $L$.

The HVS has natural capability to interpret luminance. Equation 4.34 has a stability with Weber's Law, which has been using in statistics, and also in some social studies such as psychology. In general, Weber's Law has an opportunity to percept differences between two things. In this content, the contrast of original and inpainted image is noticed by using the Weber's Law. First of all, Weber's Law is a subset of discrimination threshold experiments;

$$\Delta l = K_w I, \tag{4.38}$$

in which $K_w$ is the Weber fraction, and $I$ is the intensity of something's initial value. Discrimination threshold is represented with $\Delta l$. Weber's Law is useful for measuring the changes. And this law generally is represented as follows:

$$\Delta l = K_w(I + I_0). \tag{4.39}$$

Here, if $I$ increases, effect of $I_0$ can be eliminated. This relation is commented as $\Delta l$ approaches to general formula above Equation 4.38. On the other hand, $I$ could be around the threshold value; thus, $\Delta l$ leads to be an element of absolute threshold. According to Weber's Law, in the situation of $C_1$'s being small enough in comparison with $\mu_x^2$, luminance will be directly dependent only on R. Inpainted image's signal $\mu_y$ can be rewriting as $\mu_y = (1 + R)\mu_x$, where R is the size of luminance change relative to the background luminance. Calculating formula of the luminance is given by Wang et al. [96]:

$$\ell(\mathbf{x}, \mathbf{y}) = \frac{2(1 + R)}{1 + (1 + R)^2 + \frac{C_1}{\mu_x^2}}. \tag{4.40}$$

Second component is the contrast, and it is represented by $c(\mathbf{x}, \mathbf{y})$. $\sigma_x$ and $\sigma_y$ are components of the function. As a second component of the SSMI, the contrast is given below.

$$c(\mathbf{x}, \mathbf{y}) = \frac{2\sigma_x\sigma_y + C_2}{\sigma_x^2 + \sigma_y^2 + C_2}, \tag{4.41}$$

where $C_2 = (K_2 L)^2$ includes a small $K_2$ constant. In order to define the last component, luminance subtraction and variance normalization are necessary. Structural part of the formula is represented as shown by the following expression:

$$s(\mathbf{x}, \mathbf{y}) = \frac{\sigma_{xy} + C_3}{\sigma_x\sigma_y + C_3}, \tag{4.42}$$

where $C_3 = C_2/2$. $\sigma_{xy}$ is given as

$$\sigma_{xy} = \frac{1}{N-1}\sum_{i=1}^{N}(x_i - \mu_x)(y_i - \mu_y). \tag{4.43}$$

The final formula is obtained as the following

$$SSMI(\mathbf{x}, \mathbf{y}) = [(\ell(\mathbf{x}, \mathbf{y})]^{\alpha}.[c(\mathbf{x}, \mathbf{y})]^{\beta}, [s(\mathbf{x}, \mathbf{y})]^{\gamma}), \tag{4.44}$$

where all exponentials are greater than zero; and $\alpha$, $\beta$ and $\gamma$ are adjusted as one in order to simplify the equation. Hence, the final SSMI is obtained as follows:

$$SSMI(\mathbf{x}, \mathbf{y}) = \frac{(2\mu_x\mu_y + C_1) + (2\sigma_{xy} + C_2)}{(\mu_x^2 + \mu_y^2 + C_1)(\sigma_x^2 + \sigma_y^2 + C_2)}. \tag{4.45}$$

There is no doubt that SSMI outperforms Wang and Bovik's previous proposal [95] on the image quality assessment: universal quality index (UQI) which is the specific version of SSMI, where $C_1$ and $C_2$ are equal to zero. That index could fail if $\mu_x^2 + \mu_y^2$ and/or $\sigma_x^2 + \sigma_y^2$ are almost zero.

## 4.3 Repeated Measures ANOVA

Analysis of variance (ANOVA) assesses the significance of one or more factors by comparing the response variable means at different factor levels. The terms of between-groups and within-groups belong to ANOVA, whereas between-subjects and within-subjects are family of RANOVA. It has a capability to investigate effects for the same subject.

RANOVA makes use of the F-statistics whose formula is as follows:

$$F = \frac{MS_{conditions}}{MS_{error}}, \tag{4.46}$$

where $MS_{conditions}$ represents the mean square (variance estimate) explained by the different subjects: $MS_{conditions}$=$\frac{SS_{conditions}}{df_{conditions}}$ whereas $MS_{error}$ shows the mean square that is due to the unexplained: $MS_{error}$=$\frac{SS_{error}}{df_{error}}$. If experiments conduct under the time, instead of using $MS_{conditions}$ using the term of $MS_{time}$ is more suitable. Furthermore, $SS_{conditions}$ is calculated by the following formula:

$$SS_{conditions} = SS_b = \sum_{i=1}^{k} n_i(\bar{x}_i - \bar{x})^2. \tag{4.47}$$

in which k is the number of conditions, $n_i$ represents number of subjects under each $(i^{th})$ condition. In addition, mean score for each $(i^{th})$ condition is represented by $\bar{x}_i$ and grand mean is represented by $\bar{x}$. In independent ANOVA design, $SS_{error} = SS_w$ in which $SS_w$ represents variability within groups. However, with RANOVA, owing to the individual differences between subjects, $SS_{subjects}$, subtracting $SS_{subjects}$ from the $SS_w$ is possible because each subject is treated as a block, and it becomes a level of a factor called subject. Hence, $SS_{error}$= $SS_w$ - $SS_{subjects}$. This feature removes the between-subjects variability and $SS_{error}$ term only shows the individual variability of each condition. There is no doubt that $SS_{error}$ term is reduced and more powerful results are gained. Moreover, within-groups variation $(SS_w)$ is calculated by the same way of an independent ANOVA design by the following formula:

$$SS_w = \sum_1 (\bar{x_{i1}} - \bar{x_1})^2 + \sum_2 (\bar{x_{i2}} - \bar{x_2})^2 + ... + \sum_k (\bar{x_{ik}} - \bar{x_k})^2. \tag{4.48}$$

Here, $x_{i1}$=the score of the $(i^{th})$ subject in group 1, $x_{i2}$=the score of the $(i^{th})$ subject in group 2 and $x_{ik}$=the score of the $(i^{th})$ subject in group k. Furthermore, calculation of $SS_{subjects}$ is necessary.

$$SS_{subjects} = k \sum (\bar{x}_i - \bar{x_1})^2. \tag{4.49}$$

And finally, $SS_{error}$ can calculated by substitution of Equation 4.48 and 4.49.
$MS_{conditions}$ is a ratio of $SS_{conditions}$ and degrees of freedom(DF) is ($k$-1). $MS_{error}$ can be calculated $SS_{error}$ dividing by ($n$-1)($k$-1) DF in which n represent number of subjects. After obtaining the $MS_{conditions}$ and $MS_{error}$, F-statistic is calculated as the ratio of them given in Equation 4.46. It will be a guide to determine the results are statically significant or not.
And the following assumptions should be checked: For RANOVA, the assumptions are normality and sphericity (homogeneity of variance). Shapiro-Wilk test, otherwise, the Kolmogorov-Smirnov test can be used to check the normality assumption. Mauchly's test can be used to check sphericity assumptions. It is employed to test the hypothesis that the variances of the differences between conditions are equal or not. If normality assumption can not meet, the non-parametric tests can be applied. If there is no assumption violation, result belongs to sphericity assumed is necessary. If assumption of sphericity is not met (p<.05), corrected F values should have been consider. When $\varepsilon$ is less than .75, test results of Greenhouse-Geisser test can

be used. Otherwise, the test results of Huynh-Feldt test can be considered. If statistically signifiant results are obtained, post-hoc comparisons can be applied for the factors. The Bonferroni test is a good candidate to detect which is different from the rest [23, 24, 68, 69].

In this thesis, RANOVA is preferred because the same five images have been used to investigate whether there is a difference in terms of performance measures or not. Hence, images, methods and performances measures are elements, predictors and dependent variables, respectively.

# CHAPTER 5

# COMPARATIVE EXPERIMENTS AND RESULTS

## 5.1 Dataset

This section presents interpretation of image histogram and results of the image and mask selection. During the datasets collection process, their different features listed below and their image histograms have been taken into account. In Section 3.2 the test images are investigated. All the images are 8-bit gray levels and $256 \times 256$ pixels. Histogram of the selected images are given in Figure 5.1. Those datasets were gathered from different sources which are indicated under the figures.
In order to apply image inpainting algorithms, five images and four masks are selected.

### Results of Image Selection

Dataset collection process was conducted carefully. Those images preferred are: *Lena*, *cameraman*, *boat*, *jet plane* and *mri*. The reasons for particularly selecting these images are various. First of all, they are used extensively in the literature. Using the same reachable test images gives an opportunity to researchers for comparing their results with the others. Methods of MARS and CMARS are novel in this domain; and thus, other researchers can use the same test images to compare their results with ours. Results of the literature review is given in Section 3.2.1. From those groups listed in Table 3.1 one from each are preferred as a test image. Secondly, image exposure quality is an other criterion of our image selection process. For this aim, images were investigated as they were well-exposed or not. According to their histograms, five well-exposed ones in the literature are selected. Histograms of *cameraman* and *mri* images could be misperceived as under-exposed. Those images which include plenty of dark areas, with right-skewed histogram meet the expectation. Similarly, *jet plane* image is not an over-exposed image in terms of including mess white pixels and having left-skewed shape. Finally, the amount of gray tones in the images which can be detected from the image histograms is yet another important component. Histograms of five images are given in Figure 5.1.

Based on the last criterion, we group five images in three groups: one including all tones (i.e., *Lena*); ones including plenty of dark tones (i.e., *mri* and *cameraman*) and ones include plenty of light tones (i.e., *jet plane* and *boat*). In other words, this classification also means that gray scale pixels are grouped according to their frequencies. These images have also variety of additional features. According to image histograms, *Lena* has a typical average scene with including all mid-tones and there is no touch axes. *Boat* image consists of bright lights and tonal variations. *Cameraman* image is well-exposed image in spite of it had taken against a bright background it still includes all the details. *Jet plane* image includes plenty of light tones; in other words, includes huge white areas. *Mri* has plenty of dark tones with fine details and symmetric structures.

To sum up, including all image types in the dataset will prepare the ground for getting more accurate results in the comparisons.

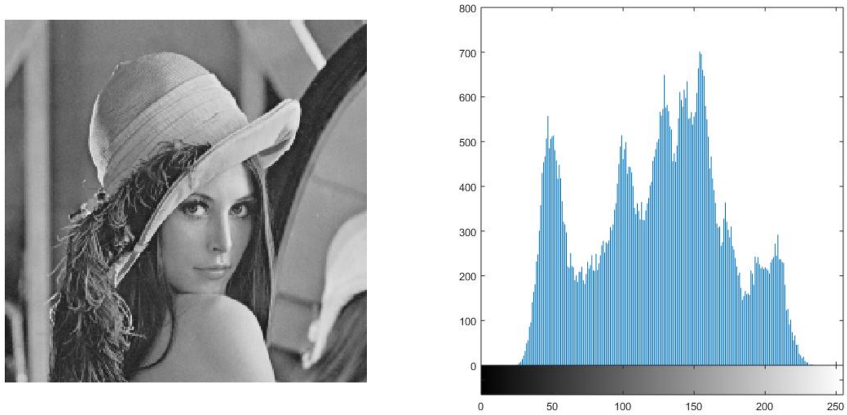


Source: Image Databases, Standard Test Images [20]

(a) Lena Image and Histogram

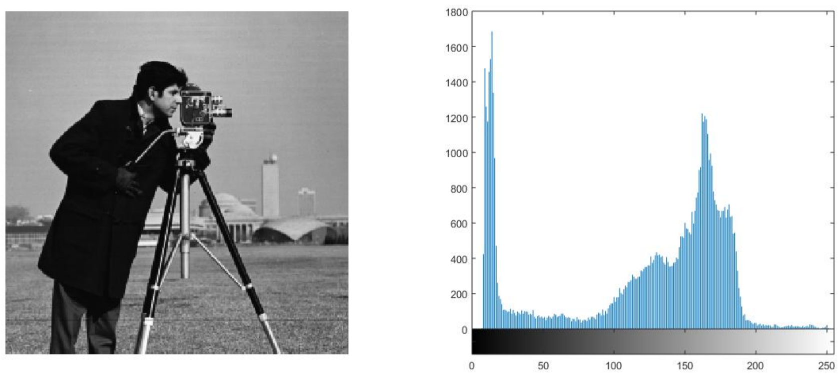


Source: Image Databases, Standard Test Images [20]

(b) Cameraman Image and Histogram

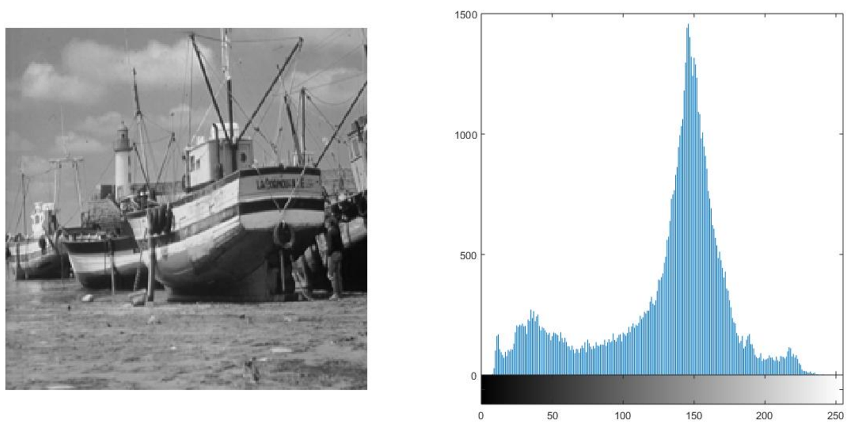


Source: Public-Domain Test Images for Homeworks and Projects [21]

(c) Boat Image and Histogram

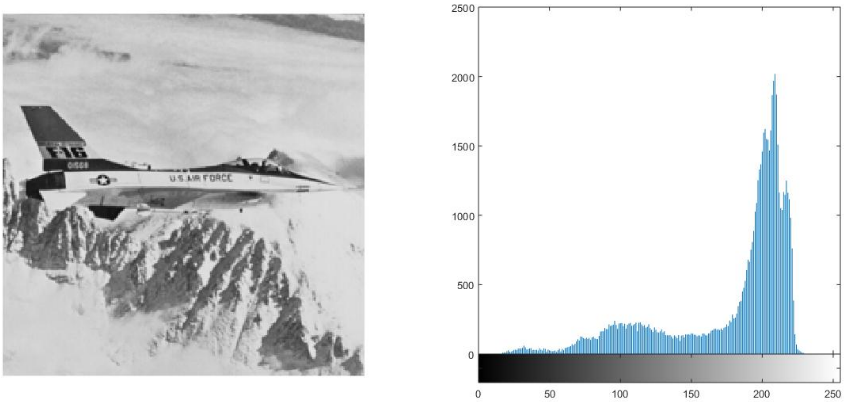


Source: Image Databases, Standard Test Images [20]

(d) Jet plane Image and Histogram

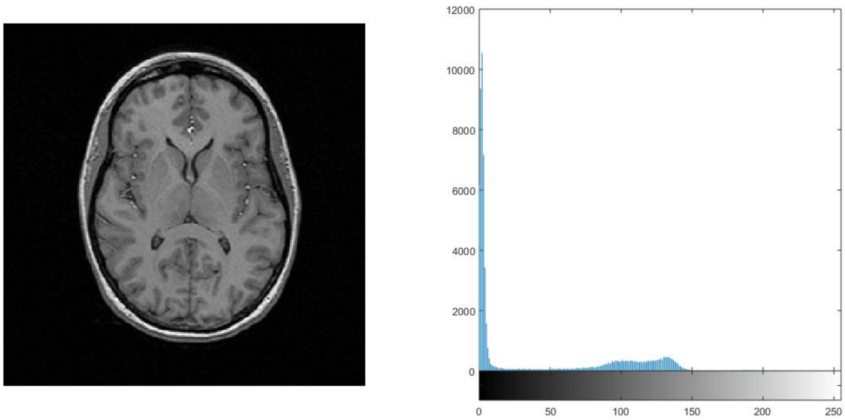


Source: Northern Arizona University, Gray Scale Images [22]

(e) MRI Image and Histogram

Figure 5.1: Used Images

### Results of Mask Selection

Occludes parts of the image can be comprised by writing the date on photography down or leading aging to scratches. In order to represent those deteriorations, researchers preferred lines or texts in their masks. In Section 3.2.2, mask properties are elaborated. Four masks are created via Adobe Illustrator program. Mask 1 and Mask 2 are fairly similar to the ones used in Firas's research [44]. Mask 3 and Mask 4 are created by the author's one of the favorite quotations of Walt Disney [93].

During the creating process different font sizes and font styles are applied. Those font styles are: light, light italic, regular, italic, bold and bold italic. Font sizes from 9pt to 36pt are preferred. Mask 4 is an intersection of Mask 3's diffent two version: twisted horizontally -50% and 50% bend. Those four masks are presented in Figure 5.2.

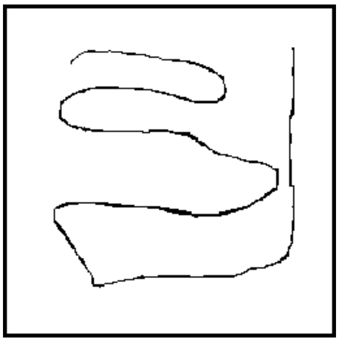

Source: Recreated by the author,
Inspired by [44]

(a) Mask 1-Thin Mask

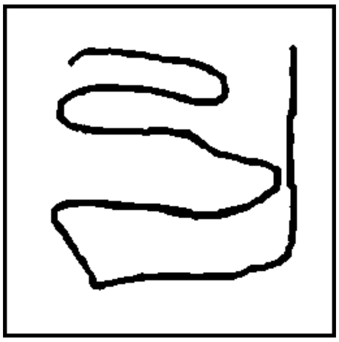

Source: Recreated by
the author

(b) Mask 2- Thick Mask


Source: Created by the author

(c) Mask 3-Text Mask

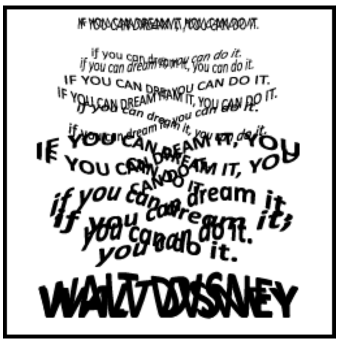

Source: Created by the author

(d) Mask 4- Superimposed text Mask

Figure 5.2: Used Masks

## 5.2 Tools

### R

In this thesis, R version 3.3.2 (2016-10-31) "Sincere Pumpkin Patch" [67] is employed in MARS method with following package:

- Earth: To build a MARS model. R Software Package and reference manual is retrieved from [52].

### MATLAB

MATLAB ® version 8.5.0.197613 (R2015a) is used in PDE, Kriging, ANNs and CMARS methods. In addition, getting the matrices, building the histograms and recreating the image included MARS method are completed via the MATLAB ®. Following toolboxes are employed:

- MOSEK ™ Optimization Toolbox is used in method of CMARS for solving the CQP [55].
- Image Processing Toolbox, version 9.2.
- Neural Network Toolbox, version 8.3.

### SPSS

SPSS ® 13.0 for Windows is employed in order to interpret the results.

### Adobe Illustrator

All masks are created via Adobe Illustrator ® version 16.0.0.

## 5.3 Applied Methods

In this research, four masks are applied to five images. Obtained 20 masked images are inpainted by using five algorithms described in Chapter 4. Furthermore, 100 outputs are gathered and evaluated under the light of three quality metrics. *Lena* image with Mask 1 is chosen in order to illustrate the method of application in detail; thus, all results given in the subsections below belongs to *Lena* image with Mask 1. In addition, results of the all images are given at the ends of the corresponding subsections. Neighbors of the corrupted parts are defined as training values except the PDE method. Masks are dilated and intersection of original image and dilated mask is taken as neighbors. *Dilation* process is mentioned in Section 2.1.3. Those neighbors are found via MATLAB ® program by creating a disk-shaped structuring element with a radius of four. This value is determined as four because it includes at least eight neighbors. Furthermore, results of inpainting checked for all methods and it is the best for all. Representation of mask *dilation* and training pixels are given in Figure 5.3.

(a) Masked Image | (b) Masked Image with Dilated Mask | (c) Training Parts of the Masked Image

Source: Created by the author

Figure 5.3: Finding Neighbors of the known pixels

After obtaining missing coordinates corresponding to the prediction values whose values turned into $256 \times 256$ matrix. Known points of the predicted matrix arranged as zero. Predicted values were nonzero if they had not predicted as black. Then, summation of matrix of masked image (unknown points are equal to zero) and predicted matrix gives the inpainted image. So, image completion is completed. Afterwards, quality metrics are calculated in order to compare the performances of the methods.

### 5.3.1 PDE

PDE code is created by Parisotto and Schonlieb for image inpainting problem in MATLAB ® [64]. These codes are modified for grayscale image. Corrupted image is reconstructed by minimizing the Equation 4.1, given in Section 4.1.1. Alternating solutions of the Euler-Lagrange equations for $u$ and $\nu$ are updated iteratively in order to solve the minimization problem. Figure 5.4b demonstrates the masked *Lena*'s segmentation results by AT algorithm given in Section 4.1.1, Equation 4.2 with 100 iteration. After 100 iteration, performance criteria is not change and for time consuming algorithm stopped $100^{th}$ iteration. Regularization parameters are defined for both $\alpha$ and $\beta$ as 100. Accuracy of AT approximation of the edge set ($\rho$) is arranged as 0.02. Those values are determined by considering the change in the inpainting image and its performance criteria. In other words, they are selected trial and error. Toleration is set to 0.00001. Weight on data fidelity should be large as mentioned in the explanation of codes and defined as 10000. Gradient matrix is created and iterative Euler-lagrange equation is solved for $u$ and $\nu$.

(a) Masked Lena

(b) Segmentation Results of the AT

Source: Created by the author

Figure 5.4: Masked Lena and Segmentation Results of the AT

### 5.3.2 Kriging

Kriging code is relased by Wolfgang Schwanghart for the MATLAB ® [63]. These codes are modified for the image inpainting case. Known locations and their corresponding values are interpreted as coordinates of training locations and their corresponding intensity values. Unsampled locations represents the missing pixels. In Kriging part, four functions are employed in image inpainting case: variogram, variogramfit, kriging and fminsearchbnd. As mentioned in Section 4.1.2 Kriging, $\hat{\mathbf{z}}^*$ represents the missing parts, and this is output of the kriging function. One of the input of kriging function is named as vstruct which is obtained from variogramfit function. Vstruct is a structure array contains all of the necessary information on the variogram. Variogram is given in Figure 5.5.

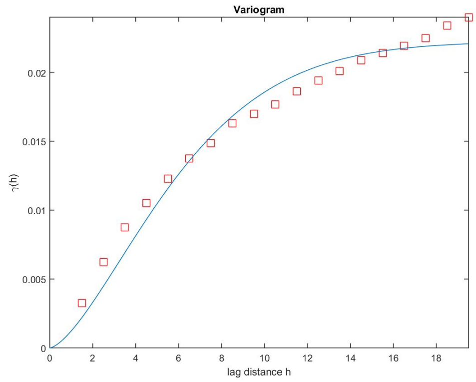


Source: Created by the author

Figure 5.5: Variogram of Lena-M1. Blue line belongs the model, red squares represents experimental semiveriograms

According to the variogram, *sill* and *range* are equal to 0.0222 and 6.7552, respectively. *Sill* is the gamma value at which the variogram levels off, whereas *range* is the corresponding lag distance of *sill* point. All distance between the observed pixels are calculated via Euclidean distance in order to obtain the variogram. Distances are grouped to 19 lag distances classes. $\mathbf{\Gamma}$ matrix is calculated; afterwards, $\mathbf{\Gamma^{-1}}$ is obtained. Multiplying $\mathbf{\Gamma^{-1}}$ and $\mathbf{g}$ vector gives us to $\boldsymbol{\lambda}$. And, finally summation of multiplication of $\boldsymbol{\lambda}$ and coordinates of the missing pixels give the prediction of the corrupted parts.

### 5.3.3 Artificial Neural Networks

The architecture is built, and after training step is over, the obtained screen shot is given in Figure 5.6a. Training process stops when the MSE of the validation samples increases continuously for more than six (default) epochs. According to result of *Lena* image with Mask 1, the best validation performance (0.0043535) is obtained at epoch 131. Correlation between the outputs and targets is shown in Figure 5.6c, and could be interpreted as a perfect correlation. Performance of the LM algorithm is given in Figure 5.6b.

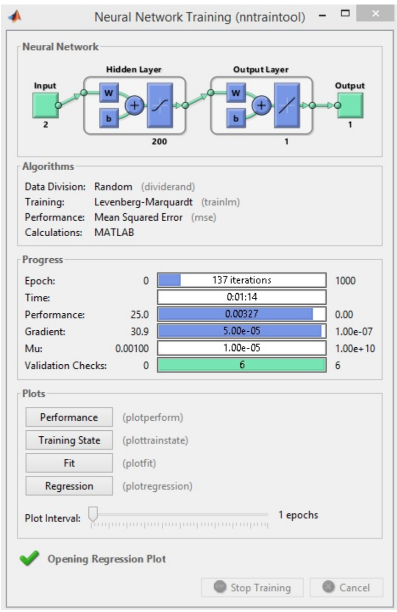


Source: Created by the author

(a) ANNs Training State

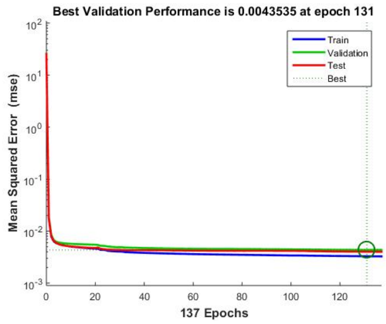


Source: Created by the author

(b) Performance of LM Algorithm

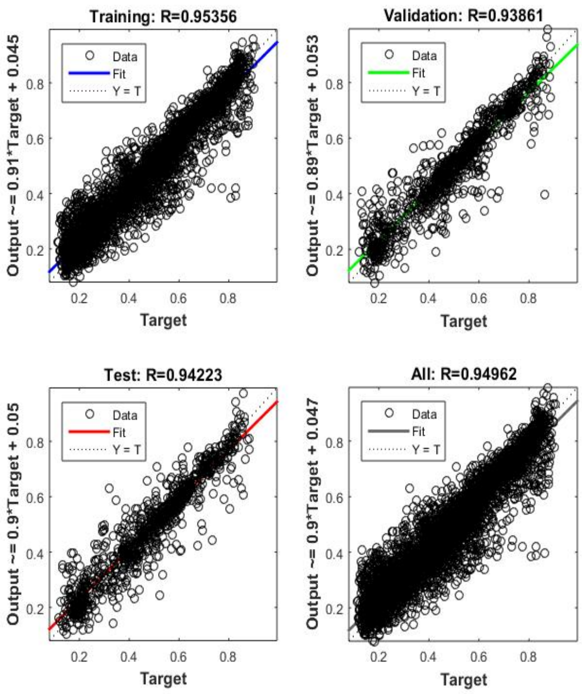


Source: Created by the author

(c) Observed versus ANN predicted values

Figure 5.6: Results of ANNs

### 5.3.4 Multivariate Adaptive Regression Splines

For this study R Earth package is used, and after obtaining the predictions, MATLAB ® is employed to put the predictions into the missing pixels. $M_{max}$ and the largest degree of interaction for masked *Lena* were defined as 150 and 2 (x and y coordinates), respectively. During $M_{max}$ determination, $GCV$ values are taken into account whether they are in increasing or decreasing status. Selecting unnecessarily small $M_{max}$ values could cause losing the terms. After determining it as 150, there is no decreasing effect on the $GCV$ value. After forward stage, number of 83 BFs are acquired and stored for the CMARS. $R^2$ changed by less than 0.0001 at 83 terms. $GCV$, $RSS$, $GR^2$, and $R^2$ are obtained as follows 0.0080, 48.18, 0.78 and 0.79, respectively. At the end of the backward stage, 78 BFs is reached and the final model is obtained.

### 5.3.5 Conic Multivariate Adaptive Regression Splines

For this study, codes of MATLAB ® are taken from [98]. First of all, obtained BFs from the forward stage of the MARS method, 83 BFs, are introduced to the algorithm. Maximum interaction is defined as two. BFs are converted to format of $\psi$ to adapt to PRSS objective function given in Chapter 4, Equation 4.21. Then, derivatives of BFs are taken, **L** matrix and construction of **D** matrix are completed and $RSS$ is calculated. MOSEK ™ Optimization Toolbox is employed for solving the CQP. Plenty of $\tilde{M}$ values, candidates of optimum solution, are obtained by solving CQP problem given in Chapter 4, Equation 4.29. Those solutions as plotted to determine to the best solutions.

User-manually determination is a key of interpretation of the performance. Minimizing balanced the objective functions $\sqrt{RSS}$ and $\|\mathbf{L}\boldsymbol{\theta}\|_2$ is important. For this purpose, the log-log scale curve of $\sqrt{RSS}$ versus $\|\mathbf{L}\boldsymbol{\theta}\|_2$ is investigated. In order to eliminate to user mistake, recursive runs were occurred. $RSS$, $\mathbf{L}\boldsymbol{\theta}$ and $GCV$ are calculated. For our illustrated sample, *Lena* with Mask 1, the best solution is gathered when $\|\mathbf{L}\boldsymbol{\theta}\|_2$ and $\sqrt{RSS}$ are taken 6.95 and 3.5, respectively. $GCV$ value is calculated as 0.0081.

## 5.4 Application Results

### 5.4.1 Outputs of Inpainted Images

In this subsection, original image, masked images and results of the all methods are given according to the following order:

| | |
|---|---|
| a | Original Image |
| b-c-d-e | Masked Images |
| f-g-h-i | Results of the PDE Method |
| j-k-l-m | Results of the ANNs Method |
| n-o-p-q | Results of the Kriging Method |
| r-s-t-u | Results of the MARS Method |
| v-w-x-y | Results of the CMARS Method |

In order to present the results, names of the masks are given under the masked images; furthermore, each image includes the abbreviated version of the method name as a caption.


(a) Original Image-Lena

(b) Mask 1 (c) Mask 2 (d) Mask 3 (e) Mask 4

(f) PDE (g) PDE (h) PDE (i) PDE

(j) ANNs (k) ANNs (l) ANNs (m) ANNs

(n) Kriging (o) Kriging (p) Kriging (q) Kriging

(r) MARS (s) MARS (t) MARS (u) MARS

(v) CMARS (w) CMARS (x) CMARS (y) CMARS

Figure 5.7: Inpainted Images of Lena Image

(a) Original Image-Boat

(b) Mask 1

(c) Mask 2


(d) Mask 3

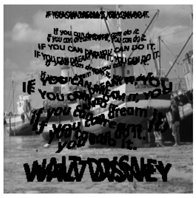

(e) Mask 4

(f) PDE

(g) PDE

(h) PDE

(i) PDE

(j) ANNs

(k) ANNs

(l) ANNs

(m) ANNs

(n) Kriging

(o) Kriging

(p) Kriging

(q) Kriging

(r) MARS

(s) MARS

(t) MARS

(u) MARS

(v) CMARS

(w) CMARS

(x) CMARS

(y) CMARS

Figure 5.8: Inpainted Images of Boat Image


(a) Original Image-Cameraman

(b) Mask 1 (c) Mask 2 (d) Mask 3 (e) Mask 4

(f) PDE (g) PDE (h) PDE (i) PDE

(j) ANNs (k) ANNs (l) ANNs (m) ANNs

(n) Kriging (o) Kriging (p) Kriging (q) Kriging

(r) MARS (s) MARS (t) MARS (u) MARS

(v) CMARS (w) CMARS (x) CMARS (y) CMARS

Figure 5.9: Inpainted Images of Cameraman Image

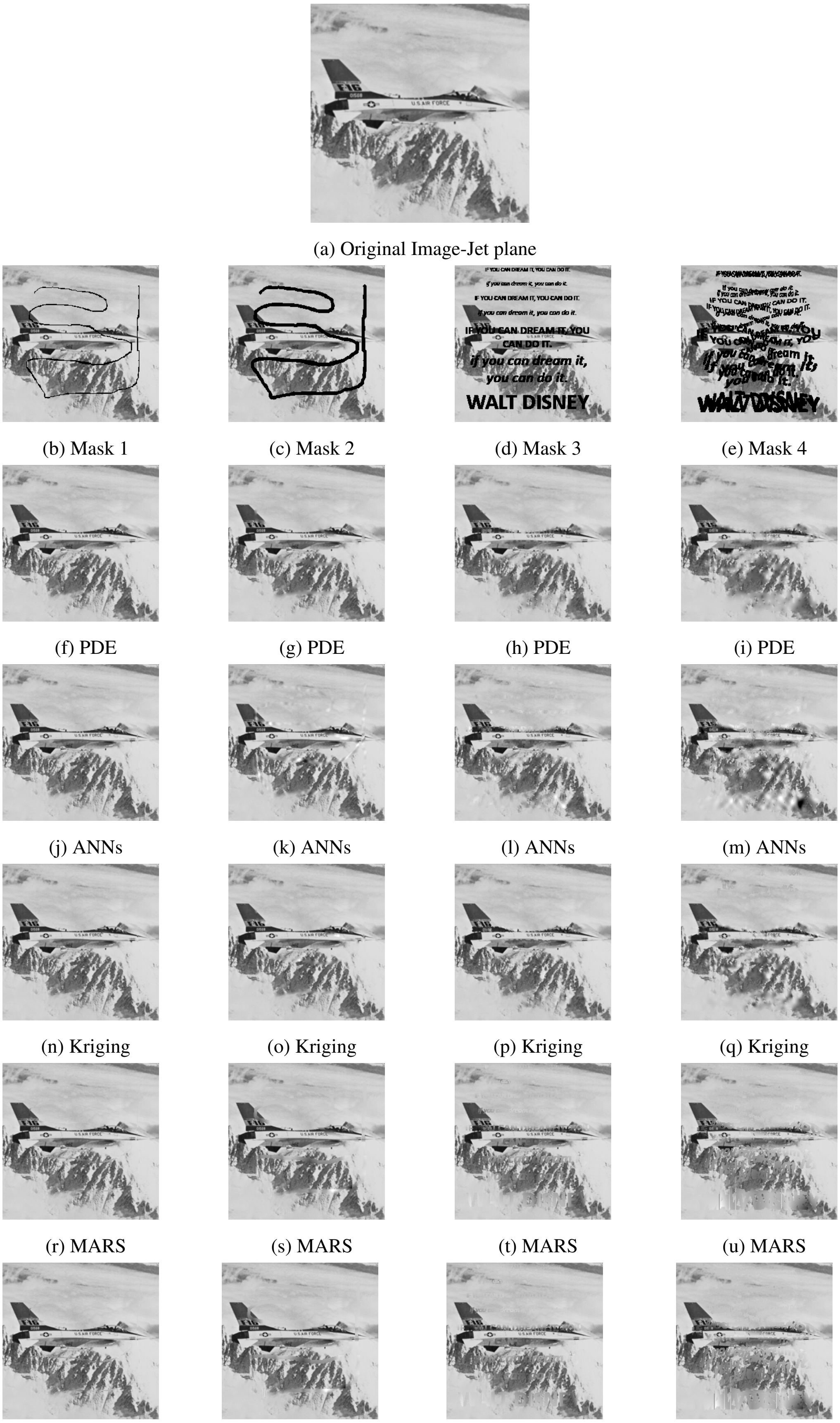


(a) Original Image-Jet plane

(b) Mask 1 (c) Mask 2 (d) Mask 3 (e) Mask 4

(f) PDE (g) PDE (h) PDE (i) PDE

(j) ANNs (k) ANNs (l) ANNs (m) ANNs

(n) Kriging (o) Kriging (p) Kriging (q) Kriging

(r) MARS (s) MARS (t) MARS (u) MARS

(v) CMARS (w) CMARS (x) CMARS (y) CMARS

Figure 5.10: Inpainted Images of Jet plane Image

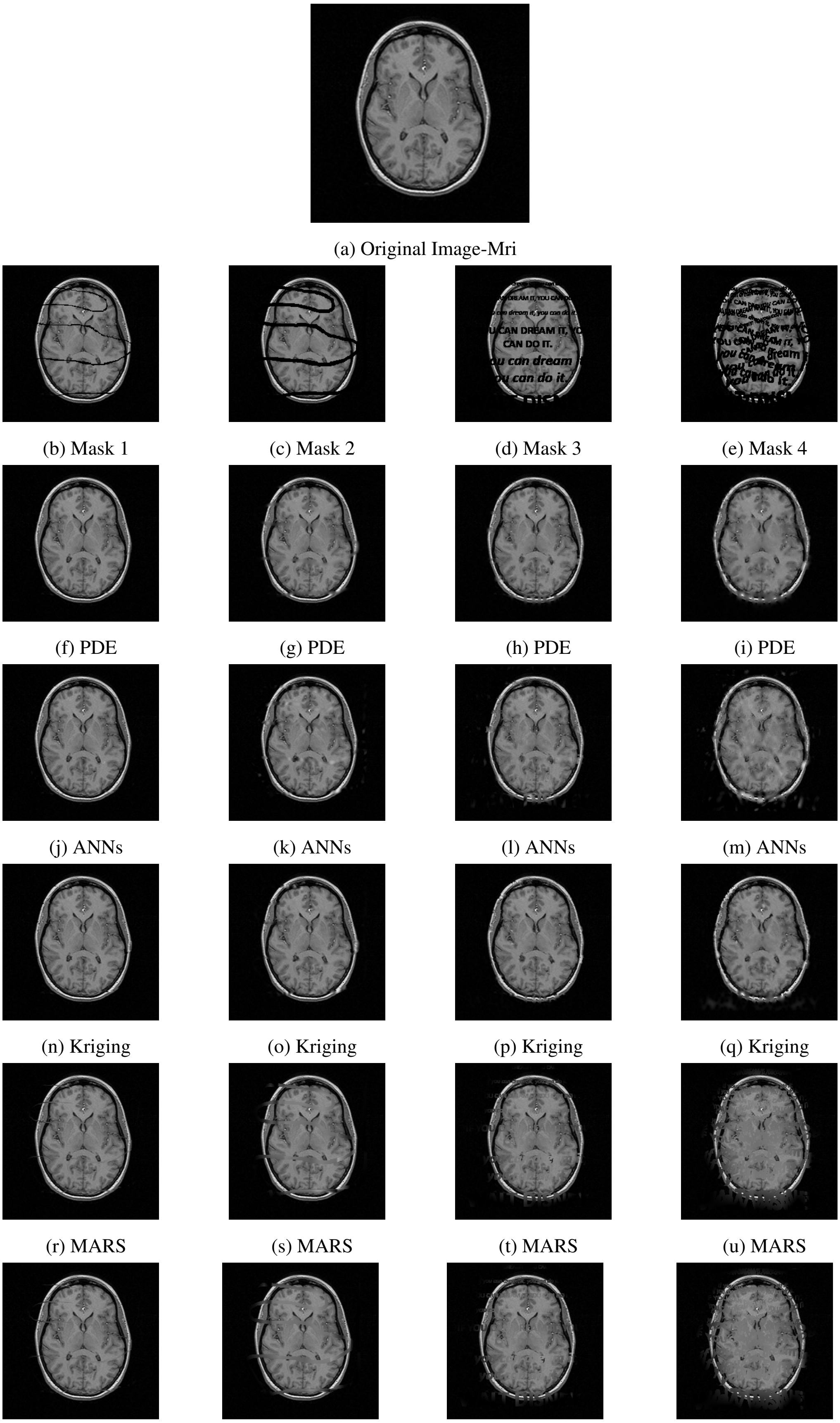

(a) Original Image-Mri

(b) Mask 1 (c) Mask 2 (d) Mask 3 (e) Mask 4

(f) PDE (g) PDE (h) PDE (i) PDE

(j) ANNs (k) ANNs (l) ANNs (m) ANNs

(n) Kriging (o) Kriging (p) Kriging (q) Kriging

(r) MARS (s) MARS (t) MARS (u) MARS

(v) CMARS (w) CMARS (x) CMARS (y) CMARS

Figure 5.11: Inpainted Images of Mri Image

### 5.4.2 Results with Quality Metrics

As mentioned in Section 4.2, the higher PSNR value indicates the higher image quality and less error. On the contrary, the lower MSE value shows the better image quality. Lastly, SSMI represents a percent, and closest values to one indicates high success of the inpainting algorithm considered.
As mentioned before, 100 outputs are evaluated in the light of three criteria. Thus, we obtained 300 numerical results. These results are interpreted in the following subsection and summarized in Chapter 6.

Table5.1: Results of the Lena image

| | Performance Criteria | Masks | Kriging | ANNs | PDE | MARS | CMARS |
|---|---|---|---|---|---|---|---|
| LENA | PSNR | M1 | 36.6533 | 38.8142 | 40.5833 | 36.5128 | 36.5168 |
| | | M2 | 31.6953 | 31.2389 | 32.8104 | 30.5337 | 30.5356 |
| | | M3 | 29.9873 | 29.5014 | 31.7136 | 27.7052 | 27.7177 |
| | | M4 | 26.0351 | 25.8371 | 27.9436 | 23.6014 | 23.5992 |
| | MSE | M1 | 2.1611e-04 | 1.3139e-04 | 8.7432e-05 | 2.2321e-04 | 2.2301e-04 |
| | | M2 | 6.7681e-04 | 7.5182e-04 | 5.2355e-04 | 8.8436e-04 | 8.8398e-04 |
| | | M3 | 0.0010 | 0.0011 | 6.7397e-04 | 0.0017 | 0.0017 |
| | | M4 | 0.0025 | 0.0026 | 0.0016 | 0.0044 | 0.0044 |
| | SSMI | M1 | 0.9873 | 0.9899 | 0.9937 | 0.9831 | 0.9832 |
| | | M2 | 0.9612 | 0.9535 | 0.9665 | 0.9464 | 0.9465 |
| | | M3 | 0.9450 | 0.9301 | 0.9580 | 0.9042 | 0.9041 |
| | | M4 | 0.8787 | 0.8506 | 0.9066 | 0.7992 | 0.7991 |

Note: PDE performs the best with respect to all criteria.

Table5.2: Results of the Boat image

| | Performance Criteria | Masks | Kriging | ANNs | PDE | MARS | CMARS |
|---|---|---|---|---|---|---|---|
| BOAT | PSNR | M1 | 36.4781 | 38.6770 | 41.0231 | 36.0910 | 36.0915 |
| | | M2 | 31.3795 | 30.2959 | 32.2000 | 29.8596 | 30.1890 |
| | | M3 | 29.8275 | 30.1231 | 32.5054 | 28.0191 | 28.0165 |
| | | M4 | 26.7869 | 25.7439 | 28.6390 | 24.5223 | 24.5239 |
| | MSE | M1 | 2.2500e-04 | 1.3561e-04 | 7.9011e-05 | 2.4598e-04 | 2.4595e-04 |
| | | M2 | 7.2786e-04 | 9.3413e-04 | 6.0257e-04 | 0.0010 | 9.5740e-04 |
| | | M3 | 0.0010 | 9.7205e-04 | 5.6165e-04 | 0.0016 | 0.0016 |
| | | M4 | 0.0021 | 0.0027 | 0.0014 | 0.0035 | 0.0035 |
| | SSMI | M1 | 0.9883 | 0.9903 | 0.9948 | 0.9839 | 0.9839 |
| | | M2 | 0.9626 | 0.9491 | 0.9682 | 0.9492 | 0.9513 |
| | | M3 | 0.9440 | 0.9354 | 0.9619 | 0.9127 | 0.9126 |
| | | M4 | 0.8759 | 0.8476 | 0.9070 | 0.8316 | 0.8316 |

Note: PDE performs the best with respect to all criteria.

Table5.3: Results of the Cameraman image

| | Performance Criteria | Masks | Kriging | ANNs | PDE | MARS | CMARS |
|---|---|---|---|---|---|---|---|
| CAMERAMAN | PSNR | M1 | 32.7880 | 34.7688 | 36.5331 | 32.4659 | 32.4559 |
| | | M2 | 28.1097 | 27.8544 | 29.2998 | 26.1997 | 26.3375 |
| | | M3 | 27.0304 | 27.4594 | 29.3773 | 24.4776 | 24.4802 |
| | | M4 | 23.3593 | 23.1782 | 25.3484 | 21.4418 | 21.4461 |
| | MSE | M1 | 5.2626e-04 | 3.3352e-04 | 2.2217e-04 | 5.6677e-04 | 5.6808e-04 |
| | | M2 | 0.0015 | 0.0016 | 0.0012 | 0.0024 | 0.0023 |
| | | M3 | 0.0020 | 0.0018 | 0.0012 | 0.0036 | 0.0036 |
| | | M4 | 0.0046 | 0.0048 | 0.0029 | 0.0072 | 0.0072 |
| | SSMI | M1 | 0.9890 | 0.9875 | 0.9944 | 0.9765 | 0.9764 |
| | | M2 | 0.9669 | 0.9428 | 0.9706 | 0.9328 | 0.9361 |
| | | M3 | 0.9468 | 0.9217 | 0.9606 | 0.8652 | 0.8652 |
| | | M4 | 0.8652 | 0.8136 | 0.9061 | 0.7775 | 0.7776 |

Note: PDE performs the best with respect to all criteria.

Table5.4: Results of the Jet plane image

| | Performance Criteria | Masks | Kriging | ANNs | PDE | MARS | CMARS |
|---|---|---|---|---|---|---|---|
| JET PLANE | PSNR | M1 | 36.3964 | 37.7787 | 40.6837 | 36.5331 | 36.5387 |
| | | M2 | 31.4047 | 30.5785 | 32.6065 | 30.5869 | 30.5798 |
| | | M3 | 29.2298 | 28.5783 | 30.6823 | 26.6196 | 26.6240 |
| | | M4 | 25.3580 | 24.2207 | 26.8607 | 23.3997 | 23.4034 |
| | MSE | M1 | 2.2928e-04 | 1.6678e-04 | 8.5433e-05 | 2.2217e-04 | 2.2189e-04 |
| | | M2 | 7.2366e-04 | 8.7528e-04 | 5.4871e-04 | 8.7360e-04 | 8.7503e-04 |
| | | M3 | 0.0012 | 0.0014 | 8.5461e-04 | 0.0022 | 0.0022 |
| | | M4 | 0.0029 | 0.0038 | 0.0021 | 0.0046 | 0.0046 |
| | SSMI | M1 | 0.9914 | 0.9902 | 0.9960 | 0.9876 | 0.9876 |
| | | M2 | 0.9711 | 0.9532 | 0.9753 | 0.9614 | 0.9611 |
| | | M3 | 0.9537 | 0.9277 | 0.9637 | 0.9086 | 0.9086 |
| | | M4 | 0.8919 | 0.8545 | 0.9173 | 0.8380 | 0.8379 |

Note: PDE performs the best with respect to all criteria.

Table5.5: Results of the Mri image

| | Performance Criteria | Masks | Kriging | ANNs | PDE | MARS | CMARS |
|---|---|---|---|---|---|---|---|
| MRI | PSNR | M1 | 35.6949 | 39.0738 | 41.0749 | 35.1368 | 35.1375 |
| | | M2 | 30.1837 | 30.5706 | 31.7149 | 28.5472 | 28.6682 |
| | | M3 | 29.2561 | 28.5617 | 31.2610 | 26.4131 | 26.4140 |
| | | M4 | 25.9795 | 24.3405 | 27.3725 | 23.3316 | 23.3316 |
| | MSE | M1 | 2.6947e-04 | 1.2377e-04 | 7.8075e-05 | 3.0642e-04 | 3.0637e-04 |
| | | M2 | 9.5857e-04 | 8.7688e-04 | 6.7377e-04 | 0.0014 | 0.0014 |
| | | M3 | 0.0012 | 0.0014 | 7.4801e-04 | 0.0023 | 0.0023 |
| | | M4 | 0.0025 | 0.0037 | 0.0018 | 0.0046 | 0.0046 |
| | SSMI | M1 | 0.9904 | 0.9887 | 0.9961 | 0.9787 | 0.9786 |
| | | M2 | 0.9637 | 0.9375 | 0.9719 | 0.9392 | 0.9325 |
| | | M3 | 0.9605 | 0.9024 | 0.9719 | 0.8696 | 0.8697 |
| | | M4 | 0.8911 | 0.7963 | 0.9313 | 0.7800 | 0.7800 |

Note: PDE performs the best with respect to all criteria.

### 5.4.3 Three-Way Repeated Measures ANOVA

In order to interpret the results three-way ANOVA is employed. First, the form of RANOVA is preferred because the same images have been used in comparisons. Note that RANOVA carries out by using the statistical software SPSS.
In this research we investigate the following research questions:

- Do different images have different effects on the method performances?
- Do methods have different performances?
- Do mask types affect performance measures?
- Which images/masks/methods differ from the rest?
- Is there an interaction between images/masks and methods?

Above testing procedure is applied three-times for each performance measures (PSNR, MSE, SSMI) separately.
First of all, we investigate the image effect and its interactions on performance measures. Images were grouped in terms of their frequency levels. *Lena* is an average image, and includes all mid-tones. *Boat* and *jet plane* have plenty of light tones whereas *cameraman* and *mri* have plenty of dark tones. Results of image effect is given in Output 5.12. According to the results, image and their interactions (image and method; image and mask; image, method and mask) are not significant factors (All $p_{values}$>.05). In other words, there is no difference in terms of image effect in the all performance measures. Then, image factor is eliminated and we repeat the analysis by taking into account the method and mask factors.
Levels of RANOVA variables are defined in different columns of the SPSS data editor.
In this thesis, we have two significant within-subject factors: Masks (M1, M2, M3, M4) and methods (KRIGING, ANNs, PDE, MARS, CMARS). And as we mentioned before, we have five images (subjects). Alpha level is selected as .05.
Output 5.13 shows the initial results of the RANOVA. It lists the level of each independent variable. The same structure is created for all measures (PSNR, MSE and SSMI).

**Tests of Within-Subjects Effects**

| Source | | Type III Sum of Squares | df | Mean Square | F | Sig. | Partial Eta Squared |
|---|---|---|---|---|---|---|---|
| im | Sphericity Assumed | 17,850 | 1 | 17,850 | 3,235 | ,323 | ,764 |
| | Greenhouse-Geisser | 17,850 | 1,000 | 17,850 | 3,235 | ,323 | ,764 |
| | Huynh-Feldt | 17,850 | . | . | . | . | ,764 |
| | Lower-bound | 17,850 | 1,000 | 17,850 | 3,235 | ,323 | ,764 |
| Error(im) | Sphericity Assumed | 5,518 | 1 | 5,518 | | | |
| | Greenhouse-Geisser | 5,518 | 1,000 | 5,518 | | | |
| | Huynh-Feldt | 5,518 | . | . | | | |
| | Lower-bound | 5,518 | 1,000 | 5,518 | | | |
| method | Sphericity Assumed | 169,134 | 4 | 42,284 | 222,063 | ,000 | ,996 |
| | Greenhouse-Geisser | 169,134 | 1,000 | 169,134 | 222,063 | ,043 | ,996 |
| | Huynh-Feldt | 169,134 | ,000 | . | . | . | ,996 |
| | Lower-bound | 169,134 | 1,000 | 169,134 | 222,063 | ,043 | ,996 |
| Error(method) | Sphericity Assumed | ,762 | 4 | ,190 | | | |
| | Greenhouse-Geisser | ,762 | 1,000 | ,762 | | | |
| | Huynh-Feldt | ,762 | ,000 | . | | | |
| | Lower-bound | ,762 | 1,000 | ,762 | | | |
| mask | Sphericity Assumed | 1499,840 | 3 | 499,947 | 881,044 | ,000 | ,999 |
| | Greenhouse-Geisser | 1499,840 | 1,000 | 1499,840 | 881,044 | ,021 | ,999 |
| | Huynh-Feldt | 1499,840 | ,000 | . | . | . | ,999 |
| | Lower-bound | 1499,840 | 1,000 | 1499,840 | 881,044 | ,021 | ,999 |
| Error(mask) | Sphericity Assumed | 1,702 | 3 | ,567 | | | |
| | Greenhouse-Geisser | 1,702 | 1,000 | 1,702 | | | |
| | Huynh-Feldt | 1,702 | ,000 | . | | | |
| | Lower-bound | 1,702 | 1,000 | 1,702 | | | |
| im * method | Sphericity Assumed | 51,596 | 4 | 12,899 | 5,030 | ,073 | ,834 |
| | Greenhouse-Geisser | 51,596 | 1,000 | 51,596 | 5,030 | ,267 | ,834 |
| | Huynh-Feldt | 51,596 | ,000 | . | . | . | ,834 |
| | Lower-bound | 51,596 | 1,000 | 51,596 | 5,030 | ,267 | ,834 |
| Error(im*method) | Sphericity Assumed | 10,258 | 4 | 2,564 | | | |
| | Greenhouse-Geisser | 10,258 | 1,000 | 10,258 | | | |
| | Huynh-Feldt | 10,258 | ,000 | . | | | |
| | Lower-bound | 10,258 | 1,000 | 10,258 | | | |
| im * mask | Sphericity Assumed | ,414 | 3 | ,138 | ,119 | ,943 | ,107 |
| | Greenhouse-Geisser | ,414 | 1,000 | ,414 | ,119 | ,788 | ,107 |
| | Huynh-Feldt | ,414 | . | . | . | . | ,107 |
| | Lower-bound | ,414 | 1,000 | ,414 | ,119 | ,788 | ,107 |
| Error(im*mask) | Sphericity Assumed | 3,466 | 3 | 1,155 | | | |
| | Greenhouse-Geisser | 3,466 | 1,000 | 3,466 | | | |
| | Huynh-Feldt | 3,466 | . | . | | | |
| | Lower-bound | 3,466 | 1,000 | 3,466 | | | |
| im * method * mask | Sphericity Assumed | 2,789 | 12 | ,232 | ,461 | ,903 | ,316 |
| | Greenhouse-Geisser | 2,789 | 1,000 | 2,789 | ,461 | ,620 | ,316 |
| | Huynh-Feldt | 2,789 | ,000 | . | . | . | ,316 |
| | Lower-bound | 2,789 | 1,000 | 2,789 | ,461 | ,620 | ,316 |
| Error(im*method*mask) | Sphericity Assumed | 6,049 | 12 | ,504 | | | |
| | Greenhouse-Geisser | 6,049 | 1,000 | 6,049 | | | |
| | Huynh-Feldt | 6,049 | ,000 | . | | | |
| | Lower-bound | 6,049 | 1,000 | 6,049 | | | |

Figure 5.12: Result of Tests of Within-Subjects Effects for Image

**Within-Subjects Factors**

Measure: psnr

| methods | masks | Dependent Variable |
|---|---|---|
| 1 | 1 | kriging_M1 |
| | 2 | kriging_M2 |
| | 3 | kriging_M3 |
| | 4 | kriging_M4 |
| 2 | 1 | nn_M1 |
| | 2 | nn_M2 |
| | 3 | nn_M3 |
| | 4 | nn_M4 |
| 3 | 1 | pde_M1 |
| | 2 | pde_M2 |
| | 3 | pde_M3 |
| | 4 | pde_M4 |
| 4 | 1 | mars_M1 |
| | 2 | mars_M2 |
| | 3 | mars_M3 |
| | 4 | mars_M4 |
| 5 | 1 | cmars_M1 |
| | 2 | cmars_M2 |
| | 3 | cmars_M3 |
| | 4 | cmars_M4 |

Figure 5.13: Structure of Within-Subjects Factors

After the normality assumption is checked, Mauchly's test is employed to test the hypothesis that the variances of the differences between conditions are equal or not. Following hypotheses are conducted:

$H_0$: Variances of the differences are equal.

versus

$H_1$: Variances of the differences are not equal.

Results are given below for each performance measures:

#### 5.4.3.1 Results of PSNR

Output 5.14 provides the mean and standard deviation for each of the images in terms of PSNR criterion.

**Descriptive Statistics**

| | Mean | Std. Deviation | N |
|---|---|---|---|
| kriging_M1 | 35,602140 | 1,6148592 | 5 |
| kriging_M2 | 30,554580 | 1,4848762 | 5 |
| kriging_M3 | 29,066220 | 1,1869406 | 5 |
| kriging_M4 | 25,503760 | 1,3014467 | 5 |
| nn_M1 | 37,822500 | 1,7752741 | 5 |
| nn_M2 | 30,107660 | 1,3065530 | 5 |
| nn_M3 | 28,844780 | 1,0168180 | 5 |
| nn_M4 | 24,664080 | 1,1237344 | 5 |
| pde_M1 | 39,979620 | 1,9382432 | 5 |
| pde_M2 | 31,726320 | 1,4197226 | 5 |
| pde_M3 | 31,107920 | 1,1746734 | 5 |
| pde_M4 | 27,232840 | 1,2441436 | 5 |
| mars_M1 | 35,347920 | 1,7076575 | 5 |
| mars_M2 | 29,145420 | 1,8405415 | 5 |
| mars_M3 | 26,646920 | 1,3932159 | 5 |
| mars_M4 | 23,259360 | 1,1225470 | 5 |
| cmars_M1 | 35,348080 | 1,7135639 | 5 |
| cmars_M2 | 29,262020 | 1,8113035 | 5 |
| cmars_M3 | 26,650480 | 1,3938892 | 5 |
| cmars_M4 | 23,260840 | 1,1212069 | 5 |

Figure 5.14: Descriptive Statistics of PSNR

Output 5.15 shows that Mauchly's test statistics is significant for methods because probability value is less than .05 ($p_{value}$=.004).

**Mauchly's Test of Sphericity[b]**

Measure: psnr

| | | | | | Epsilon[a] | | |
|---|---|---|---|---|---|---|---|
| Within Subjects Effect | Mauchly's W | Approx. Chi-Square | df | Sig. | Greenhouse-Geisser | Huynh-Feldt | Lower-bound |
| methods | ,000 | 27,722 | 9 | ,004 | ,330 | ,429 | ,250 |
| masks | ,030 | 9,552 | 5 | ,108 | ,446 | ,588 | ,333 |
| methods * masks | ,000 | . | 77 | . | ,208 | ,582 | ,083 |

Tests the null hypothesis that the error covariance matrix of the orthonormalized transformed dependent variables is proportional to an identity matrix.

a. May be used to adjust the degrees of freedom for the averaged tests of significance. Corrected tests are displayed in the Tests of Within-Subjects Effects table.

b. Design: Intercept
Within Subjects Design: methods+masks+methods*masks

Figure 5.15: Results of Mauchly's Test of Sphericity for PSNR

Thus, there are significant differences between variances of differences. Since the condition of sphericity has not been met, we consider the corrected F-ratio of Greenhouse-Geisser or Huynh-Feldt instead of sphericity assumed. In this case, $\varepsilon$ is less than .75;

consequently, results of Greenhouse-Geisser test is important.
On the contrary, the test is nonsignificant ($p_{value}$=.108) in terms of masks effect. Hence, this result is interpreted as variances are not significantly different, and the sphericity assumed result is used. The value of $\varepsilon$ is less than .75 in terms of interaction between methods and masks; hence, the results of Greenhouse-Geisser test is important. Output 5.16 includes corrected F values and F values for masks, methods and interaction between these two variables. According to results, methods are significant by different (F(1.32, 5.28)=225.97, $p_{value}$<.05). And, mask has an effect of the PSNR (because (F(3, 12)=563.57, $p_{value}$<.05) ). And there is an interaction between masks and methods (F(2.5, 10)=21.62, $p_{value}$<.05). Thus, both masks and methods are needed, as well as their interaction to explain PSNR value. In other words, the performances measured in terms of the PSNR value are related to the type of mask, the method and their interaction.

**Tests of Within-Subjects Effects**

Measure: psnr

| Source | | Type III Sum of Squares | df | Mean Square | F | Sig. | Partial Eta Squared | Noncent. Parameter | Observed Power[a] |
|---|---|---|---|---|---|---|---|---|---|
| methods | Sphericity Assumed | 205,822 | 4 | 51,455 | 225,967 | ,000 | ,983 | 903,870 | 1,000 |
| | Greenhouse-Geisser | 205,822 | 1,321 | 155,858 | 225,967 | ,000 | ,983 | 298,406 | 1,000 |
| | Huynh-Feldt | 205,822 | 1,718 | 119,813 | 225,967 | ,000 | ,983 | 388,179 | 1,000 |
| | Lower-bound | 205,822 | 1,000 | 205,822 | 225,967 | ,000 | ,983 | 225,967 | 1,000 |
| Error(methods) | Sphericity Assumed | 3,643 | 16 | ,228 | | | | | |
| | Greenhouse-Geisser | 3,643 | 5,282 | ,690 | | | | | |
| | Huynh-Feldt | 3,643 | 6,871 | ,530 | | | | | |
| | Lower-bound | 3,643 | 4,000 | ,911 | | | | | |
| masks | Sphericity Assumed | 1902,300 | 3 | 634,100 | 563,569 | ,000 | ,993 | 1690,708 | 1,000 |
| | Greenhouse-Geisser | 1902,300 | 1,339 | 1420,978 | 563,569 | ,000 | ,993 | 754,465 | 1,000 |
| | Huynh-Feldt | 1902,300 | 1,764 | 1078,598 | 563,569 | ,000 | ,993 | 993,954 | 1,000 |
| | Lower-bound | 1902,300 | 1,000 | 1902,300 | 563,569 | ,000 | ,993 | 563,569 | 1,000 |
| Error(masks) | Sphericity Assumed | 13,502 | 12 | 1,125 | | | | | |
| | Greenhouse-Geisser | 13,502 | 5,355 | 2,521 | | | | | |
| | Huynh-Feldt | 13,502 | 7,055 | 1,914 | | | | | |
| | Lower-bound | 13,502 | 4,000 | 3,375 | | | | | |
| methods * masks | Sphericity Assumed | 26,753 | 12 | 2,229 | 21,622 | ,000 | ,844 | 259,465 | 1,000 |
| | Greenhouse-Geisser | 26,753 | 2,498 | 10,709 | 21,622 | ,000 | ,844 | 54,014 | 1,000 |
| | Huynh-Feldt | 26,753 | 6,985 | 3,830 | 21,622 | ,000 | ,844 | 151,026 | 1,000 |
| | Lower-bound | 26,753 | 1,000 | 26,753 | 21,622 | ,010 | ,844 | 21,622 | ,927 |
| Error(methods*masks) | Sphericity Assumed | 4,949 | 48 | ,103 | | | | | |
| | Greenhouse-Geisser | 4,949 | 9,992 | ,495 | | | | | |
| | Huynh-Feldt | 4,949 | 27,939 | ,177 | | | | | |
| | Lower-bound | 4,949 | 4,000 | 1,237 | | | | | |

a. Computed using alpha = ,05

Figure 5.16: Result of Tests of Within-Subjects Effects for PSNR

### The Main Effect of Methods

The hypotheses of methods in RANOVA are as follows:
$H_0$: $\mu 1_{PSNR}$ = $\mu 2_{PSNR}$ = $\mu 3_{PSNR}$ = $\mu 4_{PSNR}$=$\mu 5_{PSNR}$
versus
$H_1$: Means are not all equal.
Methods are defined as 1. KRIGING, 2. ANNs, 3. PDE, 4. MARS and 5. CMARS, respectively.
Output 5.17 shows the descriptive statistics of the main effect of methods. Performances have the following rank: PDE, ANNs, KRIGING, CMARS and MARS.

**Estimates**

Measure: psnr

| methods | Mean | Std. Error | 95% Confidence Interval | |
|---|---|---|---|---|
| | | | Lower Bound | Upper Bound |
| 1 | 30,182 | ,611 | 28,486 | 31,877 |
| 2 | 30,360 | ,546 | 28,844 | 31,876 |
| 3 | 32,512 | ,613 | 30,810 | 34,214 |
| 4 | 28,600 | ,655 | 26,782 | 30,418 |
| 5 | 28,630 | ,655 | 26,812 | 30,448 |

Figure 5.17: Estimated results of method for PSNR

Output 5.18 shows the results of Bonferroni tests. According to RANOVA test, there is a difference between the methods. Post hoc tests reveal which specific methods differed.

**Pairwise Comparisons**

Measure: psnr

| (I) methods | (J) methods | Mean Difference (I-J) | Std. Error | Sig.[a] | 95% Confidence Interval for Difference[a] | |
|---|---|---|---|---|---|---|
| | | | | | Lower Bound | Upper Bound |
| 1 | 2 | -,178 | ,138 | 1,000 | -,951 | ,595 |
| | 3 | -2,330* | ,088 | ,000 | -2,824 | -1,836 |
| | 4 | 1,582* | ,103 | ,001 | 1,008 | 2,156 |
| | 5 | 1,551* | ,101 | ,001 | ,987 | 2,115 |
| 2 | 1 | ,178 | ,138 | 1,000 | -,595 | ,951 |
| | 3 | -2,152* | ,121 | ,001 | -2,829 | -1,475 |
| | 4 | 1,760* | ,228 | ,015 | ,484 | 3,035 |
| | 5 | 1,729* | ,225 | ,015 | ,469 | 2,990 |
| 3 | 1 | 2,330* | ,088 | ,000 | 1,836 | 2,824 |
| | 2 | 2,152* | ,121 | ,001 | 1,475 | 2,829 |
| | 4 | 3,912* | ,180 | ,000 | 2,903 | 4,920 |
| | 5 | 3,881* | ,174 | ,000 | 2,907 | 4,856 |
| 4 | 1 | -1,582* | ,103 | ,001 | -2,156 | -1,008 |
| | 2 | -1,760* | ,228 | ,015 | -3,035 | -,484 |
| | 3 | -3,912* | ,180 | ,000 | -4,920 | -2,903 |
| | 5 | -,030 | ,015 | 1,000 | -,112 | ,051 |
| 5 | 1 | -1,551* | ,101 | ,001 | -2,115 | -,987 |
| | 2 | -1,729* | ,225 | ,015 | -2,990 | -,469 |
| | 3 | -3,881* | ,174 | ,000 | -4,856 | -2,907 |
| | 4 | ,030 | ,015 | 1,000 | -,051 | ,112 |

Based on estimated marginal means

*. The mean difference is significant at the ,05 level.

a. Adjustment for multiple comparisons: Bonferroni.

Figure 5.18: Result of Pairwise Comparisons of method for PSNR

Here is the results of the post hoc tests:

- Kriging method is significantly different from the PDE, MARS and CMARS methods, except ANNs.
- ANNs method is significantly different from the PDE, MARS and CMARS methods, except Kriging.
- PDE method is significantly different from all methods.
- MARS method is significantly different from the Kriging, ANNs and PDE methods, except CMARS.

- CMARS method is significantly different from the Kriging, ANNs and PDE methods, except MARS.

### The Main Effect of Masks

The hypotheses of masks in RANOVA are as follows:

$H_0$: $\mu_{1_{PSNR}} = \mu_{2_{PSNR}} = \mu_{3_{PSNR}} = \mu_{4_{PSNR}}$
versus
$H_1$: Means are not all equal.
Masks are defined as Mask 1, Mask 2, Mask 3 and Mask 4, respectively.
Output 5.19 shows the descriptive statistics of the main effect of masks. Performances have the following rank: Mask 1, Mask 2, Mask 3 and Mask 4.

**Estimates**

Measure: psnr

| masks | Mean | Std. Error | 95% Confidence Interval Lower Bound | 95% Confidence Interval Upper Bound |
|---|---|---|---|---|
| 1 | 36,820 | ,761 | 34,708 | 38,932 |
| 2 | 30,159 | ,694 | 28,233 | 32,086 |
| 3 | 28,463 | ,543 | 26,956 | 29,970 |
| 4 | 24,784 | ,517 | 23,349 | 26,219 |

Figure 5.19: Estimated results of mask for PSNR

Output 5.20 shows the results of Bonferroni tests. Post hoc tests reveal which specific masks differ.

**Pairwise Comparisons**

Measure: psnr

| (I) masks | (J) masks | Mean Difference (I-J) | Std. Error | Sig.[a] | 95% Confidence Interval for Difference[a] Lower Bound | 95% Confidence Interval for Difference[a] Upper Bound |
|---|---|---|---|---|---|---|
| 1 | 2 | 6,661* | ,189 | ,000 | 5,745 | 7,576 |
| | 3 | 8,357* | ,349 | ,000 | 6,665 | 10,049 |
| | 4 | 12,036* | ,363 | ,000 | 10,276 | 13,796 |
| 2 | 1 | -6,661* | ,189 | ,000 | -7,576 | -5,745 |
| | 3 | 1,696* | ,334 | ,042 | ,077 | 3,315 |
| | 4 | 5,375* | ,368 | ,001 | 3,592 | 7,158 |
| 3 | 1 | -8,357* | ,349 | ,000 | -10,049 | -6,665 |
| | 2 | -1,696* | ,334 | ,042 | -3,315 | -,077 |
| | 4 | 3,679* | ,068 | ,000 | 3,348 | 4,010 |
| 4 | 1 | -12,036* | ,363 | ,000 | -13,796 | -10,276 |
| | 2 | -5,375* | ,368 | ,001 | -7,158 | -3,592 |
| | 3 | -3,679* | ,068 | ,000 | -4,010 | -3,348 |

Based on estimated marginal means

*. The mean difference is significant at the ,05 level.

a. Adjustment for multiple comparisons: Bonferroni.

Figure 5.20: Result of Pairwise Comparisons of mask for PSNR

Here is the results of the post hoc tests:

- All masks are significantly different from each other. (All $p_{values}$<.05).

### The Interaction Between Methods and Masks

The hypotheses of the interaction between methods and masks in RANOVA is as follows:
$H_0$: There is an interaction between the methods and masks.
versus
$H_1$: There is no an interaction between the methods and masks.
Methods are defined as 1. KRIGING, 2. ANNs, 3. PDE, 4. MARS and 5. CMARS, respectively.
Masks are defined as Mask 1, Mask 2, Mask 3 and Mask 4, respectively.
Output 5.21a shows the results of Bonferroni tests. According to RANOVA test, there is an interaction between methods and masks.

3. methods * masks

Measure: psnr

| methods | | Mean | Std. Error | 95% Confidence Interval Lower Bound | Upper Bound |
|---|---|---|---|---|---|
| 1 | 1 | 35,6021 | ,722 | 33,597 | 37,607 |
| | 2 | 30,5546 | ,664 | 28,711 | 32,398 |
| | 3 | 29,0662 | ,531 | 27,592 | 30,540 |
| | 4 | 25,5038 | ,582 | 23,888 | 27,120 |
| 2 | 1 | 37,8225 | ,794 | 35,618 | 40,027 |
| | 2 | 30,1077 | ,584 | 28,485 | 31,730 |
| | 3 | 28,8448 | ,455 | 27,582 | 30,107 |
| | 4 | 24,6641 | ,503 | 23,269 | 26,059 |
| 3 | 1 | 39,9796 | ,867 | 37,573 | 42,386 |
| | 2 | 31,7263 | ,635 | 29,964 | 33,489 |
| | 3 | 31,1079 | ,525 | 29,649 | 32,566 |
| | 4 | 27,2328 | ,556 | 25,688 | 28,778 |
| 4 | 1 | 35,3479 | ,764 | 33,228 | 37,468 |
| | 2 | 29,1454 | ,823 | 26,860 | 31,431 |
| | 3 | 26,6469 | ,623 | 24,917 | 28,377 |
| | 4 | 23,2594 | ,502 | 21,866 | 24,653 |
| 5 | 1 | 35,3481 | ,766 | 33,220 | 37,476 |
| | 2 | 29,2620 | ,810 | 27,013 | 31,511 |
| | 3 | 26,6505 | ,623 | 24,920 | 28,381 |
| | 4 | 23,2608 | ,501 | 21,869 | 24,653 |

(a) Result of Pairwise Comparisons of interaction for PSNR

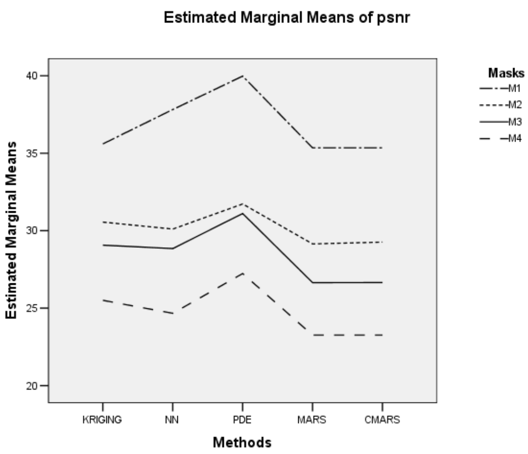


(b) Estimated marginal means for PSNR

Figure 5.21: Result of Interaction for PSNR

Here is the results of the post hoc tests in terms of PSNR criterion:

- Mean of PSNR values vary between 39.9796 to 23.3594.

- PDEs is the best performing method in all images with all masks.
- Kriging and ANNs are competing with each other.
- MARS and CMARS are competing with each other.
- All methods perform better with Mask 1.
- All methods perform worst with Mask 4.
- Mask 2, Mask 3 and Mask 4 have the same ranking: PDE, KRIGING, ANNs, CMARS and MARS.
- Mask 1 has a slightly different ranking: PDE, ANNs, KRIGING, CMARS and MARS. That is ANN performs better than KRIGING while the others are performing the same as with other masks.

#### 5.4.3.2 Results of MSE

Output 5.22 provides the mean and standard deviation for each of the images in terms of MSE criterion.

**Descriptive Statistics**

| | Mean | Std. Deviation | N |
|---|---|---|---|
| kriging_M1 | ,000293 | ,0001319 | 5 |
| kriging_M2 | ,000917 | ,0003437 | 5 |
| kriging_M3 | ,001280 | ,0004147 | 5 |
| kriging_M4 | ,002920 | ,0009808 | 5 |
| nn_M1 | ,000178 | ,0000883 | 5 |
| nn_M2 | ,001008 | ,0003378 | 5 |
| nn_M3 | ,001334 | ,0003208 | 5 |
| nn_M4 | ,003520 | ,0009039 | 5 |
| pde_M1 | ,000110 | ,0000626 | 5 |
| pde_M2 | ,000710 | ,0002801 | 5 |
| pde_M3 | ,000808 | ,0002440 | 5 |
| pde_M4 | ,001960 | ,0005857 | 5 |
| mars_M1 | ,000313 | ,0001460 | 5 |
| mars_M2 | ,001312 | ,0006450 | 5 |
| mars_M3 | ,002280 | ,0007981 | 5 |
| mars_M4 | ,004860 | ,0013849 | 5 |
| cmars_M1 | ,000313 | ,0001466 | 5 |
| cmars_M2 | ,001283 | ,0006082 | 5 |
| cmars_M3 | ,002280 | ,0007981 | 5 |
| cmars_M4 | ,004860 | ,0013849 | 5 |

Figure 5.22: Descriptive Statistics of MSE

Output 5.23 shows that Mauchly's test statistics is significant for both methods and masks because probability values are less than .05 ($p_{value}$=.001 and $p_{value}$=.020). Thus, there are significant differences between variance of differences. And the condition of sphericity has not been met, and we consider the corrected F-ratio of Greenhouse-Geisser.

**Mauchly's Test of Sphericity**[b]

Measure: mse

| Within Subjects Effect | Mauchly's W | Approx. Chi-Square | df | Sig. | Epsilon[a] Greenhouse-Geisser | Huynh-Feldt | Lower-bound |
|---|---|---|---|---|---|---|---|
| methods | ,000 | 33,609 | 9 | ,001 | ,275 | ,301 | ,250 |
| masks | ,005 | 14,287 | 5 | ,020 | ,361 | ,390 | ,333 |
| methods * masks | ,000 | . | 77 | . | ,162 | ,315 | ,083 |

Tests the null hypothesis that the error covariance matrix of the orthonormalized transformed dependent variables is proportional to an identity matrix.

a. May be used to adjust the degrees of freedom for the averaged tests of significance. Corrected tests are displayed in the Tests of Within-Subjects Effects table.

b. Design: Intercept
Within Subjects Design: methods+masks+methods*masks

Figure 5.23: Results of Mauchly's Test of Sphericity for MSE

According to Output 5.24, methods are significant (F(1.01, 4.34)=35.05, $p_{value}$<.05). And, mask has an effect of MSE (because (F(1.08, 4.33)=67.54, $p_{value}$<.05) ). And there is an interaction between masks and methods (F(1.95, 7.80)=41.03, $p_{value}$<.05). Thus, both masks and methods are needed, as well as their interaction to explain MSE value. In other words, MSE value is related to type of mask, method and interaction of mask and method.

**Tests of Within-Subjects Effects**

Measure: mse

| Source | | Type III Sum of Squares | df | Mean Square | F | Sig. | Partial Eta Squared | Noncent. Parameter | Observed Power[a] |
|---|---|---|---|---|---|---|---|---|---|
| methods | Sphericity Assumed | 2,50E-005 | 4 | 6,25E-006 | 35,048 | ,000 | ,898 | 140,193 | 1,000 |
| | Greenhouse-Geisser | 2,50E-005 | 1,099 | 2,28E-005 | 35,048 | ,003 | ,898 | 38,509 | ,995 |
| | Huynh-Feldt | 2,50E-005 | 1,204 | 2,08E-005 | 35,048 | ,002 | ,898 | 42,206 | ,997 |
| | Lower-bound | 2,50E-005 | 1,000 | 2,50E-005 | 35,048 | ,004 | ,898 | 35,048 | ,990 |
| Error(methods) | Sphericity Assumed | 2,85E-006 | 16 | 1,78E-007 | | | | | |
| | Greenhouse-Geisser | 2,85E-006 | 4,395 | 6,49E-007 | | | | | |
| | Huynh-Feldt | 2,85E-006 | 4,817 | 5,93E-007 | | | | | |
| | Lower-bound | 2,85E-006 | 4,000 | 7,14E-007 | | | | | |
| masks | Sphericity Assumed | ,000 | 3 | 5,21E-005 | 67,535 | ,000 | ,944 | 202,605 | 1,000 |
| | Greenhouse-Geisser | ,000 | 1,083 | ,000 | 67,535 | ,001 | ,944 | 73,116 | 1,000 |
| | Huynh-Feldt | ,000 | 1,170 | ,000 | 67,535 | ,001 | ,944 | 79,014 | 1,000 |
| | Lower-bound | ,000 | 1,000 | ,000 | 67,535 | ,001 | ,944 | 67,535 | 1,000 |
| Error(masks) | Sphericity Assumed | 9,25E-006 | 12 | 7,71E-007 | | | | | |
| | Greenhouse-Geisser | 9,25E-006 | 4,331 | 2,14E-006 | | | | | |
| | Huynh-Feldt | 9,25E-006 | 4,680 | 1,98E-006 | | | | | |
| | Lower-bound | 9,25E-006 | 4,000 | 2,31E-006 | | | | | |
| methods * masks | Sphericity Assumed | 1,67E-005 | 12 | 1,39E-006 | 41,026 | ,000 | ,911 | 492,312 | 1,000 |
| | Greenhouse-Geisser | 1,67E-005 | 1,949 | 8,58E-006 | 41,026 | ,000 | ,911 | 79,970 | 1,000 |
| | Huynh-Feldt | 1,67E-005 | 3,777 | 4,43E-006 | 41,026 | ,000 | ,911 | 154,966 | 1,000 |
| | Lower-bound | 1,67E-005 | 1,000 | 1,67E-005 | 41,026 | ,003 | ,911 | 41,026 | ,996 |
| Error(methods*masks) | Sphericity Assumed | 1,63E-006 | 48 | 3,40E-008 | | | | | |
| | Greenhouse-Geisser | 1,63E-006 | 7,797 | 2,09E-007 | | | | | |
| | Huynh-Feldt | 1,63E-006 | 15,109 | 1,08E-007 | | | | | |
| | Lower-bound | 1,63E-006 | 4,000 | 4,08E-007 | | | | | |

a. Computed using alpha = ,05

Figure 5.24: Result of Tests of Within-Subjects Effects for MSE

### The Main Effect of Methods

The hypotheses of methods in RANOVA are as follows:

$H_0$: $\mu_{1_{MSE}} = \mu_{2_{MSE}} = \mu_{3_{MSE}} = \mu_{4_{MSE}} = \mu_{5_{MSE}}$

versus

$H_1$: Means are not all equal.

Methods are defined as 1. KRIGING, 2. ANNs, 3. PDE, 4. MARS and 5. CMARS, respectively.

Output 5.25 shows the descriptive statistics of the main effect of methods. Performances have the following rank: PDE, KRIGING, ANNs, CMARS and MARS.

**Estimates**

Measure: mse

| methods | Mean | Std. Error | 95% Confidence Interval | |
|---|---|---|---|---|
| | | | Lower Bound | Upper Bound |
| 1 | ,00135 | ,000 | ,001 | ,002 |
| 2 | ,00151 | ,000 | ,001 | ,002 |
| 3 | ,00090 | ,000 | ,001 | ,001 |
| 4 | ,00219 | ,000 | ,001 | ,003 |
| 5 | ,00218 | ,000 | ,001 | ,003 |

Figure 5.25: Estimated results of method for MSE

Output 5.26 shows the results of Bonferroni tests. According to RANOVA test, there is a difference between the methods. Post hoc tests reveals which specific methods differ.

**Pairwise Comparisons**

Measure: mse

| (I) methods | (J) methods | Mean Difference (I-J) | Std. Error | Sig.[a] | 95% Confidence Interval for Difference[a] | |
|---|---|---|---|---|---|---|
| | | | | | Lower Bound | Upper Bound |
| 1 | 2 | ,000 | ,000 | ,708 | -,001 | ,000 |
| | 3 | ,000* | ,000 | ,048 | 4,63E-006 | ,001 |
| | 4 | -,001* | ,000 | ,025 | -,002 | ,000 |
| | 5 | -,001* | ,000 | ,024 | -,002 | ,000 |
| 2 | 1 | ,000 | ,000 | ,708 | ,000 | ,001 |
| | 3 | ,001* | ,000 | ,005 | ,000 | ,001 |
| | 4 | -,001 | ,000 | ,146 | -,002 | ,000 |
| | 5 | -,001 | ,000 | ,140 | -,002 | ,000 |
| 3 | 1 | ,000* | ,000 | ,048 | -,001 | -4,63E-006 |
| | 2 | -,001* | ,000 | ,005 | -,001 | ,000 |
| | 4 | -,001* | ,000 | ,031 | -,002 | ,000 |
| | 5 | -,001* | ,000 | ,029 | -,002 | ,000 |
| 4 | 1 | ,001* | ,000 | ,025 | ,000 | ,002 |
| | 2 | ,001 | ,000 | ,146 | ,000 | ,002 |
| | 3 | ,001* | ,000 | ,031 | ,000 | ,002 |
| | 5 | 7,04E-006 | ,000 | 1,000 | -2,02E-005 | 3,43E-005 |
| 5 | 1 | ,001* | ,000 | ,024 | ,000 | ,002 |
| | 2 | ,001 | ,000 | ,140 | ,000 | ,002 |
| | 3 | ,001* | ,000 | ,029 | ,000 | ,002 |
| | 4 | -7,04E-006 | ,000 | 1,000 | -3,43E-005 | 2,02E-005 |

Based on estimated marginal means

*. The mean difference is significant at the ,05 level.

a. Adjustment for multiple comparisons: Bonferroni.

Figure 5.26: Result of Pairwise Comparisons of method for MSE

Here is the results of the post hoc tests:

- Kriging method is significantly different from the PDE, MARS and CMARS methods, except ANNs.
- ANNs method is significantly different from PDE.
- PDE method is significantly different from all methods.

- MARS method is significantly different from KRIGING and PDE.
- CMARS method is significantly different from KRIGING and PDE.

### The Main Effect of Masks

The hypotheses of masks in RANOVA are as follows:
$H_0$: $\mu_{1_{MSE}} = \mu_{2_{MSE}} = \mu_{3_{MSE}} = \mu_{4_{MSE}}$
versus
$H_1$: Means are not all equal.
Masks are defined as Mask 1, Mask 2, Mask 3 and Mask 4, respectively.
Output 5.27 shows the descriptive statistics of the main effect of masks. Performances have the following rank: Mask 1, Mask 2, Mask 3 and Mask 4.

**Estimates**

Measure: mse

| masks | Mean | Std. Error | 95% Confidence Interval Lower Bound | 95% Confidence Interval Upper Bound |
|---|---|---|---|---|
| 1 | ,00024 | ,00005 | ,000 | ,000 |
| 2 | ,00105 | ,00020 | ,001 | ,002 |
| 3 | ,00160 | ,00023 | ,001 | ,002 |
| 4 | ,00362 | ,00046 | ,002 | ,005 |

Figure 5.27: Estimated results of mask for MSE

Output 5.28 shows the results of Bonferroni tests. Post hoc tests revealed which specific masks differed.

**Pairwise Comparisons**

Measure: mse

| (I) masks | (J) masks | Mean Difference (I-J) | Std. Error | Sig.[a] | 95% Confidence Interval for Difference[a] Lower Bound | 95% Confidence Interval for Difference[a] Upper Bound |
|---|---|---|---|---|---|---|
| 1 | 2 | -,001* | ,000 | ,032 | -,002 | -9,46E-005 |
| | 3 | -,001* | ,000 | ,010 | -,002 | ,000 |
| | 4 | -,003* | ,000 | ,007 | -,005 | -,001 |
| 2 | 1 | ,001* | ,000 | ,032 | 9,46E-005 | ,002 |
| | 3 | -,001* | ,000 | ,015 | -,001 | ,000 |
| | 4 | -,003* | ,000 | ,005 | -,004 | -,001 |
| 3 | 1 | ,001* | ,000 | ,010 | ,000 | ,002 |
| | 2 | ,001* | ,000 | ,015 | ,000 | ,001 |
| | 4 | -,002* | ,000 | ,006 | -,003 | -,001 |
| 4 | 1 | ,003* | ,000 | ,007 | ,001 | ,005 |
| | 2 | ,003* | ,000 | ,005 | ,001 | ,004 |
| | 3 | ,002* | ,000 | ,006 | ,001 | ,003 |

Based on estimated marginal means

*. The mean difference is significant at the ,05 level.

a. Adjustment for multiple comparisons: Bonferroni.

Figure 5.28: Result of Pairwise Comparisons of mask for MSE

Here is the results of the post hoc tests:

- All masks are significantly different from each other.

### The Interaction Between Methods and Masks

The hypotheses of the interaction between methods and masks in RANOVA is as follows:

$H_0$: There is an interaction between the methods and masks.

versus

$H_1$: There is no an interaction between the methods and masks.

Methods are defined as 1. KRIGING, 2. ANNs, 3. PDE, 4. MARS and 5. CMARS, respectively.

Masks are defined as Mask 1, Mask 2, Mask 3 and Mask 4, respectively.

Output 5.29a shows the results of Bonferroni tests. According to RANOVA test, there is a difference between the interaction between methods and masks.

**3. methods * masks**

Measure: mse

| methods | masks | Mean | Std. Error | 95% Confidence Interval Lower Bound | 95% Confidence Interval Upper Bound |
|---|---|---|---|---|---|
| 1 | 1 | ,0002932 | ,000 | ,000 | ,000 |
| | 2 | ,0009174 | ,000 | ,000 | ,001 |
| | 3 | ,0012800 | ,000 | ,001 | ,002 |
| | 4 | ,0029200 | ,000 | ,002 | ,004 |
| 2 | 1 | ,0001782 | ,000 | 6,85E-005 | ,000 |
| | 2 | ,0010076 | ,000 | ,001 | ,001 |
| | 3 | ,0013344 | ,000 | ,001 | ,002 |
| | 4 | ,0035200 | ,000 | ,002 | ,005 |
| 3 | 1 | ,0001104 | ,000 | 3,27E-005 | ,000 |
| | 2 | ,0007097 | ,000 | ,000 | ,001 |
| | 3 | ,0008076 | ,000 | ,001 | ,001 |
| | 4 | ,0019600 | ,000 | ,001 | ,003 |
| 4 | 1 | ,0003129 | ,000 | ,000 | ,000 |
| | 2 | ,0013116 | ,000 | ,001 | ,002 |
| | 3 | ,0022800 | ,000 | ,001 | ,003 |
| | 4 | ,0048600 | ,001 | ,003 | ,007 |
| 5 | 1 | ,0003131 | ,000 | ,000 | ,000 |
| | 2 | ,0012833 | ,000 | ,001 | ,002 |
| | 3 | ,0022800 | ,000 | ,001 | ,003 |
| | 4 | ,0048600 | ,001 | ,003 | ,007 |

(a) Result of Pairwise Comparisons of interaction for MSE

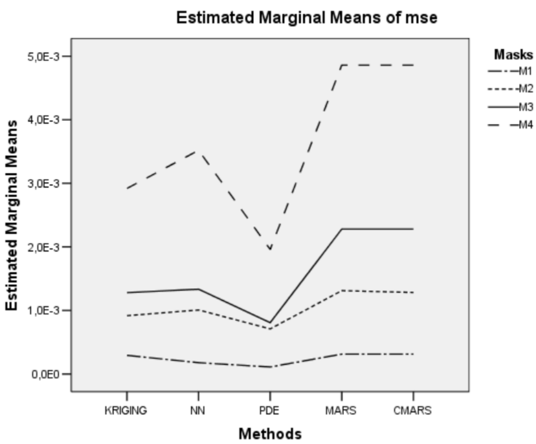


(b) Estimated marginal means for MSE

Figure 5.29: Result of Interaction for MSE

Here is the results of the post hoc tests in terms of MSE criterion:

- Mean of MSE values vary between 1.10E-4 to 4.86E-3.
- PDEs is the best performing method in all images with all masks.

- Kriging and ANNs are competing with each other.
- MARS and CMARS are competing with each other.
- All methods perform better with Mask 1.
- All methods perform worst with Mask 4.
- Mask 1 has the following ranking: PDE, ANNs, KRIGING, MARS and CMARS.
- Mask 2 has the following rank: PDE, KRIGING, ANNs, CMARS and MARS.
- Mask 3 and Mask 4 have the same ranking: PDE, KRIGING, ANNs following by equal performances of CMARS and MARS.

#### 5.4.3.3 Results of SSMI

Output 5.30 provides the mean and standard deviation for each of the images in terms of SSMI criterion.

**Descriptive Statistics**

| | Mean | Std. Deviation | N |
|---|---|---|---|
| kriging_M1 | ,98928 | ,0016362 | 5 |
| kriging_M2 | ,96510 | ,0039579 | 5 |
| kriging_M3 | ,95000 | ,0069853 | 5 |
| kriging_M4 | ,88056 | ,0111892 | 5 |
| nn_M1 | ,98932 | ,0012008 | 5 |
| nn_M2 | ,94722 | ,0069417 | 5 |
| nn_M3 | ,92346 | ,0127598 | 5 |
| nn_M4 | ,83252 | ,0260157 | 5 |
| pde_M1 | ,99500 | ,0010368 | 5 |
| pde_M2 | ,97050 | ,0034022 | 5 |
| pde_M3 | ,96322 | ,0052780 | 5 |
| pde_M4 | ,91366 | ,0109061 | 5 |
| mars_M1 | ,98196 | ,0043964 | 5 |
| mars_M2 | ,94580 | ,0108148 | 5 |
| mars_M3 | ,89206 | ,0227644 | 5 |
| mars_M4 | ,80526 | ,0283333 | 5 |
| cmars_M1 | ,98194 | ,0044529 | 5 |
| cmars_M2 | ,94550 | ,0115689 | 5 |
| cmars_M3 | ,89204 | ,0227038 | 5 |
| cmars_M4 | ,80524 | ,0282854 | 5 |

Figure 5.30: Descriptive Statistics of SSMI

Output 5.31 shows that Mauchly's test statistics is significant for methods ($p_{value}$=.011) and Greenhouse-Geisser test is important. On the other hand, the condition of sphericity has been met for masks.

Mauchly's Test of Sphericity[b]

Measure: ssmi

| Within Subjects Effect | Mauchly's W | Approx. Chi-Square | df | Sig. | Epsilon[a] Greenhouse-Geisser | Huynh-Feldt | Lower-bound |
|---|---|---|---|---|---|---|---|
| methods | ,000 | 24,596 | 9 | ,011 | ,315 | ,392 | ,250 |
| masks | ,036 | 9,029 | 5 | ,128 | ,415 | ,510 | ,333 |
| methods * masks | ,000 | . | 77 | . | ,140 | ,231 | ,083 |

Tests the null hypothesis that the error covariance matrix of the orthonormalized transformed dependent variables is proportional to an identity matrix.

a. May be used to adjust the degrees of freedom for the averaged tests of significance. Corrected tests are displayed in the Tests of Within-Subjects Effects table.

b. Design: Intercept
Within Subjects Design: methods+masks+methods*masks

Figure 5.31: Results of Mauchly's Test of Sphericity for SSMI

Output 5.32 includes corrected F values and F values for masks, methods and interaction between these two variables. According to results, methods are significant (F(1.26, 5.04)=34.58, $p_{value}$<.05). And, mask type has an effect of MSE (because (F(3, 12)=431.01, $p_{value}$<.05) ). And there is an interaction between masks and methods (F(1.68, 6.73)=31.80, $p_{value}$<.05).
Thus, methods, masks and interaction between masks and methods need to explain the SSMI value.

Tests of Within-Subjects Effects

Measure: ssmi

| Source | | Type III Sum of Squares | df | Mean Square | F | Sig. | Partial Eta Squared | Noncent. Parameter | Observed Power[a] |
|---|---|---|---|---|---|---|---|---|---|
| methods | Sphericity Assumed | ,047 | 4 | ,012 | 34,584 | ,000 | ,896 | 138,338 | 1,000 |
| | Greenhouse-Geisser | ,047 | 1,259 | ,038 | 34,584 | ,002 | ,896 | 43,532 | ,998 |
| | Huynh-Feldt | ,047 | 1,566 | ,030 | 34,584 | ,001 | ,896 | 54,169 | 1,000 |
| | Lower-bound | ,047 | 1,000 | ,047 | 34,584 | ,004 | ,896 | 34,584 | ,989 |
| Error(methods) | Sphericity Assumed | ,005 | 16 | ,000 | | | | | |
| | Greenhouse-Geisser | ,005 | 5,035 | ,001 | | | | | |
| | Huynh-Feldt | ,005 | 6,265 | ,001 | | | | | |
| | Lower-bound | ,005 | 4,000 | ,001 | | | | | |
| masks | Sphericity Assumed | ,269 | 3 | ,090 | 431,011 | ,000 | ,991 | 1293,032 | 1,000 |
| | Greenhouse-Geisser | ,269 | 1,244 | ,216 | 431,011 | ,000 | ,991 | 536,099 | 1,000 |
| | Huynh-Feldt | ,269 | 1,531 | ,176 | 431,011 | ,000 | ,991 | 659,779 | 1,000 |
| | Lower-bound | ,269 | 1,000 | ,269 | 431,011 | ,000 | ,991 | 431,011 | 1,000 |
| Error(masks) | Sphericity Assumed | ,002 | 12 | ,000 | | | | | |
| | Greenhouse-Geisser | ,002 | 4,975 | ,001 | | | | | |
| | Huynh-Feldt | ,002 | 6,123 | ,000 | | | | | |
| | Lower-bound | ,002 | 4,000 | ,001 | | | | | |
| methods * masks | Sphericity Assumed | ,024 | 12 | ,002 | 31,802 | ,000 | ,888 | 381,626 | 1,000 |
| | Greenhouse-Geisser | ,024 | 1,683 | ,014 | 31,802 | ,000 | ,888 | 53,520 | 1,000 |
| | Huynh-Feldt | ,024 | 2,768 | ,009 | 31,802 | ,000 | ,888 | 88,039 | 1,000 |
| | Lower-bound | ,024 | 1,000 | ,024 | 31,802 | ,005 | ,888 | 31,802 | ,983 |
| Error(methods*masks) | Sphericity Assumed | ,003 | 48 | 6,24E-005 | | | | | |
| | Greenhouse-Geisser | ,003 | 6,732 | ,000 | | | | | |
| | Huynh-Feldt | ,003 | 11,073 | ,000 | | | | | |
| | Lower-bound | ,003 | 4,000 | ,001 | | | | | |

a. Computed using alpha = ,05

Figure 5.32: Result of Tests of Within-Subjects Effects for SSMI

### The Main Effect of Methods

The hypotheses of methods in RANOVA are as follows:
$H_0$: $\mu_{1_{SSMI}}$ = $\mu_{2_{SSMI}}$ = $\mu_{3_{SSMI}}$ = $\mu_{4_{SSMI}}$=$\mu_{5_{SSMI}}$
versus
$H_1$: Means are not all equal.
Output 5.33 shows the descriptive statistics of the main effect of methods. Performances have the following rank: PDE, KRIGING, ANNs, MARS and CMARS.

**Estimates**

Measure: ssmi

| methods | Mean | Std. Error | 95% Confidence Interval | |
|---|---|---|---|---|
| | | | Lower Bound | Upper Bound |
| 1 | ,9462 | ,0022 | ,940 | ,952 |
| 2 | ,9231 | ,0051 | ,909 | ,937 |
| 3 | ,9606 | ,0021 | ,955 | ,967 |
| 4 | ,9063 | ,0072 | ,886 | ,926 |
| 5 | ,9062 | ,0073 | ,886 | ,926 |

Figure 5.33: Estimated results of method for SSMI

Output 5.34 shows the results of Bonferroni tests. According to RANOVA test, there is a difference between the methods.

**Pairwise Comparisons**

Measure: ssmi

| (I) methods | (J) methods | Mean Difference (I-J) | Std. Error | Sig.[a] | 95% Confidence Interval for Difference[a] | |
|---|---|---|---|---|---|---|
| | | | | | Lower Bound | Upper Bound |
| 1 | 2 | ,023 | ,006 | ,193 | -,011 | ,057 |
| | 3 | -,014* | ,001 | ,001 | -,020 | -,009 |
| | 4 | ,040 | ,007 | ,050 | -5,89E-005 | ,080 |
| | 5 | ,040 | ,007 | ,055 | -,001 | ,081 |
| 2 | 1 | -,023 | ,006 | ,193 | -,057 | ,011 |
| | 3 | -,037* | ,007 | ,049 | -,075 | ,000 |
| | 4 | ,017 | ,004 | ,117 | -,005 | ,038 |
| | 5 | ,017 | ,004 | ,102 | -,004 | ,038 |
| 3 | 1 | ,014* | ,001 | ,001 | ,009 | ,020 |
| | 2 | ,037* | ,007 | ,049 | ,000 | ,075 |
| | 4 | ,054* | ,008 | ,023 | ,010 | ,098 |
| | 5 | ,054* | ,008 | ,025 | ,009 | ,099 |
| 4 | 1 | -,040 | ,007 | ,050 | -,080 | 5,89E-005 |
| | 2 | -,017 | ,004 | ,117 | -,038 | ,005 |
| | 3 | -,054* | ,008 | ,023 | -,098 | -,010 |
| | 5 | 9,00E-005 | ,000 | 1,000 | -,002 | ,002 |
| 5 | 1 | -,040 | ,007 | ,055 | -,081 | ,001 |
| | 2 | -,017 | ,004 | ,102 | -,038 | ,004 |
| | 3 | -,054* | ,008 | ,025 | -,099 | -,009 |
| | 4 | -9,00E-005 | ,000 | 1,000 | -,002 | ,002 |

Based on estimated marginal means

*. The mean difference is significant at the ,05 level.

a. Adjustment for multiple comparisons: Bonferroni.

Figure 5.34: Result of Pairwise Comparisons of method for SSMI

Here is the results of the post hoc tests:

- Kriging method is significantly different from PDE.
- ANNs method is significantly different from PDE.
- PDE method is significantly different from all methods except ANNs.
- MARS method is significantly different from PDE.
- CMARS method is significantly different from PDE.

### The Main Effect of Masks

The hypotheses of masks in RANOVA are as follows:

$H_0$: $\mu_{1_{SSMI}} = \mu_{2_{SSMI}} = \mu_{3_{SSMI}} = \mu_{4_{SSMI}}$

versus

$H_1$: Means are not all equal.

Masks are defined as Mask 1, Mask 2, Mask 3 and Mask 4, respectively.

Output 5.35 shows the descriptive statistics of the main effect of masks. Performances have the following rank: Mask 1, Mask 2, Mask 3 and Mask 4.

**Estimates**

Measure: ssmi

| masks | Mean | Std. Error | 95% Confidence Interval | |
|---|---|---|---|---|
| | | | Lower Bound | Upper Bound |
| 1 | ,988 | ,001 | ,985 | ,990 |
| 2 | ,955 | ,003 | ,947 | ,963 |
| 3 | ,924 | ,005 | ,912 | ,937 |
| 4 | ,847 | ,007 | ,827 | ,868 |

Figure 5.35: Estimated results of mask for SSMI

Output 5.36 shows the results of Bonferroni tests.

**Pairwise Comparisons**

Measure: ssmi

| (I) masks | (J) masks | Mean Difference (I-J) | Std. Error | Sig.[a] | 95% Confidence Interval for Difference[a] | |
|---|---|---|---|---|---|---|
| | | | | | Lower Bound | Upper Bound |
| 1 | 2 | ,033* | ,002 | ,000 | ,023 | ,042 |
| | 3 | ,063* | ,004 | ,000 | ,045 | ,081 |
| | 4 | ,140* | ,006 | ,000 | ,109 | ,171 |
| 2 | 1 | -,033* | ,002 | ,000 | -,042 | -,023 |
| | 3 | ,031* | ,003 | ,002 | ,018 | ,044 |
| | 4 | ,107* | ,005 | ,000 | ,084 | ,131 |
| 3 | 1 | -,063* | ,004 | ,000 | -,081 | -,045 |
| | 2 | -,031* | ,003 | ,002 | -,044 | -,018 |
| | 4 | ,077* | ,003 | ,000 | ,060 | ,093 |
| 4 | 1 | -,140* | ,006 | ,000 | -,171 | -,109 |
| | 2 | -,107* | ,005 | ,000 | -,131 | -,084 |
| | 3 | -,077* | ,003 | ,000 | -,093 | -,060 |

Based on estimated marginal means

*. The mean difference is significant at the ,05 level.

a. Adjustment for multiple comparisons: Bonferroni.

Figure 5.36: Result of Pairwise Comparisons of mask for SSMI

Here is the results of the post hoc tests:

- All masks are significantly different from each other.

### The Interaction Between Methods and Masks

The hypotheses of the interaction between methods and masks in RANOVA is as follows:

$H_0$: There is an interaction between the methods and masks.

versus

$H_1$: There is no an interaction between the methods and masks.

Output 5.37a shows the results of Bonferroni tests. According to RANOVA test, there is a difference between the interaction between methods and masks. Here is the

**3. methods * masks**

Measure: ssmi

| methods | masks | Mean | Std. Error | 95% Confidence Interval Lower Bound | Upper Bound |
|---|---|---|---|---|---|
| 1 | 1 | ,98928 | ,001 | ,987 | ,991 |
| | 2 | ,96510 | ,002 | ,960 | ,970 |
| | 3 | ,95000 | ,003 | ,941 | ,959 |
| | 4 | ,88056 | ,005 | ,867 | ,894 |
| 2 | 1 | ,98932 | ,001 | ,988 | ,991 |
| | 2 | ,94722 | ,003 | ,939 | ,956 |
| | 3 | ,92346 | ,006 | ,908 | ,939 |
| | 4 | ,83252 | ,012 | ,800 | ,865 |
| 3 | 1 | ,99500 | ,000 | ,994 | ,996 |
| | 2 | ,97050 | ,002 | ,966 | ,975 |
| | 3 | ,96322 | ,002 | ,957 | ,970 |
| | 4 | ,91366 | ,005 | ,900 | ,927 |
| 4 | 1 | ,98196 | ,002 | ,977 | ,987 |
| | 2 | ,94580 | ,005 | ,932 | ,959 |
| | 3 | ,89206 | ,010 | ,864 | ,920 |
| | 4 | ,80526 | ,013 | ,770 | ,840 |
| 5 | 1 | ,98194 | ,002 | ,976 | ,987 |
| | 2 | ,94550 | ,005 | ,931 | ,960 |
| | 3 | ,89204 | ,010 | ,864 | ,920 |
| | 4 | ,80524 | ,013 | ,770 | ,840 |

(a) Result of Pairwise Comparisons of interaction for SSMI

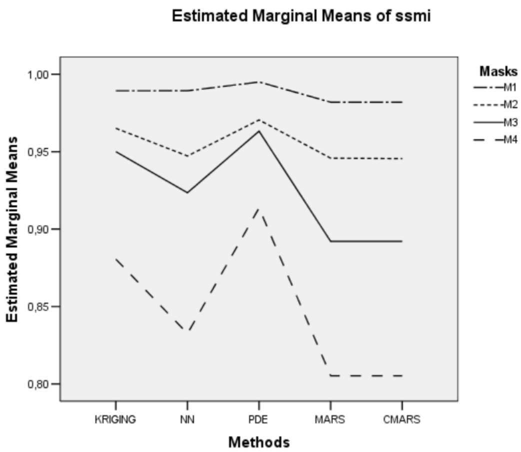


(b) Estimated marginal means for SSMI

Figure 5.37: Result of Interaction for SSMI

results of the post hoc tests in terms of SSMI criterion:

- Mean of SSMI values vary between .99 to .81.
- PDEs is the best performing method in all images with all masks.
- Kriging and ANNs are competing with each other.
- MARS and CMARS are competing with each other.
- All methods perform better with Mask 1.
- All methods perform worst with Mask 4.

- Mask 1 has the following ranking: PDE, ANNs, KRIGING, MARS and CMARS.
- Mask 2, Mask 3 and Mask 4 have the same ranking: PDE, KRIGING, ANNs, MARS and CMARS.

# CHAPTER 6

# CONCLUSION

The main purpose of this research is to examine the comparison of the computational inpainting methods' performances. Results of effects of methods, masks, images and their interaction are elaborated in Section 5.4.3. Summarized results are given below via bullets:

- Image type; in other words, frequency of the grayscale values of the image does not affect the performance.
- All performances are related to type of mask, inpainting methods and their interaction.
- From Mask 1 to Mask 4 performances of the all methods decline according to all performance measures. In addition, effects of the all masks are significantly different from each other. That was one of the expected result of our research because missing pixels are increasing from Mask 1 to Mask 4.
- PDEs is the best performing method in all images with all masks with respect to all criteria considered. Our results boost the results of the literature review. PDEs were good at small missing parts such as scratches and cracks.
- ANNs and KRIGING are competing with each other. In Mask 1, ANNs method provides better results than KRIGING method; however with other masks, KRIGING method provides better results than ANNs method with respect to all performance criteria. This slightly change between the ANNs and KRIGING is because of the mechanism of KRIGING algorithm. Mask 2, 3 and 4 cover the images of 9% to 26% whereas Mask 1 covers the only 3%. Actually,

the calculated distances become more meaningful when there are more missing parts.

- MARS and CMARS are competing with each other. According to results, CMARS has better performances because of eliminated the backward stage of the MARS method. The harsh point of CMARS was user-manually determination one of the initial value for the second step of its algorithm. If user-manually determination handover the automatic determination by algorithms, CMARS algorithm would be faster than MARS with better inpainted images.

- In this research, running times are not involved but from Mask 1 to Mask 4 as we expected algorithms needed more time to inpaint images. In addition, as mentioned in literature review, PDEs were time efficient followed by MARS, CMARS, ANNs and KRIGING.

- SSMI criterion yields HVS. According to this criterion, ANNs, KRIGING, MARS and CMARS have similar performances. If perception of visual and running time are important, MARS and CMARS can be better candidates than ANNs and KRIGING. In addition, CMARS has a slightly better performance than MARS with respect to PSNR and MSE criteria. If this slight difference is important, CMARS can be selected as the best among the interpolation based inpainting considered.

This research is the first in terms of using MARS and CMARS methods in image inpainting domain. Possible future work can be using these methods on object removing case. Yet another possible future work can be changing the main focus as examining the comparison of method performances on position of missing pixel. There is no doubt that location of the missing pixel and its neighbors are more important than it is seen. If some parts and their neighbors are completely destroyed; in other words, there is no background information, different ANNs techniques such as using an image database can be a good candidate to inpaint. Also, we investigated gray level images, those methods could be examined in color images. Furthermore, this study can be extended to video processing. Instead of inpainting the old photographs, inpainting the old movies will add more value to today's world.

# REFERENCES


[1] Abayomi-Alli, A. A., et al. "Adaptive Regression Splines Models for Predicting Facial Image Verification and Quality Assessment Scores.", Balkan Journal of Electrical & Computer Engineering, Vol.3, No.1, 2015.

[2] Acar, Sibel. *Intersections: Architecture and Photography in Victorian Britain*, MA Thesis, Department of History of Architecture, Institute of Social Sciences, Middle East Technical University, Ankara, Turkey, Sep. 2009.

[3] Banday, Mahroosh, and Sharma, Richa. "Image Inpainting – An Inclusive Review of the Underlying Algorithm and Comparative Study of the Associated Techniques." *International Journal of Computer Applications*, Volume 98, No.17, Jul. 2014.

[4] Beers, Wim C. M. van, and Kleijnen, Jack P.C. "Kriging Interpolation in Simulation: A Survey." *Proceedings of the 2004 Winter Simulation Conference*, 2004.

[5] Bertalmio, Marcelo, et al. "Image Inpainting." Computer GRAPHics and Interactive Techniques (SIGGRAPH), New Orleans, LU, pp. 417-424, Jan. 2000.

[6] Bertalmio, Marcelo, et al. "Navier-Stokes, Fluid Dynamics, and Image and Video Inpainting." Computer Vision and Pattern Recognition (CVPR), Hawai, pp:355–362, Dec. 2001.

[7] Bertalmio, Marcelo, et al. "Simultaneous Structure and Texture Image Inpainting." *IEEE Transactions on Image Processing*, Vol. 12, No:8, August 2003, pp. 882-889. Retrieved from `http://www.math.ucla.edu/~lvese/PAPERS/01217265.pdf`. Accessed Apr. 2018.

[8] Bogdan M. Wilamowski, et al. "Improved Computation for Levenberg–Marquardt Training." *IEEE Transactions on Neural Networks*, Vol. 21, No. 6, Jun. 2010.

[9] Bostan Aslantaş, Pınar. *Analysis and Modeling of Spatially and Temporally Varying Meteorological Parameter: Precipitation Over Turkey* PhD Thesis. Geodetical and Geographical Information Technologies Department, Institute of Natural and Applied Sciences, Middle East Technical University, Ankara, Turkey, Feb. 2013.

[10] Cardinal, David. "Harnessing Histograms", PC Magazine, 19 Oct. 2004. *PCMag,* `https://www.pcmag.com/article2/0,2817,1658448,00.asp`. Accessed Apr. 2018.

[11] Carlisle, David, et al. "The Great, Big List of LaTeX Symbols." 7 Feb. 2001. Retrieved from `https://www.rpi.edu/dept/arc/training/latex/LaTeX_symbols.pdf`. Accessed Apr. 2018.

[12] Chan Tony F., and Shen, Jianhong. "Local inpainting models and TV inpainting." *SIAM Journal on Applied Mathematics*, Vol. 62, Jan. 2001.

[13] Chan, Tony, and Shen, Jianhong. "Mathematical Models for Local Non-Texture Inpaintings.", *SIAM J. Appl. Math.*, 62(3), pages 1019–1043, Jul. 2002.

[14] Chan Tony F., and Shen, Jianhong. "Non-Texture Inpainting by Curvature Driven Diffusion (CDD)." *CLA Computational and Applied Mathematics*, pp:00-35, Sep. 2000.

[15] Chang, Lin, and Chongxiu Yu. "New Interpolation Algorithm for Image Inpainting." *International Conference on Physics Science and Technology (ICPST)*, 2011.

[16] Criminisi, Antonio, et al. "Object Removal by Exemplar-Based Inpainting.", *Computer Vision and Pattern Recognition*, 15 Jul. 2003.

[17] Criminisi, Antonio, et al. "Region Filling and Object Removal by Exemplar-Based Image Inpainting." *IEEE Transactions on Image Processing*, Vol.13, No.9:1200-1212, Sep. 2004.

[18] Dataset collection of Einstein. Image Databases, Images from Digital Image Processing, 3rd edition, by Gonzalez and Woods. *Image processing place,* `http://www.imageprocessingplace.com/DIP-3E/dip3e_book_images_downloads.htm`. Accessed Apr. 2018.

[19] Dataset collection of Chemical Plant. Image Database. Volume 3: Miscellaneous. *USC Viterbi,* `https://minghsiehee.usc.edu/volume-3-miscellaneous/`. Accessed Apr. 2018.

[20] Dataset collection of Lena, Living room, Woman Dark Hair, Pirate, Cameraman, Mandril, Peppers, House, Lake, Walkbridge and Jetplane. *Image Databases*, `http://www.imageprocessingplace.com/root_files_V3/image_databases.htm`. Accessed Apr. 2018.

[21] Dataset collection of Barbara and Boat. *Public-Domain Test Images for Homeworks and Projects*, `https://homepages.cae.wisc.edu/~ece533/images/`. Accessed Apr. 2018.

[22] Dataset collection of MRI. Northern Arizona University, NAU Electrical Engineering, Home page of Dr. Phillip A. Mlsn. *Grayscale Images*, `http://www.cefns.nau.edu/~pam7/EE442/grayscale/grayscaleimgs.html`, Accessed Apr. 2018.

[23] Davis, C.S. Statistical Methods for the Analysis of Repeated Measures, New York, NY: Springer-Verlag, 2003.

[24] Dean, S. and Illowsky, B. "F Distribution and ANOVA: The F Distribution And The F Ratio" `https://www.saylor.org/site/wp-content/uploads/2011/06/MA121-6.3.2-s3.pdf`, Accessed Jul. 2018.

[25] Efros, A. A. and Freeman, W. T. "Image quilting for texture synthesis and transfer." in SIGGRAPH, ACM, 2001.

[26] Emile-Male, Gilberte. *The Restorer's Handbook of Easel Painting*. Van Nostrand Reinhold, New York, Aug. 1977.

[27] Equation Editor for LaTeX. Retrieved from `https://www.codecogs.com/latex/eqneditor.php`. Accessed Apr. 2018.

[28] Fadnavis, Shreyas. "Image Interpolation Techniques in Digital Image Processing: An Overview." *International Journal of Engineering Research and Applications*, ISSN : 2248-9622, Vol. 4, Issue 10, Part-1, Oct. 2014, pp.70-73. Retrieved from `https://www.researchgate.net/publication/301889708_Image_Interpolation_Techniques_in_Digital_Image_Processing_An_Overview` Accessed Apr. 2018.

[29] Fang, et al. "A Systolic Tree-Searched Vector Quantizer for Real-Time Image Compression." *Proc. VLSI Signal Processing IV IEEE Press*, NY, 1990.

[30] Fawzi, A., et al. "Image Inpainting Through Neural Networks Hallucinations." *Image, Video, and Multidimensional Signal Processing Workshop (IVMSP)*, Aug. 2016.

[31] Friedman, Jerome H. "Multivariate Adaptive Regression Splines." *The Annals of Statistics*, Vol. 19, No. 1, Mar. 1991, pp. 1-67.

[32] Friedman, Jerome H. "Fast MARS." Department of Statistics, Stanford University, May. 1993.

[33] Gandhi, Snehal, et al. "Performance Analysis and Optimization of Patch Based Image Restoration Techniques for Diversified Field Images." *International Journal of Advanced Research in Computer Science and Software Engineering*, Volume 4, Issue 2, Feb. 2014.

[34] Gonzalez, Rafael C., and Richard E. Woods. *Digital Image Processing.* Pearson Prentice Hall, 2008.

[35] Gupta, Dipalee, and Choubey Siddhartha. "Discrete Wavelet Transform for Image Processing." *International Journal of Emerging Technology and Advanced Engineering*, ISSN 2250-2459, ISO 9001:2008 Certified Journal, Volume 4, Issue 3, Mar. 2015.

[36] Hamill, Michele. *Preserving Your Family Photographs.* Cornell University Library Department of Preservation and Conservation, Ithaca, NY, 2001.

[37] Hastie, Trevor, et al. *The Elements of Statistical Learning Data Mining, Inference, and Prediction*, Springer Series in Statistics, Springer New York, 2009, ISBN 978-0-387-84857-0.

[38] "How to Read a Histogram." *Vertheim.com*, `www.vertheim.com/how-to-read-a-histogram.html`. Accessed Apr. 2018.

[39] Hutchinson, Jamie. *Information Age Madonna*, *IEEE Professional Communication Society Newsletter*, Volume 45 Number 3, May./Jun. 2001. `http://www.lenna.org/pcs_mirror/may_june01.pdf`. Accessed Apr. 2018.

[40] "Ill Posed Problem: Definition." *StatisticsHowTo,* `http://www.statisticshowto.com/ill-posed-problem-definition/`. Accessed Jul. 2018.

[41] "Image Types in the Toolbox." *MathWorks,* `https://www.mathworks.com/help/images/image-types-in-the-toolbox.html#f14-33397`. Accessed Apr. 2018.

[42] Jähne Bernd. *Digital Image Processing.* 5th revised and extended edition, Springer. ISBN 3-540-67754-2, 2002.

[43] Jain, Viren, and Seung, H.Sebastian. "Natural Image Denoising with Convolutional Networks." *Advances in Neural Information Processing Systems*, 21:769–776, 2008.

[44] Jassim, Firas A. "Image Inpainting by Kriging Interpolation Technique." *World of Computer Science and Information Technology Journal (WCSIT)*, ISSN: 2221-0741 Vol. 3, No. 5, 91-96, 2013.

[45] Kaiming, He, and Sun, Jian "Statistics of Patch Offsets for Image Completion." 12th European Conference on Computer Vision (ECCV), 2012.

[46] Kandimalla, Ashok. "The Two Tools of Trade Part-1", Issue of Smart Photography, pages(70-74), Nov. 2013.

[47] Kandimalla Ashok. "The Two Tools of Trade Part-2", Issue of Smart Photography, pages(78-82), Dec. 2013.

[48] Landy, Michael S. "Weber's Law and Fechner's Law", *PSYCH-UA.44, Lab in Perception, Fall, 2014. Michael S. Landy Homepage* `http://www.cns.nyu.edu/~msl/courses/0044/handouts/Weber.pdf`, Accessed Jan. 2018.

[49] Leggat, Robert. *History of Photography from Its Beginnings Till the 1920s.* 1 Dec. 1995.

[50] Lindberg, Siv. *Perceptual Determinants of Print Quality.* PhD Thesis. Stockholm University, Faculty of Social Sciences, Department of Psychology, 2004.

[51] Mahon, Basil. *The Man Who Changed Everything: The Life of James Clerk Maxwell.* Chichester, West Sussex, England, Wiley, 2003.

[52] Milborrow, Stephen. R Software Package and Reference Manual. Earth: Multivariate Adaptive Regression Spline Models. Retrieved from `https://cran.r-project.org/web/packages/earth/`. Accessed Apr. 2018.

[53] Mohammadi, Pedram, et al. "Subjective and Objective Quality Assessment of Image: A Survey." Preprint Submitted to Elsevier, 28 Jun. 2014.

[54] Morley, John. "Academic Phrasebank." The University of Manchester, 2014. Retrieved from `http://www.kfs.edu.eg/com/pdf/2082015294739.pdf`. Accessed Jan. 2018.

[55] MOSEK™ Software, A very powerful commercial software for CQP. Copenhagen: MOSEK™ ApS, 1997, Aug. 2014. Retrieved from `http://www.mosek.com`. Accessed Apr. 2018.

[56] Mumford, David, and Shah, Jayant. "Optimal approximation by piecewise smooth functions and associated variational problems." *Communications on Pure and Applied Mathematics*, vol. 42, pp. 577-684, 1989.

[57] Munson, David C. *A note on Lena*, *IEEE Transactions on Image Processing*, VOL. 5. NO. 1. Jan. 1996 Retrieved from `https://perso.liris.cnrs.fr/christian.wolf/research/misc/lena.pdf`. Accessed Apr. 2018.

[58] Naryškin, Romanas. "Underexposure vs Overexposure - A Beginner's Guide." *Photography Life,* 5 Mar. 2018. `https://photographylife.com/underexposure-and-overexposure-in-photography`. Accessed Apr. 2018.

[59] Ndajah, Peter, et al. "An Investigation on the Quality of Denoised Images." *International Journal of Circuit, Systems, and Signal Processing*, 5(4), pp.423-434, 2011.

[60] Ndajah, Peter. "An Investigation on the Quality of Denoised Images." *International Journal of Circuits, system and signal processing*, Issue 4, Volume 5:423–434, 2011.

[61] "New York State Archives." *Matting and Framing,* http://www.archives.nysed.gov/records/memory/matting-and-framing. Accessed Apr. 2018.

[62] Oliveria, Manuel M., et al. "Fast Digital Image Inpainting" *International Conference on Visualization, Imaging and Image Processing (VIIP 2001)*, Marbella, Spain. 3 Sep. 2001.

[63] "Ordinary Kriging Codes by Wolfgang Schwanghart" Retrieved from https://www.mathworks.com/matlabcentral/fileexchange/29025-ordinary-kriging?requestedDomain=true. Accessed Apr. 2018.

[64] "PDE Codes by Simone Parisotto. Detailed Matlab implementation of five classic inpainting methods (AMLE, Harmonic, Mumford-Shah, Cahn-Hilliard, Transport) described in "Partial Differential Equation Methods for Image Inpainting" (Carola-Bibiane Schönlieb, Cambridge University Press, 2015)." Retrieved from https://www.mathworks.com/matlabcentral/fileexchange/55326-matlab-codes-for-the-image-inpainting-problem?s_tid=srchtitle. Accessed Apr. 2018.

[65] Pedersen, Marius, et al. "Image Quality Metrics for the Evaluation of Print Quality." *Image Quality and System Performance VIII*, vol. 7867, no. 7867702, ser. 1, 2011. 1, doi:10.1117/12.876472. http://www.imaging.org/site/PDFS/Reporter/Articles/2011_26/REP26_2_EI2011_PEDERSEN_7867_1.pdf. Accessed Apr. 2018.

[66] Quirós, Elia, et al. "Testing Multivariate Adaptive Regression Splines(MARS) as a Method of Land Cover Classification of TERRA-ASTER Satellite Images." *Sensors*, 9, 9011-9028; doi:10.3390/s91109011, ISSN 1424-8220, 2009.

[67] R Core Team (2013). R: A language and environment for statistical computing. R Foundation for Statistical Computing, Vienna, Austria. Retrieved from http://www.R-project.org

[68] "Repeated Measures Designs" *Discovering Statistics*, https://www.discoveringstatistics.com/repository/repeatedmeasures.pdf. Accessed Jul. 2018.

[69] "Repeated Measures ANOVA." *Laerd,* https://statistics.laerd.com/statistical-guides/

repeated-measures-anova-statistical-guide.php. Accessed Jul. 2018.

[70] Reddy, V. Raveendrea, et al. "Speed Control of Induction Motor Drive Using Artificial Neural Networks- Levenberg-Marquardt Backpropogation Algorithm." *International Journal of Applied Engineering Research*, ISSN 0973-4562 Volume 13, Number 1, 2018, pp. 80-85.

[71] Russ, John C. *The Image Processing Handbook.* Sixth Edition, CRC Press, Boca Raton FL,ISBN 1-4398-4045-0, 2011.

[72] Russell, Tony, et al. "MLA Formatting and Style Guide." *The Purdue OWL,* Purdue U Writing Lab, 28 Mar. 2018, https://owl.english.purdue.edu/owl/resource/747/01/. Accessed Apr. 2018.

[73] Sapkal, Monali S., and Kadbe, Premanand. "Kriging Interpolation Technique Basis Image Inpainting." *International Journal of Latest Trends in Engineering and Technology (IJLTET)*, Vol. 6, Issue Jan. 2016.

[74] Schmidt-Thieme, Lars. "Nächste-Nachbar- und Kernel-Verfahren." Information Systems and Machine Learning Lab (ISMLL): Machine Learning. Institute for Business Economics and Information Systems & Institute for Computer Science University of Hildesheim. Winter Term 2007. Course Notes. Retrieved from https://www.ismll.uni-hildesheim.de/lehre/ml-07w/skript/. Accessed Apr. 2018.

[75] Schönlieb, Carola-Bibiane. *Partial Differential Equation Methods for Image Inpainting.* Cambridge University Press, 2015.

[76] Sephton, Peter. "Forecasting Recessions: Can We Do Better on MARS?" Federal Reserve Bank of St. Louis, pp. 39-49, Mar./Apr. 2001.

[77] Shiffman, Daniel. "Color." *Processing*, https://processing.org/tutorials/color/. Accessed June 2018.

[78] Skien, J.O., et al. "Top-kriging – geostatistics on stream networks." *Hydrol. Earth Syst. Sci.*, 10, 277–287, 2006.

[79] Stack Exchange for LaTeX. Retrieved from https://tex.stackexchange.com/. Accessed Apr. 2018.

[80] "Structural Similarity (SSIM) Index for Measuring Image Quality - MATLAB Ssim", *MathWorks*, https://www.mathworks.com/help/images/ref/ssim.html. Accessed Apr. 2018.

[81] Szeliski, Richard. *Computer Vision: Algorithms and Applications.* Springer, 2010.

[82] Table Generator for LaTeX. Retrieved from http://www.tablesgenerator.com/#. Accessed Apr. 2018.

[83] Taylan, Pakize, et al. "New approaches to regression by generalized additive models and continuous optimization for modern applications in finance, science and technology." *Optimization*, 56(5-6), 2007, ISSN 02331934.

[84] "Technology", *BBCNews*, http://www.bbc.com/news/technology-19260550, Accessed Apr. 2018.

[85] Telea, Alexandru. "An Image Inpainting Technique Based On The Fast Marching Method." *Journal Of Graphics Tools*, Vol. 9, No. 1: 25—36, 2004.

[86] Thanki, Bansi B. "Overview of an Image Inpainting Techniques." *International Journal For Technological Research In Engineering*, Volume 2, Issue 5, Jan. 2015.

[87] "The costliest art mishaps." *BBC News,* http://www.bbc.com/news/world-asia-34059664. Accessed Apr. 2018.

[88] "Thesis Manual and LaTeX Template" *Graduate School of Natural and Applied Sciences*, http://fbe.metu.edu.tr/thesis-manual. Accessed Apr. 2018.

[89] Umbaugh, Scott E. *Digital Image Processing and Analysis, Human and Computer Vision Applications with CVIPtools*, CRC Press, Second Edition, 2011.

[90] "Variogram calculation and interpretation" *Geostatistical Software & Services*,http://www.statios.com/resources/04-variogram.pdf. Accessed Apr. 2018.

[91] Virdee, T.S., and Kottegoda, N.T. "A brief review of kriging and its application to optimal interpolation and observation well selection." *Hydrological Sciences Journal*, 29:4, 367-387, DOI: 10.1080/02626668409490957, 1984. Retrieved from https://doi.org/10.1080/02626668409490957. Accessed Apr. 2018.

[92] Walden, Sarah. *The Ravished Image*. St. Martin's Press, New York, 1 Aug. 1985.

[93] "Walt Disney Quotes." *BrainyQuote,* https://www.brainyquote.com/authors/walt_disney. Accessed on 22 Apr. 2018.

[94] Wang, Zhou, and Bovik, Alan C. "Mean Squared Error: Love It or Leave It? - A new look at signal fidelity measures." *IEEE Signal Processing Magazine*, vol. 26, no. 1, pp. 98-117, Jan. 2009.

[95] Wang, Zhou, and Bovik, Alan C. "A universal image quality index." *IEEE Signal Processing letters*, vol. 9, no.3, pp. 81-84, Mar. 2002.

[96] Wang, Zhou, et al. "Image Quality Assessment: From Error Visibility to Structural Similarity." *IEEE Transactions on Image Processing*, vol. 13, no. 4, pp. 600-612, Apr. 2004.

[97] Wang, Zhou, et al. "Structural Approaches to Image Quality Assessment in Handbook of Image and Video Processing." in Handbook of Image and Video Processing, 2nd edition, Al Bovik, ed., Academic Press, 2005.

[98] Weber, G., Batmaz, İ., Köksal, G., Taylan, P., and Yerlikaya-Özkurt, F. "CMARS: A new contribution to nonparametric regression with multivariate adaptive regression splines supported by continuous optimisation." Preprint 2009-16, Institute of Applied Mathematics, Middle East Technical University, 06800 Ankara, Turkey, Sep. 2009.

[99] "What is the reason Lena Söderberg's photo is used widely to test algorithms in image processing?" *Quora*, `shorturl.at/eSW34`. Accessed Apr. 2018.

[100] Wu, Jiying, and Ruan, Qiuqi. "A Novel Hybrid Image Inpainting Model." *International Conference on Audio, Language and Image Processing(ICALIP)*, May. 2008.

[101] Xie, Junyuan, et al. "Image denoising and Inpainting with Deep Neural Networks." *Advances in Neural Information Processing Systems* 25, pages 350-358, 2012.

[102] Yadav, Neha, et al. *An Introduction to Neural Network Methods for Differential Equations.* Springer, Netherlands, 2015.

[103] Yılmaz, Yavuz. *Daily Natural Gaz Consumption Prediction by MARS and CMARS Models for residential Users in Ankara.* MSc Thesis. Scientific Computing, Institute of Applied Mathematics, Middle East Technical University, Ankara, Turkey, Aug. 2015.

[104] Yuan, Ganzhao, and Ghanem, Bernard. "$\ell$ TV: A New Method for Image Restoration in the Presence of Impulse Noise." *Conference on Computer Vision and Pattern Recognition(CVPR)*, 2015. *CVPR 2015*,`https://www.cv-foundation.org/openaccess/CVPR2015.py`. Accessed Apr. 2018.

[105] Zhou, Jun, and Robles-Kelly, Antonio. "Image Inpainting Based on Local Optimization." *International Conference on Pattern Recognition (ICPR)*, Oct. 2010.

[106] Çavuşlu, Mehmet Ali, et al. "Hardware Implementation of Neural Network Training with Levenberg-Marquardt Algorithm." *TBV Bilgisayar Bilimleri ve Mühendisliği Dergisi*, 5. Cilt, s:31-38, 2012.

[107] Özmen, Neslihan. *Image Segmentation and Smoothing via Partial Differential Equations.* MSc Thesis. Scientific Computing, Institute of Applied Mathematics, Middle East Technical University, Ankara, Turkey, Feb. 2009.

# APPENDIX A

# IMAGE TYPES

MATLAB ® has a useful Image Processing Toolbox ™ which allows the users to make the following operations: import, export and exploration, geometric transformation and image registration, image filtering and enhancement, image segmentation and analysis, deep learning for image processing, 3-D volumetric image processing, code generation and CPU computing. In general, images are defined as four basic types as shown in the following Table A.1.

TableA.1: Interpretation of Image Types

| **Image Type** | **Interpretation** |
|---|---|
| Binary<br>(Also known as a, bilevel image) | Logical array containing only 0s and 1s,<br>interpreted as black and white, respectively. |
| Indexed<br>(Also known as a pseudocolor image) | Array of class logical,uint8, uint16,single, or double<br>whose pixel values are direct indices into a colormap.<br>The colormap is an m-by-3 array of class,double.<br>For single or double,arrays, integer values range from [1, p*].<br>For logical, uint8, or,uint16 arrays, values range from [0,p-1].<br>*p is the length of the colormap. |
| Grayscale<br>(Also known as an intensity,<br>gray scale, or gray level image) | Array of class uint8,uint16, int16,single, or double<br>whose pixel values specify intensity values.<br>For single or double,arrays, values range from [0, 1].<br>For uint8,values range from [0,255].<br>For uint16, values,range from [0, 65535].<br>For int16, values,range from [-32768, 32767]. |
| Truecolor<br>(Also known as an,RGB image ) | m-by-n-by-3 array of,class uint8, uint16,single, or double<br>whose pixel values specify intensity values.<br>For single or double,arrays, values range from [0, 1].<br>For uint8,values range from [0, 255].<br>For uint16, values range from [0,65535]. |

Source: MathWorks, Image Types in the Toolbox. [41]

## A.1 Binary

A binary image consists of two discrete values: zero or one; zero represents black, other white. It contains 1-bit per pixel data. Because of its capability of saving storage and fast transmitting advantages, binary image can be a good alternative to send/receive facsimile automatic xerox (FAX) images. Using threshold operation on grayscale images is a widespread method of creating binary image. That operation omits the information on the image but detecting the edge of the object could be a good guide for optical character recognition (OCR) application [89], page 50-51.

## A.2 Indexed

Image indexing is an image representation method which converts the color to index number corresponding value of palette. The higher the number of color palette is, the better the image reflects natural traces.

## A.3 Grayscale

Instead of color information, grayscale images contain brightness levels. Oxford Dictionary defines brightness as: “The quality or state of giving out or reflecting light”. Without color information, grayscale images are defined as monochrome image. This means grayscale image has 256 shades of gray. The usual grayscale image consists of 8-bit per pixel (8bpp) data, which indicates a fluctuation of the gray tones from zero to 255 (Number of 256 brightness levels).

## A.4 RGB

In the image processing area, color images consist of RGB colors in which each monochrome color band includes 8-bit brightness information of the image data. Thanks to some color transformation transactions hue, saturation and lightness (HSL) could be obtained. Lightness is the intensity of the color whereas hue is the color perception. The saturation is a measure to decide whether the image is deep or pale.

People are familiar with RGB and HSL values in Word Paint program. In Figure A.1 a middle purple is represented in terms of RGB and HSL values.

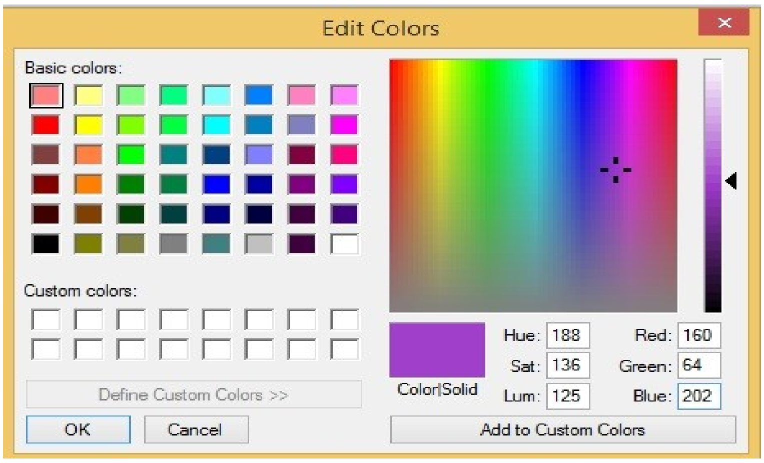


Source: Created by the author

Figure A.1: Representation of RGB and HSL values

Hence, R=160, G=64 and B=202 indicates a middle purple with H=188, S=136 and L=125 corresponding HSL values. Scott [89] introduced equations to convert RGB values to HSL values. Color images are converted to grayscale images with a following equation [89], page 50-51:

$$Y = 0.299R + 0.587G + 0.144B \tag{A.1}$$